Clustering of strong replicators associated with active promoters is sufficient to establish an early-replicating domain

Caroline Brossas, Anne-Laure Valton, Sergey V Venev, Sabarinadh Chilaka, Antonin Counillon, Marc Laurent, Coralie Goncalves, Bénédicte Duriez, Franck Picard, Job Dekker, et al.

Clustering of strong replicators associated with active promoters is sufficient to establish an early-replicating domain

Caroline Brossas[1], Anne-Laure Valton[2,5], Sergey V. Venev[2], Sabarinadh Chilaka[3], Antonin Counillon[1], Marc Laurent[1], Coralie Goncalves[1], Bénédicte Duriez[1], Franck Picard[4], Job Dekker[2,5] and Marie-Noëlle Prioleau[1]*

[1] Université de Paris, CNRS, Institut Jacques Monod, Equipe Labellisée Association pour la recherche sur le cancer, Paris, 75013, France

[2]University of Massachusetts Medical School, Program in Systems Biology, Department of Biochemistry and Molecular Pharmacology, Worcester, MA 01605, USA

[3]Present address: Centre for Immunology, University of Glasgow, G12 8QQ, United Kingdom

[4] Université de Lyon, Université Lyon 1, CNRS, Laboratoire de Biométrie et Biologie Evolutive UMR 5558, Villeurbanne, France.

[5] Howard Hughes Medical Institute, Chevy Chase, MD, 20815, USA

* Correspondence: marie-noelle.prioleau@ijm.fr

Abstract

Vertebrate genomes replicate according to a precise temporal program strongly correlated with their organization into A/B compartments. Until now, the molecular mechanisms underlying the establishment of early-replicating domains remain largely unknown. We defined two minimal *cis*-element modules containing a strong replication origin and chromatin modifier binding sites capable of shifting a targeted mid-late replicating region for earlier replication. The two origins overlap with a constitutive or a silent tissue specific promoter. When inserted side-by-side, these modules advance replication timing over a 250 kb region through the cooperation with one endogenous origin located 30 kb away. Moreover, when inserted at two chromosomal sites separated by 30 kb, these two modules come into close physical proximity and form an early-replicating domain establishing more contacts with active A compartments. The synergy depends on the presence of the active promoter/origin. Our results show that clustering of strong origins located at active promoters can establish early-replicating domains.

Keywords: Replication timing/ Replication origin/ Nuclear organization/ Chromatin accessibility/ Promoter

Running title: Formation of an early-replicating domain

Introduction

A precise, cell type-specific temporal program governs the duplication of vertebrate genomes (Ryba *et al*, 2010). The genome-wide mapping of replication origins with different methods has revealed a high density of efficient site-specific origins in early-replicated domains, whereas late regions are usually origin-poor (Prioleau & MacAlpine, 2016). Replication timing (RT) domains are correlated with the organization of chromosomes into two main types of compartments: compartment A, which is accessible and replicated early, and compartment B, which is more condensed and replicated late (Ryba *et al*, 2010). These compartments, which display greater interaction within themselves rather than across them, were initially defined by the Hi-C method, at a resolution of 1 megabase (Lieberman-Aiden *et al*, 2009). The only major player in the RT program for which the mode of action has been elucidated is Rif1 (Knott *et al*, 2012; Yamazaki *et al*, 2012; Cornacchia *et al*, 2012). Rif1 has a global repressive effect on genome-wide DNA replication. This effect is mediated by the recruitment of protein phosphatase 1, which opposes the Dbf4-dependent kinase (DDK) activity required for origin firing (Hiraga *et al*, 2014). Consistent with this direct role, ChIP analyses of Rif1 throughout the mouse genome revealed an overlap between Rif1 associated domains and late replication (Foti *et al*, 2016). However, only regions associated with Rif1 but not with the nuclear lamina switch to early replication in a context of Rif1 depletion. This finding suggests that other major players, such as the nuclear lamina, are also involved in controlling late replication (Duriez *et al*, 2019). One key question that remains concerns whether some late-replicating domains are so robustly constrained by their nuclear compartmentalization that the targeting of a very efficient origin associated with early timing control elements could not locally advance the timing of their replication. The underlying

question is whether a late domain is defined by the deficiency of an early-firing signal together with an accumulation of signals imposing the late-firing of many potential initiation sites. A related question is whether early-replicated domains are defined solely by the absence of a strong negative signal, such as association with the nuclear lamina and/or Rif1. Alternatively, early constant timing regions (CTRs) may result fortuitously from the more or less synchronous firing of a cluster of replicons, each with its own individual local early timing control elements. This hypothesis is supported by the high density of efficient origins mostly associated with transcription start sites (TSS) and thus proximal to sites associated with open chromatin marks in early-replicated domains (Picard *et al*, 2014). In agreement with this model, a recent study showed that stem-cell specific early-replicating domains in mouse are controlled by stem-cell specific *cis*-elements located in promoter and enhancer regions (Sima *et al*, 2019). Moreover, several elements spanning altogether 30 kb had to be deleted so that the early domain switched from early to late, suggesting redundancy between these elements along early domains and their potential capacity to act remotely. Here we put forward the central role of constitutive promoters in the formation of constitutive early-replicating domains and strongly suggests that spatial connections between strong initiation sites play a key role in this fundamental process.

Results

Cooperation between two minimal autonomous replicons impacts on RT at a large scale

The current study is based on the method we developed to quantify the magnitude of the RT shift induced by the insertion of an ectopic DNA sequence into a specific mid-late-replicating locus (chr1:72,565,520 bp, galGal5) (Hassan-Zadeh *et al*, 2012 and Appendix Figure S1). Here we confirmed our previous data on a much larger number of cell lines modified in the same targeted region, allowing a statistical quantification of RT shifts (Figure 1 and Appendix Table S1). The tissue specific β^A-*globin* promoter containing a strongly active replication origin flanked by 2XFIV (Footprint IV of cHS4 insulator element is a binding site for the Upstream Stimulatory Factor (USF) (West *et al*, 2004)) significantly advanced RT (Figure1 (ii), *p*-value = 4.57E-05) and to the same extent as the active *β-actin* constitutive promoter containing an active replication

origin (Figure EV1A) (Figure 1 (iii), *p*-value = 3.38E-03). Finally, the combination of these two minimal modules (*β^A-globin+β-actin* constructs) imposed a stronger shift to earlier replication at the inserted locus than the presence of a single minimal module alone (Figure 1 (iv), *p*-value = 3.25 E-03 between (ii) and (iv); *p*-value = 2.66E-03 between (iii) and (iv) and Figure EV1 and Hassan-Zadeh *et al*, 2012). These endogenous origins/promoters are naturally found in early-replicating domains in DT40 cells (Appendix Figure S2) and therefore constitute excellent models to understand how early domains might be established. Insertion of this large construct on the two homologous chromosomes (2x (*β^A-globin+β-actin)* cell line) allowed us to observe a 250 kb region displaying an advance RT compared to a WT cell line (Figure 2A and Appendix Figure S3). A zoom in centred on the site of insertion confirmed that this site is naturally a termination zone (TZ) flanked by two initiation zones (IZ) (Figure 2B). RT profiles obtained from S1 to S4 fractions showed that the IZ about 30 kb upstream of the site of insertion (IZ.1) is activated in S3 in WT cells whereas the IZ located 60 kb downstream (IZ.2) is activated already in S2. IZ.1 and IZ.2 correspond to strong initiation sites detected by the short nascent strand (SNS) assay (Massip *et al*, 2019). Profiles observed at the same region in a cell line modified on both chromosomes (2x (*β^A-globin+β-actin)* cell line) showed firing of the IZ.1 in S1 whereas the IZ.2 is unchanged compared to the WT cell line. Moreover, in this line, IZ.1 is then extended in S2 on the 3' direction towards the insertion site, revealing the activation of origins brought by the inserted construct. These changes led to a 30 kb shift of the TZ downstream of the site of insertion. Overall, this result suggested that the large *β^A-globin+β-actin* construct impacted strongly on the RT profile of its surrounding regions in two different ways: it advanced significantly the RT of a 30 kb upstream strong endogenous origin from S3 to S1 and induced strong initiation in S2 due to efficient firing of replication origins present inside the construct.

Two advanced replicons separated by 30 kb synergize to form a synthetic early-replicating region that interacts more with A compartments

Our observation suggested that the large *β^A-globin+β-actin* construct might cooperate with endogenous replication origins located about 30 kb upstream. To further test this hypothesis, we inserted two large autonomous replicons 30 kb apart at sites 1 and 3 (insertion site 1; chr1:72,565,520 bp and insertion site 3; chr1: 72,536,061 bp, galGal5, Figure 2B) and tested their impact on RT. The autonomous replicon at site 3 was similar to the one at site 1 except that the gene used conferred puromycin-N-acetyltransferase resistance (*PuroR*, insertion site 3, Figure 3A). We assessed the impact of RT changes in the middle of our modified region, by introducing a reporter construct in a central position (Insertion site 2; chr1: 72,548,590 bp, galGal5, Figure 2B) between the two autonomous replicons (1+2+3) or on the other chromosome (1+3) (Figure 3A). The reporter construct consisted of the erythroid-specific *β^A-globin* origin/promoter linked to the green fluorescent protein (*GFP*) reporter gene and a 1.6 kb fragment of human chromosome 7 (h.K7; chr7:26,873,165-26,874,805 bp, hg38) containing no replication origin (Figure 3A). We found that the *GFP* reporter construct had no impact on RT when inserted alone at site 2 (-ΔL+ΔE= -5.1%, Figure EV2A). We then showed that the *β^A-globin+β-actin* construct inserted at site 1 had similar effects on RT when associated with *GFP* reporter construct insertion at site 2 on the same or the other chromosome (compare Figure EV1B with Figure EV2B and C and Hassan-Zadeh *et al*, 2012). These results confirm the neutral impact on RT of inserting the *GFP* reporter construct at site 2. We then investigated whether the insertion of a single autonomous replicon at site 3 was able to advance RT as efficiently as insertion at site 1. We confirmed that the *β^A-globin+β-actin* construct induced a substantial shift in RT when inserted at this new genomic position (-ΔL+ΔE= +26.8% for clone 1 and -ΔL+ΔE= +22% for clone 2, Figure EV2D). This shift was similar to the one observed in *β^A-globin+β-actin* clones after insertion at site 1 (*p*-value = 0.133 between (i) and (iii), Figure 3). As previously shown, the insertion of the *GFP* reporter construct at site 2 had no impact on RT when associated with a single autonomous replicon at site 3 on either the same or the other chromosome (Figure EV2, compare -ΔL+ΔE values between D. and E.). Insertion of two autonomous replicons at sites 1 and 3, with (1+2+3) or without (1+3) the central *GFP* reporter construct, resulted in larger shift in RT over the whole of the genomic region targeted (Figure EV3A and B, -ΔL+ΔE= +63.3% and +70.3% for 1+2+3 insertions and -ΔL+ΔE= +65.2%, +84.2%, +57.3%, for

1+3 insertions). A quantitative analysis revealed that the differences in RT between cell clones with one and two autonomous replicons were significant (*p*-value=0.01554 between (i) and (ii) and *p*-value=0.03571 between (ii) and (iii), Figure 3A). Overall, these results strongly suggest that two similar independent advanced replicons, 30 kb apart, can synergize to control the extent of the RT shift.

Genome-scale studies have shown that RT is strongly correlated with A/B compartments in human cells, suggesting spatial proximity of regions of similar RT within the nucleus (Ryba *et al*, 2010). We tested whether the large change in RT of the modified chromosome is accompanied by a change in the way the inserted origins interact with A and B compartments. This system allows us to assess how the early replicating allele (allele 1+3) interacts with A and B compartments compared to the allele with the endogenous RT (allele 2) (Figure 3B). We conducted Hi-C to assess compartment status genome wide and to measure long-range chromatin interactions for allele 1+3 and allele 2 at the same time. We first examined interactions between inserted sequences at alleles 1+3 and 2 and chromosome 1 (chr1). The profile of interactions of allele 1+3 with chr1 and allele 2 with chr1, demonstrates alternating patterns in the p-arm of chr1, whereas in the q-arm the two profiles show more overlap (Figure 3C and Appendix Figure S4A, D). Most of the loci that show preferred interactions with allele 1+3 coincide with loci located within A compartment domains (Figure 3C and Appendix Figure S4A, D). To further quantify the observed preference, we calculated average distance-corrected interactions between allele 1+3/allele 2 and regions of chr1 according to their compartment status (Figure 3D and Appendix Figure S4B, E). Averaged interactions confirm that allele 1+3 interacts more with A compartment than with B compartment both for p and q-arms of chr1, unlike allele 2 which shows smaller preference for A compartment in the q-arm, and no association with either A or B compartment in the p-arm. Our observations regarding allele 2 are in line with the WT compartment status of the mid-late insertion site, as shown by an eigenvector 1 (EV1) value near zero (see also Figure 7A below). We assessed the significance of the interaction preferences by re-calculating the average interactions of allele 1+3/allele 2 and regions of chr1 with randomly shuffled compartment status (EV1) (Figure 3D, Appendix Figure S4 B, E) (see Methods for details). We further looked if allele 1+3 and allele 2 demonstrated any preferential interactions with other chromosomes in the genome, by comparing

their density of interactions (averaged interactions normalized by chromosome length, see Methods for details). The number of interactions with chr9 is disproportionately higher for allele 1+3 than for allele 2 compared to other chromosomes (Figure 3E, Appendix Figure S4 C, F) showing that allele 1+3 interacts more with chr9. Our results show that allele1+3 interacts more with specific A compartments located on chr1 and globally more with chr9. These specific interactions coincide with several strong replication origins and high gene density for chr9, however precise mechanistic understanding will require further investigation.

The constitutive *β-actin* promoter/origin is required for the synergic action of the two replicons separated by 30 kb

We have already shown that the large autonomous replicon used in this study is composed of two strong origins associated either with an active (*β-actin)* or an inactive (*β^A-globin)* promoter (Hassan-Zadeh *et al*, 2012 and Appendix Figure S2 and Figure EV4A). MNase (micrococcal nuclease) titration analyses confirmed a differential chromosomal accessibility of the two minimal modules inserted separately at site 1 (Figure EV4B and C and Appendix Figure S5). However, both minimal modules individually can induce a significant RT shift (Figure 1). To understand in more details the mechanisms involved in the synergy observed in the large *β^A-globin*+*β-actin* construct, we tested for each minimal construct the effect of a double insertion at sites 1 and 3 on the same chromosome. We observed that similarly to the large autonomous replicon, the *β-actin* promoter induced a stronger shift in RT when inserted at 1+3 positions (Figure 4A and Figure EV3C). By contrast, two inactive *β^A-globin* promoters did not produce any advanced RT when inserted at 1+3 sites (Figure 4B and Figure EV5). We observed for a subset of clones even a decrease in the intensity of the RT after the second insertion, a reproducible observation that cannot be explained yet. However, this last result showed that the minimal replicon containing an inactive promoter

is not able to synergize when located at two remoted positions. Moreover, it showed that the synergy observed with constructs containing the active *β-actin* promoter (small or large modules) did not result from the simple two-fold increase in the number of active origins in the analysed region. This result suggests that an unknown specific mechanism allowed two strong origins associated with an active TSS and separated by 30 kb to advance their RT.

The formation of the early-replicating domain is associated with the spatial proximity of the two advanced replicons

We tested the hypothesis whether the synergy between the two advanced replicons leading to the formation of an early-replicating domain involved spatial proximity between the replicons concerned. 3C experiments, after crosslinking, digestion, ligation and PCR with loci specific primers, measure the frequency of interactions between any two genomic loci. We thus could have used 3C to assess the interactions between the two advanced replicons. However, there are limitations inherent to our system: First, allele 1+3 and allele 2 share common sequences. There are two insertion sites on allele 1+3 and only one insertion site on allele 2 (Figure 3B). Therefore, we can only quantify the interactions within allele 1+3 (*i.e.* interactions between the two early replicons) without controls for allele 2. Second, the two early replicons located on allele 1+3 have almost similar sequences resulting in only few primers that would be 3C compatible. Third, 4C experiments could be another possibility but normalization is not trivial and interpretation of the data can be challenging in this case of different insertions on different alleles. Cre/*loxP* site-specific recombination has been successfully used in yeast and bacteria to assess the relative probabilities of different regions of the genome colliding with each another (Burgess & Kleckner, 1999; Hildebrandt & Cozzarelli, 1995). Since Cre/loxP sites are inside our constructs, we used this elegant Cre/loxP system instead of 3C to evaluate the spatial proximity between the two autonomous replicons located 30 kb apart. We assessed the capacity of the 5' recombination element located in the β^A*-globin+β-actin* construct at site 3 (*loxP_RE*,

yellow triangle, Figure 5A) to recombine with the 3' recombination element in the *β^A-globin+β-actin* construct at site 1 (*loxP_LE*, green triangle, Figure 5A). The percentage of chromosomes modified by this recombination (Figure 5C and Appendix Figure S6A, large 1+3 excision) was quantified in cell clones with 1+2+3 and 1+3 configurations, 1 h, 8 h, 24 h and 48 h after the induction of the Cre recombinase. We evaluated the frequency of random contacts by constructing new clones in which the advanced replicon inserted at site 1 was replaced by a *loxP_LE* element alone (Figure 5A, *loxP_LE* (1)+ *β^A-globin+β-actin* (3)). We quantified the large excision product of the modified chromosome by semi-quantitative PCR on the whole cell population with a specific primer pair (Figure 5B, Up large excision and Low large excision). The percentage of cells containing this excision product increased steadily over time, from 6 to 14% after 1 h to 43% to 89% of the cells after 48 h of Cre recombinase induction (Figure 5C and Appendix Figure S6A). By contrast, only small amounts of this product were detected in three independent clones carrying the *loxP_LE* (1)+ *β^A-globin+β-actin* (3) configuration, (from 3% after 1 h to 12% of the cells after 48 h of Cre recombinase induction; Figure 5C and Appendix Figure S6A). Recombination rates varied by five to eightfold between the two types of configuration, as reported for yeasts harboring different combinations of *loxP* sites (Burgess & Kleckner, 1999). Since the *loxP_LE* element is located either at the end of the actively transcribed *BsR* gene or alone at site 1 in the two configurations, we investigated whether the difference in recombination efficiency might be due to differences in chromatin accessibility at this position. We therefore tested the chromatin accessibility of *loxP_LE* at site 1 in the two configurations by assessing the MNase sensitivity (Figure 6A,B). The heterochromatin region located upstream from the early-replicating *β-globin* locus was used as a control for the condensed state and the transcriptionally active *MED14* promoter for the open state (Litt *et al*, 2001; Prioleau *et al*, 1999). We detected similar small amounts of DNA release from *loxP_LE* in both configurations, for all MNAse concentrations showing that the *loxP_LE* element had similar accessibility in both configurations. Since two *β-actin* constructs can also synergize when inserted at sites 1 and 3 (Figure 4A), we tested their capacity to recombine after Cre recombinase induction. We observed a similar behavior as previously with the large *β^A-globin+β-actin* construct (Figure 5C and Appendix Figure S6B). Overall, our data strongly suggest the existence of molecular contacts between the

two constructs synergistically acting on RT. The formation of the early-replicating domain is, thus, linked to a spatial connection between the two advanced replicons containing an active promoter and located 30 kb apart. It suggests that the two advanced replicons might form a chromatin loop.

The close spatial proximity of the two advanced replicons is not associated with an increase in chromatin accessibility

We then investigated whether the synergy of the two autonomous replicons associated with their physical proximity affected the chromatin accessibility of these replicons or of one of the genomic regions located within the early-replicating domain. We addressed this question by quantifying, nuclease-treated chromatin in 1+2+3 and 1+3 cell lines, by qPCR with specific primer sets specifically amplifying at either one or both autonomous *β^A-globin+β-actin* replicons, at the central *GFP* reporter transgene, at the three insertion sites or at control loci (Figure 6A,B). We compared chromatin accessibility between these cell lines and the one having only one *β^A-globin+β-actin* construct inserted at site 1 (Figure EV4D.). We observed an increase in total nucleosome release at insertion site 3 relative to insertions sites 1 and 2 and condensed chromatin controls, for all MNAse concentrations. The chromatin of this insertion site is, therefore, more accessible than that at sites 1 and 2 (Figure 6, insertion site 3). The *β-actin* module harbors the same pattern of accessibility as observed with one autonomous replicon (compare Figure 6B. and Figure EV4C.). Nucleosomes embedded within the upstream 2xFIV element of the *β^A-globin+β-actin* construct at site 3 (5' 2xFIV-3) and within the *PuroR* gene were more susceptible to MNAse, regardless of MNAse concentration, than nucleosomes embedded at similar positions (5' 2xFIV-1 and *BsR* gene) in the *β^A-globin+β-actin* construct at site 1. The chromatin at this site is, therefore, also more exposed, probably reflecting the greater accessibility of the unmodified site 3. The *GFP* reporter construct in the middle of the early-replicating domain (1+2+3) or on the other mid-late-replicating unmodified chromosome (1+3), released similar small amounts of material for all MNAse concentrations as were detected for heterochromatin regions or at the unmodified site 2. We can conclude from these results that two modules composed of 5.6 kb of accessible

chromatin and containing efficient replicators separated by 30 kb are sufficient to create an early-replicated domain when inserted into a naturally closed mid-late-replicating region. These two constructs can establish spatial connections without increasing the accessibility of their own chromatin, or the accessibility of the chromatin located in the middle of the early-replicating domain.

Two late-replicating environments embedded into a B compartment are permissive to a shift towards earlier replication after the site-specific insertion of a large autonomous replicon

It remains unknown whether late-replicating regions are permissive to early timing control elements. One hypothesis is that the nuclear and chromatin organizations of late-replicating domains impose robust constraints that prevent earlier firing. We addressed this question directly, by investigating whether the *β^A-globin+β-actin* construct behaves as efficiently when targeted to regions naturally displaying very late replication and located in a B compartment. We selected two late-replicating regions from the genome-wide RT profile obtained for wt DT40 cells. One of these regions was located 2 Mb upstream from the previously studied mid-late-replicating region on chromosome 1 (Late1 chr1:70,523,649 and mid-late chr1:72,565,520 bp, galGal5; Figure 7A) and the other was located 105.4 Mb downstream from this mid-late-replicating region (Late2 chr1:177,936,192 bp, galGal5, Figure 7B). The late 2 locus is characterized by gene depletion over a 500 kb region in contrast to the late 1 locus (Figure 7). In addition, we know from a previous study that the two late loci are found at the nuclear periphery in DT40 cells. However, the late 2 locus is more tightly associated with nuclear lamina than the late 1 (Figure 6 in (Duriez *et al*, 2019)). Altogether, it strongly suggests that the late 2 locus is a constitutive late domain whereas the late 1 locus might be a facultative late domain. We confirmed that these two regions were, indeed, replicated much later than the previously studied region (Figure 8A, B, Without). We calculated -ΔL+ΔE values for cell clones containing the *β^A-globin+β-actin* transgene inserted into these late-replicating regions (Figure 8). We observed a strong impact on RT of transgene insertion at the late 1 site (Figure 8A). The RT shift was comparable with the one observed following insertions into the previously studied mid-late-replicating region (-ΔL+ΔE = +29.3% for clone 1

and +51.7% for clone 2, Figure 8A. versus smallest and greatest -ΔL+ΔE values calculated for eight clones: +23.3% and 52.9%, respectively, in the mid-late-replicating region, Figure 1). However, in the late 2 region, we detected a slightly lower, but nevertheless significant shift in RT, than that induced in a mid-late-replicating region (-ΔL+ΔE = +16.1% for clone 1, +19.1% for clone 2 and +21.3% for clone 3, Figure 8B). Our findings confirm the robustness of the previously identified combination of *cis*-elements to advance the RT. We show here that the *β^A-globin+β-actin* combination can impose local autonomous control over RT in at least three chromosomal regions, one replicating in mid-late S phase and the other two displaying late replication among which one is a constitutive late domain (Late 2).

Discussion

The DNA RT program has emerged as a system that integrates genome regulation and the three-dimensional organization of the genome. From these observations was proposed the replication domain model in which each RT domain acts as a regulatory unit, determining when the replicons within its boundaries can fire. We challenged this model, by disturbing naturally mid-late- and late-replicating domains after site-specific insertion of constructs containing critical *cis*-elements known to regulate origin firing. Based on the work described here, we identified five important principles underlying the establishment and maintenance of domains of early and late replication: (1) A strong origin embedded into an accessible chromatin structure can significantly advance the RT of a mid-late-replicating region; (2) Two replicators carrying timing information can act in cooperation if located in close proximity; (3) Strong autonomous replicons overlapping an active promoter can act in synergy on RT even when separated by 30 kb to form early-replicated regions; (4) The formation of an early-replicating domain results locally in the formation of a spatial connection between the advanced replicons and on a larger scale in an increase of contacts with the A compartment; (5) The RT of late-replicating domains can be advanced locally by a strong autonomous replicon, but the final RT is also influenced by chromosomal context.

Molecular mechanisms shaping efficient replicons carrying timing information

Studies in *S. cerevisiae* have suggested that the correct temporal activation of origins during S-phase involves the activation of early-firing origins, because these origins have a greater "accessibility" to firing factors, which are present in limiting amounts. After firing, the limiting factors are released and can bind to and activate less accessible origins, and so on (Douglas & Diffley, 2012). This theory suggests that the RT of a region directly reflects the accessibility to these limiting factors of specific regions bound by pre-RCs. In vertebrate cells, there is a strong correlation between early replication and the accumulation of open chromatin marks, consistent with a role for the openness of chromatin in the recruitment of these potential limiting factors (Picard *et al*, 2014; Ryba *et al*, 2010). We previously identified a combination of *cis*-elements constituting an independent replicon with the capacity to advance RT of a 250 kb mid-late-replicating region significantly (Hassan-Zadeh *et al*, 2012 and Figure 2A). This construct contains only promoters and regulatory motifs naturally present in the chicken genome (one tissue-specific promoter, one constitutive promoter and four FIVs elements), linked to either the *IL2R* reporter gene or the *blasticidin* gene selection cassette. Moreover, autonomous replicon activity is driven only by endogenously expressed *trans*-factors. Investigation of the chromatin structure of each independent unit revealed a number of different features, highlighting the potential diversity of *cis*-elements involved in RT control in vertebrates. One of the elements identified contains the β^A*-globin* erythroid tissue-specific promoter which cannot drive transcription in the DT40 lymphoid cell line. The other element contains the constitutive *β-actin* promoter linked to a gene for selection. This strong origin/promoter facilitates the local opening of chromatin structure and the acquisition of H3K4me3 and H3K9K27ac marks at the inserted position (Figure EV4E). These findings are consistent with the observation that the synthetic activation of transcription, but not nuclear repositioning, shifts the RT of several mid-late-replicating loci to mid-early in mouse ES cells (Therizols *et al*, 2014). Our first observation shows that, at least at this mid-late-replicated chromosomal position, origins located within the β^A*-globin* and *β-actin* promoters are highly efficient, because they were able to advance RT locally in a population-based timing assay. We were unable to estimate the fraction of cells in which

these two replicators were activated, but the significant shift in RT towards earlier replication strongly suggests that they are activated in a large proportion of cells. Based on genome-wide studies and our recent genetic study, we suggest that most vertebrate origins consist of a G-quadruplex motif linked to an as yet undefined *cis*-element, and that replicators overlapping a promoter tend to be the most effective (Besnard *et al*, 2012; Cayrou *et al*, 2012; Valton *et al*, 2014). Both the *β^A-globin* and *β-actin* promoters/origins contain several G-quadruplex motifs and locally induce strong SNS enrichment when inserted ectopically, thereby satisfying the criteria for a "canonical strong origin" (Hassan-Zadeh *et al*, 2012 and Appendix Figure S2).

Statistical analyses showed that these origins together with *cis*-elements controlling chromatin structure could act in cooperation when located close together by providing more effective timing information. This result supports the hypothesis that early-replicating domains result from the clustering of origins embedded within an open chromatin structure. Consistent with this hypothesis, genome-wide mapping of replication origins by the SNS method in human and mouse cells has shown the clustering of efficient replication origins within early-replicated domains, forming small initiation zones of several kilobases, mostly located around TSS containing a CpG island (CGI) (Cayrou *et al*, 2015; Picard *et al*, 2014). Our two linked RT shift-inducing constructs are thus reminiscent of the organization of the endogenous structure of early-replicated domains.

Early replicators can advance RT locally in late-replicating domains

We investigated the possible dominance of late-replicating domains over replicators carrying early timing information, by assessing the capacity of the same previously dissected combination of *cis*-elements to function as an independent replicon in genomic regions that are naturally replicated in late S-phase. This construct has the ability to advance significantly the RT at three chromosomal loci (one replicated in mid-late S-phase and two in late S-phase), demonstrating the robustness of the signal embedded in this specific construct. With respect to the replication domain model, these findings suggest that any type of chromosomal environment, including a large constitutive late domain, is permissive for the formation of an

autonomous advanced replicon. However, the observation that the final RT for the modified region was more advanced for the region normally replicated in mid-late S-phase than for that normally replicated in late S-phase suggests that there may be two layers of regulation, at the local and large scales. Both these levels of regulation must be taken into account if we are to understand how large replication domains are constructed. Our data suggest that late-replicating domains are also defined by a lack of signals associated with autonomous early replicons. Consistent with this hypothesis, one mechanism proposed for the regulation of late-replicated regions associated with common fragile sites involves a low density of replication initiation events (Letessier *et al*, 2011). Less abundant but nevertheless efficient origins can also be detected in late-replicating domains by the SNS method. A recent study investigated the role of H4K20me marks in controlling late-firing origins. It showed that the conversion of K20me1 to K20me3 enhances ORCA recruitment and MCM loading at already defined origins required for the correct replication of heterochromatin (Brustel *et al*, 2017). Interestingly, the loss of Suv4-20h, which is responsible for this methylation, delays RT for 15% of the mouse genome. Late origins are, therefore, also defined by a specific chromatin organization facilitating the coordination of late-firing and counteracting the overall repressive effect of heterochromatic regions without providing early-firing signals.

Robust early-replicated domains can be formed by synergy between efficient early replicators separated by several tens of kilobases

We investigated the formation of early-replicating domains further, by inserting two identical strong combinations of early origins into the same chromosome, at sites 30 kb apart. This distance is within the range of average spacing between strong initiation sites or zones detected by the SNS method in early-replicated domains. To our surprise, we found that these two inserted constructs advanced RT to a much greater extent when inserted together than when inserted alone. We found that the presence of the two constructs favored physical contact between these two remote regions. We suspect that this spatial connection is required for the synergic effect on RT, although we have no definitive proof that this is the

case. Interactions between active promoters have been observed by several methods, including the recent production of an ultrahigh-resolution Hi-C map during neural differentiation in mice (Bonev *et al*, 2017; Li *et al*, 2012). Moreover, a recent study proposed that origins of replication tend to cluster even more efficiently than promoters themselves (Jodkowska *et al*, 2019). These results are consistent with our observations, because our construct shown to act synergically contains the constitutive *β-actin* promoter. In *S. cerevisiae* the Fkh1/2 transcription factors have been shown to be directly involved in the early-firing of a large group of origins (Knott *et al*, 2012). It has recently been shown that this function involves direct interaction with Dbf4, the regulatory unit of the essential DDK firing factor (Fang *et al*, 2017). Based on the dimerization capacity of Fkh1/2 and the observation that early-firing origins associated with Fkh1/2 tend to cluster, it was suggested that this clustering might even increase the efficiency of Fkh1/2 for the local recruitment of Dbf4 to early replication factories (Knott *et al*, 2012). Recently, replication initiators containing intrinsically disordered regions (IDRs) have been described in *Drosophila melanogaster* and constitute a new class of phase separating elements that undergo liquid-liquid phase separation (LLPS) upon DNA binding *in vitro*. These elements may drive through IDR-IDR interactions a spatial co-localization of multiple active replication origins within a nuclear zone, which could also favor a better accessibility to firing factors (Parker 2019). We thus suggest that the close proximity of two strong autonomous replicators carrying early timing information here locally increased the efficiency of limiting firing factor recruitment in a similar manner. Most efficient early-firing origins are associated with active promoters containing CGI. This model is, therefore, consistent with genome-wide observations, validating our synthetic approach.

Methods

Plasmid construction

The targeting vectors for homologous recombination in DT40 cells were constructed with the multisite Gateway Pro kit (Thermo Fischer Scientific #12537100), as previously described (Hassan-Zadeh *et al*, 2012). The same entry vectors as before were used for the 5′ and 3′ target arms for specific insertion at site 1 in the mid-late-replicating region (chr1:72,565,520 bp, galGal5) (Hassan-Zadeh *et al*, 2012). New arms

were prepared for specific targeting at sites 2 (chr1: 72,548,589 bp, galGal5) and 3 (chr1: 72,536,060 bp, galGal5) in the mid-late-replicating region, and at sites 1 (Late1 chr1:70,523,649 bp, galGal5) and 2 (Late2 chr1:177,936,192 bp, galGal5) in the late regions. The 5' and 3' target arms for homologous recombination were amplified from DT40 genomic DNA with the primer pairs listed in Appendix Table S3.

We used four entry vectors to generate the new *β^A-globin+β-actin* construct inserted at site 1: two entry vectors containing the 5′ and 3′ target arms for specific insertion at site 1 (Appendix Table S3) and two new entry vectors. The first contained two copies of FIV linked to the *β^A-globin* promoter (2xFIV_ *β^A-globin*). The 2XFIV_ *β^A-globin* entry vector was used as a template for PCR amplification with the following primers: 2XFIV_*β^A-globin*-Up/Low (Appendix Table S3). The second entry vector (2xFIV_*β-actin+BsR*) contained the 2xFIV elements upstream from the *β-actin* promoter linked with the *blasticidin* resistance gene (*BsR*), flanked by *loxP* sites. This construct was made by amplifying the *β-actin* promoter from the pLox*BsR* vector (Arakawa *et al*, 2001) such that *XhoI* and 2xFIV sequences were added upstream from the promoter with the following primers: 2XFIV_*β-actin*-Up/Low (Appendix Table S3). The PCR product was inserted into the previously described *β-actin+BsR* entry vector (Hassan-Zadeh *et al*, 2012), between the *XhoI* site located upstream from the *β-actin* promoter and the *BglII* site at the end of the promoter by ligation with T4 DNA ligase (BioLabs #M0202S), and the 2xFIV_*β-actin+BsR* entry vector was selected after sequence verification. The corresponding final vector was generated by recombining compatible *att* sites between the entry vectors, with LR clonase. For electroporation, the final vector was linearized with *ScaI* (NEB #R3122S).

We used four entry vectors to generate the *β^A-globin+β-actin* construct inserted at site 3. We used two entry vectors containing the 5′ and 3′ target arms for specific insertion at site 3 (Appendix Table S3), the previously described 2XFIV_ *β^A-globin* entry vector and a new entry vector (2xFIV_*β-actin+PuroR*) containing the 2xFIV sequence upstream from the *β-actin* promoter linked with the *puromycin* resistance (*PuroR*) gene, flanked by *loxP* sites. This construct was made by amplifying part of the entry vector from the previously described *β^A-globin+β-actin* vector such that the *attB* sites were flanked by the *XhoI* restriction site and 2xFIV sequences on one side of the recombined region and the *XhoI* sequence on the

other, with the following primer pair: *XhoI*+2xFIV-Up/Low (Appendix Table S3). The *β-actin* promoter associated with the *PuroR* gene cassette was produced by *XhoI* digestion of the pLoxPuro plasmid (Arakawa *et al*, 2001). The final 2xFIV*_β-actin+PuroR* entry vector for insertion at site 3 was generated by *XhoI* digestion of the PCR product and ligation with T4 DNA ligase. The corresponding 2xFIV*_β-actin+PuroR* entry vector was selected after sequence verification. The final vector was generated by recombining compatible *att* sites between the four entry vectors, with LR clonase. For electroporation, the final vector was linearized with *PvuI* (NEB #R3150S).

We used four entry vectors to generate the *GFP* reporter construct inserted at site 2. We used two entry vectors containing the 5′ and 3′ target arms for specific insertion at site 2 (Appendix Table S3), one entry vector previously described and containing a similar *β-actin+BsR* cassette flanked by two *loxP* sites (Hassan-Zadeh *et al*, 2012) and one new entry vector (*β^A-GFP*-h.K7). This entry vector contained the *β^A-globin* promoter sequence amplified from the previously described 2xFIV_ *β^A-globin* entry vector with the following primer pair: β^A-Up/Low, the *GFP* gene sequence amplified from the peGFP plasmid (Clontech #6085-1) with the following primer pair: *GFP*-Up/Low and part of human chromosome 7 (chr7:26,873,165-26,874,805 bp, hg38) amplified from human genomic DNA with the following primer pair: h.K7-Up/Low (Appendix Table S3). The β^A-Up and h.K7-Low primers were associated with the corresponding *attB* sites for Gateway recombination. These three DNA fragments were combined with the In-Fusion HD cloning plus kit (Takara #638909), introduced into the corresponding entry vector with BP clonase (Thermo Fisher Scientific #11789020) and selected after sequence verification. The final vector was generated by recombining compatible *att* sites between the four entry vectors, with LR clonase (Thermo Fisher Scientific #12538120). For electroporation, the final vector was linearized with *Pvu*I (NEB #R3150S).

The *loxP_LE* sequence was inserted into site 1 by the insertion of a larger construct composed of the *loxP_LE*-h.K7+ *β-actin+BsR* elements followed by site-specific Cre recombinase excision. This construct was generated by the association of two entry vectors containing the 5′ and 3′ target arms for specific insertion at site 1, a previously described entry vector containing a similar *β-actin+BsR* selection cassette (Hassan-Zadeh *et al*, 2012) and a new entry vector (*loxP_RE*-h.K7). This entry vector contained part of the

human chromosome 7 sequence amplified from human genomic DNA with the following primer pair containing the upstream *loxP_RE* sequence: *loxP_RE*-h.K7-Up/Low (Appendix Table S3). The *loxP_RE*-h.K7-Up and the *loxP_RE*-h.K7-Low primers were associated with the corresponding *attB* sites. The PCR products were introduced into the corresponding entry vector with BP clonase and selected after sequence verification. The final vector was generated by recombining compatible *att* sites between the four entry vectors, with LR clonase. For electroporation, the final vector was linearized with *PvuII* (NEB #R3151S). We used four entry vectors to generate the new *β^A-globin+β-actin* construct inserted at site late 1 and late 2: two entry vectors containing the 5′ and 3′ target arms for specific insertion at site late 1 or late 2 (Appendix Table S3) and the previously described *β^A-globin* and *β-actin+BsR* entry vectors (Hassan-Zadeh *et al*, 2012). We used three entry vectors to generate the *β-actin* construct inserted at site 1 and 3: the previously described *β-actin+BsR* or *β-actin+PuroR* entry vector (Hassan-Zadeh *et al*, 2012), one entry vector containing the 3′ target arm for specific insertion at site 1 or 3 and a new entry vector containing the 5′ target arm for specific insertion at site 1 or 3 flanked by att sequences necessary for Gateway recombination using three entry vectors (Appendix Table S3).

Cell culture and transfection

DT40 cells were grown in RPMI 1640 Glutamax (Thermo Fisher Scientific #61870010) containing 10% FBS, 1% chicken serum, 0.1 mM β-mercaptoethanol, 200 U/mL penicillin, 200 µg/mL streptomycin and 1.75 µg/mL amphotericin B, at 37°C, under an atmosphere containing 5% CO_2. We transfected DT40 cells as previously described (Hassan-Zadeh *et al*, 2012). Cell clones were selected on media containing a final concentration of 20 µg/ml blasticidin or 1 µg/ml puromycin, depending on the resistance gene carried by the transgene. Genomic DNA was extracted from cells in lysis buffer (10 mM Tris pH8.0; 25 mM NaCl; 1 mM EDTA and 200 µg/mL proteinase K). Clones into which the plasmid DNA was integrated were screened by PCR with primer pairs designed to bind on one side of the insertion site such that one primer bound within the construct and the other primer bound just upstream or downstream from the arm used for recombination, as previously described (Hassan-Zadeh *et al*, 2012)(Appendix Figure S7 and Appendix

Table S4). The insertion of constructs into the same chromosome or the other chromosome was determined by long-range PCR (Appendix Figure S8). For each clone tested, genomic DNA was extracted with the DNeasy Blood & Tissue kit (Qiagen #69504). We designed primer pairs amplifying in the part of the genome between constructs to control for DNA extraction quality (Ctrl), and primer pairs amplifying the two tested constructs to test the insertions (Appendix Table S4). The LR 1+2 primer pair was used to amplify the h.K7 part of the *GFP* reporter construct inserted at site 2 and the *IL2R* gene within the *β^A-globin+β-actin* construct inserted at site 1. The LR 2+3 primer pair was used to amplify the *PuroR* gene within the *β^A-globin+β-actin* construct inserted at site 3 and the *GFP* gene within the *GFP* reporter construct inserted at site 2. The LR 1+3 primer pair was used to amplify the *PuroR* gene within the *β^A-globin+β-actin* construct inserted at site 3 and the *IL2R* gene within the *β^A-globin+β-actin* construct inserted at site 1, regardless of the presence or absence of the central construct. The LR *loxP_LE*(1)+ *β^A-globin+β-actin* (3) primer pair was used to amplify the *PuroR* gene within the *β^A-globin+β-actin* construct inserted at site 3 and the *loxP_LE* element inserted at site 1, regardless of the presence or absence of the central construct. PCR was performed with the Long PCR Enzyme Mix (Thermo Fisher Scientific #K0181) under following conditions: initial denaturation at 94°C for 3 minutes, followed by 10 cycles of 95°C for 20 s, 68°C for 14 minutes, followed by 20 cycles of 95°C for 20 s, 68°C for 18 minutes and a final extension phase of 10 minutes at 68°C. Quantitative PCR (qPCR) was carried out for each clone, on 4 ng of genomic DNA, with a primer binding to the transgene (With on the *GFP* reporter construct, With on *β^A-globin+β-actin* construct, With on *β-actin* and *loxP_LE* on the loxP site inserted at site 1), and a primer binding close to insertion site 1 and amplifying both alleles (Both or insertion site 1 + 5 kb), to confirm that only one copy of the transgene had been inserted (Appendix Table S2 and S3).

Cre-loxP excision

In this study, we used the DT40 Cre1 subclone, which constitutively expresses a tightly regulated Cre recombinase fused to a mutated estrogen receptor (Mer) (Arakawa *et al*, 2001). This inactive Mer-Cre-Mer fusion protein can be transiently activated in the presence of 4-hydroxytamoxifen, resulting in the efficient

excision of genomic regions flanked by two recombination signals (*loxP* sites) inserted in the same direction. We also used a modified inducible Cre recombination system involving two different mutant loxP sites (*loxP_RE* and *loxP_LE*). After Cre recombination, these two mutants are converted into a new nonfunctional loxP site (*loxP_RE+LE*) that is not recognized by the Cre recombinase, thereby preventing additional recombination events (Arakawa *et al*, 2001). For the excision of the genomic DNA flanked by loxP sites, we treated 3 x 10^5 cells with 5 μM 4-hydroxytamoxifen (Sigma Aldrich #T176) for two days. Subclones were obtained by plating dilutions of the treated cell suspension at a density of 50, 150, and 1500 viable cells per 10 ml in 96-well flat-bottomed microtiter plates. Genomic DNA was extracted from single subclones and analyzed by PCR with specific primer pairs (Appendix Table S4). We assessed the excision of the *β-actin +BsR* selection cassette in clones with the *GFP* reporter construct inserted at site 2, with a primer pair amplifying the polyA sequence of the both *BsR* and *GFP* genes and the downstream part of the 3' arm of insertion site 2 (Appendix Figure S7, primer pair #3-4, BsR excision site 2, Appendix Table S4). We assessed the excision of the *β-actin+PuroR* selection cassette in clones with the β^A*-globin+β-actin* construct inserted at site 3 and already containing the β^A*-globin* construct at site 1 (Hassan-Zadeh *et al*, 2012), with a primer pair amplifying the polyA sequence of the both *IL2R* and *PuroR* genes and the downstream part of the 3' arm of insertion site 3 (Appendix Figure S7, primer pair #5-6, *PuroR* excision at site 3, Appendix Table S4). All clones were cultured for 72 h in selective media containing the appropriate antibiotic, to confirm PCR results.

For the large 1+3 excision kinetic, 3 x 10^6 cells were treated with 5 μM 4-hydroxytamoxifen for 1, 8, 24, 48 h before genomic DNA extraction with the DNeasy Blood & Tissue kit (Qiagen #69504). The large 1+3 excision was quantified by semiquantitative PCR with the large excision primer pair and the Ctrl primer pair used for normalization (Figure 5, Appendix Figure S6 and Appendix Table S4). Calibration was based on a standard curve generated with various amounts of genomic DNA (16 ng to 160 ng) obtained from a previously isolated clone in which the large recombination had occurred. For each set of excision kinetic conditions, 64 ng or 160 ng of genomic DNA was tested (for amplification with the Ctrl or the large excision primer pair, respectively). PCR was performed with the Herculase II fusion DNA polymerase (Agilent

Technologies #600675) under the following conditions: initial denaturation at 98°C for 4 minutes, followed by 25 cycles of 98°C for 30 s, 57°C for 45 s, 72°C for 2 minutes, and a final extension phase for 3 minutes at 72°C. After migration of the PCR products on a 0.8% agarose gel and SYBR Safe staining, the mean intensity of each signal was quantified with Image J, corrected with the local background mean intensity and normalized with the mean intensity of the signal obtained in the control amplification.

RT analysis

The RT experiments presented in Figure 8, Figures EV1, EV2, EV3 and EV5 were performed as previously described (Hassan-Zadeh *et al*, 2012). Briefly, about 10^7 exponentially growing cells were pulse-labeled with 5-Bromo-2'-deoxyuridine (BrdU, Sigma-Aldrich #B9285) for 1 h and sorted into four S-phase fractions, from early to late S phase. The collected cells were treated with lysis buffer (50 mM Tris pH 8.0; 10 mM EDTA pH 8.0; 300 mM NaCl; 0.5% SDS, 0.2 mg/ml of freshly added proteinase and 0.5 mg/ml of freshly added RNase A), incubated at 65°C for 2 h and stored at -20°C, in the dark. Genomic DNA was isolated from each sample by phenol-chloroform extraction and alcohol precipitation and sonicated four times for 30s each, at 30s intervals, in the high mode at 4°C in a Bioruptor water bath sonicator (Diagenode), to obtain fragments of 500 to 1000 bp in size. The sonicated DNA was denatured by incubation at 95°C for 5 minutes. We added monoclonal anti-BrdU antibody (BD Biosciences #347580) at a final concentration of 3.6 µg/ml in 1x IP buffer (10 mM Tris pH 8.0, 1 mM EDTA pH 8.0, 150 mM NaCl, 0.5% Triton X-100, and 7 mM NaOH). We used 30 µl or 50 µl of protein-G-coated magnetic beads (from Ademtech #4342 or Thermo Fisher Scientific #10004D, respectively) per sample to pull down the anti-BrdU antibody. Beads and BrdU-labeled nascent DNA were incubated for 2-3 hours at 4°C, on a rotating wheel. The beads were then washed once with 1x IP buffer, twice with wash buffer (20 mM M Tris pH 8.0, 2 mM EDTA pH 8.0, 250 mM NaCl, 0.25% Triton X-100) and then twice with 1x TE buffer pH 8.0. The DNA was eluted by incubating the beads at 37°C for 2 h in 250 µl 1x TE buffer pH 8.0, to which we added 1% SDS and 0.5 mg/ml proteinase K. DNA was purified by phenol-chloroform extraction and alcohol precipitation and resuspended in 50 µl TE.

For Repli-seq analyses, immunoprecipitated NS from the four S-phase fractions collected by flow cytometry or from an asynchronous cell population were amplified by whole-genome amplification (GenomePlex Complete Whole Genome Amplification kit #WGA2; Sigma) according to the manufacturer's recommendations to obtain sufficient DNA amount. After amplification, libraries were constructed with the NEBNext Ultra II DNA Library Prep Kit for Illumina (NEB #E7645S) following the manufacturer's instructions with minor modifications. For the adaptor ligation, undiluted adaptor and no size selection were used. The library amplification was performed using NEB-Next Multiplex Oligos for Illumina (NEB #E7710S) with nine different NEB-Next index primer and the NEB-Next Universal PCR Primer (NEB #E6861A) with three PCR cycles. Library purification was performed with the SPRI-select Reagent kit (Beckman coulter #B23317), and the final elution step was reduced to 33µl of 0.1×TE. The mean size of the library molecules determined on an Agilent Bio-analyser High Sensitivity DNA chip (Agilent technologies, #5067–4626) was 330-350 bp. Sequencing was performed on a NextSeq 500 Illumina sequencer with a High Output 150 cycles flow cell (paired-end reads of 75 bp) according to standard procedures. For each sample, 15-20 M of reads were generated. All Illumina sequencing runs were performed at the GENOM'IC facility of the Cochin Institute.

Repli-Seq data processing

Paired-end sequencing data were mapped on the galGal5 chicken genome using bowtie2 (Langmead & Salzberg, 2012). For each timing fraction, replication timing was computed using 50kb sliding windows at 10kb intervals, normalized by the global and local genomic coverage of the asynchonous cell population, to normalize for total and local coverage variations. Then the centered and standardized timing profiles were smoothed using cubic splines (smooth.spline function of R). In order to provide a single RT profile combining all fractions, we used the method proposed by (Du *et al*, 2019), by computing the weighted average WA = (0.917*G1) + (0.750*S1) + (0.583*S2) + (0.417*S3) + (0.250*S4) + (0*G2). An increase in WA indicates an earlier timing.

Flow cytometry analysis

After BrdU incorporation, DT40 cells were washed twice with PBS, fixed in 75% ethanol and stored at -20°C. On the day of sorting, fixed cells were resuspended at a final concentration of 2.5 x 10^6 cells/mL in 0.1% IGEPAL in PBS (Sigma, #CA-630), 50 µg/ml propidium iodide and 0.5 mg/ml RNase A, and incubated for 30 minutes at room temperature. Cells were sorted with an INFLUX 500 cell sorter (Cytopeia, BD Biosciences). Four fractions of S-phase cells (S1-S4), each containing 5x10^4 cells, were collected and further treated for locus-specific RT analyses. Two fractions of S-phase cells (S1-S2), each containing 10^5 cells were collected and further treated for genome-wide RT analyses.

MNAse digestions

We cross-linked 30x10^6 exponentially growing cells by incubation for 5 min with 1% (v/v) freshly prepared formaldehyde (Thermo Fisher Scientific, #28908) at room temperature. Fixation was stopped by adding glycine to a final concentration of 0.125 M and incubating for five minutes at room temperature, with stirring. Cells were then washed three times in cold PBS and their nuclei were extracted in 3 mL of lysis buffer (10 mM Tris-HCl pH 7.5, 10 mM NaCl, 3 mM $MgCl_2$, 0.2% Triton X-100, 0.5 mM EGTA pH 8.0, 1 mM DTT, 1x protease inhibitor cocktail (Sigma, #P8340)) for 5 minutes at 4°C, centrifuged and resuspended in digestion buffer (10 mM Tris-HCl pH 7.5, 10 mM NaCl, 3 mM $MgCl_2$, 1 mM $CaCl_2$, 1x protease inhibitor cocktail (Sigma, #P8340)). Micrococcal Nuclease (MNase; Thermo Fisher Scientific, #EN0181) digestions were performed for 15 minutes at 37°C, using either a final concentration of 10 U/mL for ChIp analyses or a series of four exponentially increasing concentrations of MNase (2.5, 10, 40 and 160 U/mL) for chromatin accessibility analyses. The reaction was stopped by adding 0.1 volumes of stop buffer (200 mM EDTA pH 8.0, 40 mM EGTA pH 8.0). For ChIp analyses, MNase digestion conditions were established so as to produce mostly mono- to hexa-nucleosome fragments of 150 bp to 1000 bp. Chromatin was then diluted by a factor of two in 2x complement buffer (40 mM Tris-HCl pH 8.0, 300 mM NaCl, 2% Triton X-100) and sonicated 20 times for 30s each, at 30s intervals in the high mode at 4°C in a Bioruptor water bath sonicator (Diagenode). For chromatin accessibility analyses, the lowest MNAse concentration

generated a mixture of oligo-, di- and mono-nucleosomes, whereas the highest concentration produced mostly mono-nucleosomes (Appendix Figure S5A). After digestion, DNA molecules were extracted in phenol-chloroform and precipitated with ethanol and were then subjected to a size selection process with the SPRI-select Reagent kit (Beckman coulter #B23317) using a 0.5X ratio to remove DNA molecules of more than 1000 bp in length (Appendix Figure S5B). The MNAse titration approach can be used to determine whether nucleosome release requires low or high levels of MNAse. Low levels of MNAse release large numbers of nucleosomes in accessible regions, leading to higher levels of DNA molecules. Nucleosomes embedded in less accessible regions are less likely to be released with such low levels of MNAse. Moreover, this approach provides additional information about the accessibility of loci. Indeed, highly inaccessible or condensed regions are not sensitive to higher concentrations of MNAse, whereas the chromatin of accessible regions is rapidly digested under the same conditions.

Chromatin immunoprecipitation

Immunoprecipitation was performed overnight at 4°C, in a final volume of 200 µl of 1x IP buffer (20 mM Tris-HCl pH 8.0, 2 mM EDTA pH 8.0, 150 mM NaCl, 1% Triton-X100 and 0.1% SDS) on an amount of chromatin corresponding to 10 µg of DNA, with anti-trimethylated K4H3 (AbCam, #ab8580), anti-dimethylated K4H3 (Millipore, #07-030) or anti-acetylated K9K27H3 (Millipore, #06-599) antibodies, according to the manufacturer's recommendations. Immunocomplexes were pulled down with 50 µl of protein-G-coated magnetic beads (Thermo Fisher Scientific, Dynabeads Protein G, #10004D) per sample. Beads and immunocomplexes were incubated for two hours at 4°C, on a rotating wheel. The beads were then washed once with 1x IP buffer, twice with wash B buffer (20 mM M Tris pH 8.0, 2 mM EDTA pH 8.0, 250 mM NaCl, 0.25% Triton X-100) and then twice with 1x TE buffer pH 8.0. For the anti-trimethylated K4H3 antibody, the wash buffer contained 500 mM NaCl, and an additional washing step was performed with buffer C (10 mM Tris-HCl pH 8.0, 1 mM EDTA pH 8.0, 1% sodium deoxycholate, 1% NP40, 250 mM LiCl). The DNA was eluted by incubating the beads for 2 h at 37°C with 250 µl 1x TE buffer pH 8.0, to which we added 1% SDS and 0.5 mg/ml proteinase K. Cross-linking was reversed by overnight incubation

at 65°C and samples were further treated with 10 µg of RNase A for 15 minutes at 37°C, and with 20 µg of proteinase K for 1 h at 56°C. DNA was purified by phenol-chloroform extraction, precipitated in alcohol and resuspended in 100 µl TE.

RNA extraction and reverse transcription

Total RNA were extracted from $5x10^6$ cells with the Nucleospin RNA kit (Macherey Nagel, #740955). The integrity of the extracted RNA was assessed with an Agilent 2100 bioanalyzer (Agilent RNA 6000 Nano Kit, #5067-1511) and 20 µg of total RNA was then treated with 4 units of DNAse I (NEB, #M0303S) for 1 h at 37°C. The enzyme was inactivated by adding 5 mM EDTA and incubating the reaction mixture for 10 min at 75°C. The RNA was then purified by phenol-chloroform extraction and ethanol precipitation. Reverse transcription reactions (RT-QPCR+) were then performed with 5 µg of RNA and random hexamers (NEB, S1330S), using the Superscript III Reverse Transcriptase (Thermo Fisher Scientific, #18080093) according to the manufacturer's instructions. Negative controls (RT-QPCR-) were performed with the same procedure, but without the addition of reverse transcriptase. The comparison of RT-QPCR+ and RT-QPCR- samples was used to validate DNAseI treatment and the complete digestion of the genomic DNA in the RNA samples.

Real-time PCR quantification of DNA

The Roche Light Cycler 2.0 detection system and the Absolute Q-PCR SYBR green capillary mix (Thermo Fisher Scientific, #AB1285B) were used for the real-time PCR quantification of BrdU-labeled nascent strands (NS) or genomic DNA extracted from 4-hydroxytamoxifen-treated clonal cell lines. For all reactions, real-time PCR was performed under the following cycling conditions: initial denaturation at 95°C for 15 minutes, followed by 50 cycles of 95°C for 15 s, 60°C for 30 s, 72°C for 20 s, and fluorescence measurement. Following PCR, a thermal melting profile was used for amplicon identification.

The Roche Light Cycler 480 detection system and the Light Cycler 480 SYBR Green I Master mix (Roche Applied Science, # 04707516001) were used for the real-time PCR quantification of ChIp DNA, MNAse-

digested DNA and cDNA. For all reactions, real-time PCR was performed under the following cycling conditions: initial denaturation at 95°C for 5 minutes, followed by 50 cycles of 95°C for 10 s, 61°C for 20 s, 72°C for 20 s and fluorescence measurement. Following PCR, a thermal melting profile was used for amplicon identification.

For both quantification methods, standard curves were generated from four-fold dilutions of the corresponding genomic DNA. Serial dilutions of plasmids containing the loci of interest were used as standards for cDNA quantification. Each reaction was performed at least in duplicate. The second-derivative maximum method was used to quantify sequences, as described in the Light Cycler Software.

For BrdU-labeled NS quantification, we used primer pairs binding to mitochondrial DNA to normalize enrichment in each S-phase fraction (Mitochondrial DNA), an early-replicated region (Early timing control) for the control of cell sorting, a genomic position located 5 kb downstream from insertion site 2 (Both), amplifying both alleles, for the control of accurate qPCR measurements and the studied regions in the transgenes. Specific primer pairs amplifying in the transgene (With) or the site of insertion in the wt allele (Without) were used (Appendix Table S4). In the case of clones with one or two autonomous replicons associated with the GFP reporter construct inserted on the other chromosome, we used a primer pair amplifying the GFP reporter construct to quantify the wt chromosome (Without on GFP reporter at site 2, Appendix Table S4) and a primer pair amplifying insertion site 2 to quantify the modified shifting chromosome (With at insertion site 2, Appendix Table S4).

Based on both the one-hour BrdU pulse labeling used and the mean rate of fork progression, estimated at 1.5 kb/min in DT40 cells (Maya-Mendoza *et al*, 2007), the resolution of our RT experiments cannot exceed a 90 kb window. Thus, for the analysis of RT within our 30 kb genomic region targeted with one, two or three constructs, we systematically used the With and Without primer pairs in central position 2. For the quantitative analyses, we analyzed independent clones. In Figure 1, N=10 for (i) from Hassan-Zadeh *et al*, 2012 and Valton et al., 2014, N=8 for (ii) from Hassan-Zadeh *et al*, 2012, Valton et al. 2014 and , N= 7 for (iii) from Hassan-Zadeh *et al*, 2012 and this article Figure EV1A and N=8 for (iv) from Hassan-Zadeh *et al*, 2012 and this article, Figure EV1B. In Figure 3, N=8 for (i) the same clones as (iv) in Figure 1, N=5 for

(ii) from Figure EV3A and B, N=3 for (iii) from this article Figure EV2 D and E. For statistical analysis, the outliers values detected with the R outliers package were excluded from the analysis (clone 4 in Figure EV1A).

For ChIp DNA and MNAse-digested DNA quantifications, we used primer pairs amplifying the wt allele at insertion sites 1, 2 and 3 (Wt allele insertion site 1, 2 or 3), the condensed region of the endogenous *β-globin* locus, as a control for the heterochromatin state (cond 1 and 2), the *BU1A* promoter (*BU1A* pro) or the *MED14* promoter (*MED14* pro), as a control for the active chromatin state, at a genomic position located 5 kb downstream from insertion site 1 (1 +5 kb), amplifying both alleles and the inserted transgenes, at the positions studied (Figure 6, Figure EV4 and Appendix Table S4).

For the quantification of MNAse-digested DNA, data are presented as total chromatin input relative to condensed genomic regions (cond1 and cond2). For each clonal cell line, the mean values obtained for the two condensed genomic regions for each digestion were arbitrarily set to 1 and used to normalize independent clones for each transgenic line separately and between all transgenic lines.

For ChIp DNA quantifications, data are presented as Ip/Input signal relative to the signal for the *BU1A* promoter (*BU1A* pro) used for normalization between transgenic lines.

For cDNA quantification, we used primer pairs amplifying the second exon of the *BU1A* gene as a control for transcribed genes, the junction of exons 3-4 of the *MED14* gene and the inserted transgenes, at the studied positions (Figure EV4 and Appendix Table S4).

Hi-C methods

Hi-C was performed as described previously (Belaghzal et al., 2017) with some minor modifications. Briefly, 10 million formaldehyde cross-linked cells (1% formaldehyde for the wild types and 2% formaldehyde for the clones) were lysed and digested overnight at 37°C with 400 units of *DpnII* (NEB). Next, the DNA ends were marked with biotin-14-dATP (Thermo Fisher Scientific #19524016) for 4 hours at 23°C and ligated for 4 hours at 16°C. To remove proteins and reverse crosslink, DNA was treated with proteinase K overnight at 65°C. DNA was then purified using phenol:chloroform and biotin was removed

from unligated ends. Ligation products were fragmented by sonication to an average size of 200bp and size selected with Ampure XP beads (Beckman Coulter, # A63880) to fragments ranging from 100 to 350 bp. End repair was performed on the DNA fragments to obtain blunt ends and biotinylated ligation products were purified using streptavidin beads (Thermo Fisher Scientific #65001). dA-tailing was then performed and the TrueSeq DNA LT kits Set A (Illumina, #15041757) was used for adapter ligation and PCR amplification. PCR primers were removed using Ampure XP beads. The libraries were sequenced using 50 bp paired end reads on Illumina HiSeq4000.

Hi-C data processing

Hi-C libraries were processed using the distiller pipeline (https://github.com/mirnylab/distiller-nf). Briefly, reads were mapped to the chicken reference assembly galGal5 using bwa mem to map fastq pairs in a single-side fashion (-SP). The specific sequences of each inserted construct (allele 1+3 and allele 2) were pooled together and placed in the original galGal5 fasta file as two additional chromosomes to be able to map and balance them in the following procedure. Alignments were parsed and pairs were classified using the pairtools package (https://github.com/mirnylab/pairtools) to generate pairs files. Uniquely mapped pairs were kept and duplicated pairs arising from PCR were removed. Pairs with high mapping quality scores on both sides (MAPQ > 30) were kept and aggregated into contact matrices in the cooler format using the cooler package (Abdennur & Mirny, 2020). Data was binned and stored into multiresolution cooler files (1kb, 2kb, 5kb, 10kb, 25kb, 50kb, 100kb, 250kb, 500kb, 1Mb). All contact matrices were normalized using the iterative correction normalization (Imakaev et al, 2012) after ignoring the first 2 diagonals to avoid short-range ligation artifacts at a given resolution. Low-coverage bins were excluded using the MADmax (maximum allowed median absolute deviation) filter on genomic coverage, described in (Schwarzer et al, 2017), using the default parameters. WT replicate 1 has 82,394,530 mapped reads with 37% cis interactions, WT replicate 2 has 139,022,250 mapped reads with 29% cis interactions, clone 4 has 541 023 662 mapped reads with 79.3% cis interactions, clone 5 has 542 918 613 mapped reads with 78.5% cis interactions (Appendix Table S5).

Additional filtering of Hi-C interactions

For all of the quantification analyses it is important to ignore the following regions: 1) large translocation on the p-arm of chr1 chr1:9,000,000-9,500,000 (Appendix Figure S9 A,B) 2) smaller translocation on the p-arm of chr1 chr1:32,270,000-32,770,000 (Appendix Figure S9 A,B) 3) beta-A globin promoter region that is included in the allele 1+3 and allele 2 inserts chr1:194,569,000-194,572,000 (Appendix Figure S9 C)) beta-actin promoter region that is included in the allele 1+3 insert chr14:4,194,000-4,197,000. Regions 3) and 4) were removed because we cannot properly assign the interactions that involved β^{A}*globin* or β-actin promoters to inserts or the endogenous loci.

A/B compartments

A and B compartments were assigned using an eigenvector decomposition procedure (Imakaev et al, 2012) implemented in the cooltools package (https://github.com/mirnylab/cooltools, http://doi.org/10.5281/zenodo.3553140). Eigenvector decomposition was performed on observed-over-expected cis contact matrices binned at 250 kb on each library and at 100kb on the pooled libraries for a better resolution of compartments. The first eigenvectors (EV1) positively correlated with gene density were used to assign A and B compartment status to each bin. EV1 calculated at 100kb was used for all quantitative analyses that involved compartment status, if not stated otherwise.

Hi-C Allele specific analysis

In order to quantify preferential interactions of allele 1+3 and allele 2 with A and B compartments we performed the following:

(1) We corrected for distance decay as the alleles were mapped as independent chromosomes (see above) but the insertion site is located on chr1. Thus, we divided the frequency of interactions of alleles 1+3 / 2

with chromosome 1 by the expected value for each bin based on genomic distance from the insertion site. (2) We calculated the average interaction of allele 1+3 / 2 with compartment A and B on chr1 p and q-arms, where compartment status A was assigned if eigenvector 1 value > 0 and compartment status B if eigenvector 1 value < 0. (3) To test the significance of observed interaction preference, we randomly shuffled the A and B compartment status 1,000 times and calculated the difference between average interactions of a given allele with compartment A and compartment B 'difference allele 1+3 / 2 A – B' for every iteration. We then calculated the p-value for the observed value of 'difference allele 1+3 / 2 A – B'.

In order to test if allele 1+3 and allele 2 demonstrate any preferential interactions with other chromosomes, i.e. trans-interactions, we performed the following:

(1) Due to the sparsity and lack of distance decay for trans-data, we averaged interactions on the scale of individual chromosomes and normalized them by corresponding chromosome lengths; we refer to this measure as density of interactions. (2) We compared the density of interactions between allele 1+3 and allele 2 with chromosomes larger than 5,000,000 bp (Figure 3E and Appendix Figure S4 C,F and Appendix Figure S9D).

Code is available on github: https://github.com/dekkerlab/allelic-rt-supplement.git

Data availability

The datasets produced in this study have been deposited in the GEO database (https://www.ncbi.nlm.nih.gov/geo/) with the accession number GSE153566.

Acknowledgments

The authors thank the members of the laboratory of M-N.P for useful insights and discussions. We thank G.Felsenfeld and R.Veitia for critical reading of the manuscript. We thank J-F Bercher for his help in defining the most accurate quantitative method for measuring RT shifts. We thank Griselda Wentzinger and Magali Fradet for performing cell sorting at ImagoSeine Institut Jacques Monod platform. Sequencing of

replication timing data was performed by the GENOM'IC core facility at Institut Cochin-Paris. We thank Ankita Nand for doing the initial mapping of the Hi-C data. This work was supported by grants from the Association pour la Recherche sur le Cancer (Equipe Labellisée) and the Agence Nationale pour la Recherche (ANR-15-CE12-0004-01), and from the National Human Genome Research Institute (HG003143 to JD). M-N.P and B.D are supported by Inserm. JD is an investigator of the Howard Hughes Medical Institute.

Author Contributions

CB, BD and M-NP planned and supervised the project. FP performed bioinformatic analysis of the repli-seq data, ALV, SV and JD conceived the Hi-C experiments, ALV conducted the Hi-C experiments. ALV and SV performed bioinformatic analysis of the Hi-C data. For all other experiments CB and M-NP designed the methodology, CB, SC, AC, ML, CG conducted the experiments, CB, BD and MN-P analyzed and validate the data, CB provided visualization of the data. CB and M-NP wrote the manuscript with input from FP, ALV and SV.

Conflict of Interests

The authors declare no conflict of interests.

References

Abdennur N & Mirny LA (2020) Cooler: scalable storage for Hi-C data and other genomically labeled arrays. *Bioinformatics* **36:** 311–316

Arakawa H, Lodygin D & Buerstedde JM (2001) Mutant loxP vectors for selectable marker recycle and conditional knock-outs. *BMC Biotechnol.* **1:** 7

Besnard E, Babled A, Lapasset L, Milhavet O, Parrinello H, Dantec C, Marin J-M & Lemaitre J-M (2012) Unraveling cell type-specific and reprogrammable human replication origin signatures associated with G-quadruplex consensus motifs. *Nat. Struct. Mol. Biol.* **19:** 837–844

Bonev B, Mendelson Cohen N, Szabo Q, Fritsch L, Papadopoulos GL, Lubling Y, Xu X, Lv X, Hugnot J-P, Tanay A & Cavalli G (2017) Multiscale 3D Genome Rewiring during Mouse Neural Development. *Cell* **171:** 557-572.e24

Brustel J, Kirstein N, Izard F, Grimaud C, Prorok P, Cayrou C, Schotta G, Abdelsamie AF, Déjardin J, Méchali M, Baldacci G, Sardet C, Cadoret J-C, Schepers A & Julien E (2017) Histone H4K20 tri-methylation at late-firing origins ensures timely heterochromatin replication. *EMBO J.* **36:** 2726–2741

Burgess SM & Kleckner N (1999) Collisions between yeast chromosomal loci in vivo are governed by three layers of organization. *Genes Dev.* **13:** 1871–1883

Cayrou C, Ballester B, Peiffer I, Fenouil R, Coulombe P, Andrau J-C, van Helden J & Méchali M (2015) The chromatin environment shapes DNA replication origin organization and defines origin classes. *Genome Res.* **25:** 1873–1885

Cayrou C, Coulombe P, Puy A, Rialle S, Kaplan N, Segal E & Méchali M (2012) New insights into replication origin characteristics in metazoans. *Cell Cycle* **11:** 658–667

Cornacchia D, Dileep V, Quivy J-P, Foti R, Tili F, Santarella-Mellwig R, Antony C, Almouzni G, Gilbert DM & Buonomo SBC (2012) Mouse Rif1 is a key regulator of the replication-timing programme in mammalian cells. *EMBO J.* **31:** 3678–3690

Douglas ME & Diffley JFX (2012) Replication timing: the early bird catches the worm. *Curr. Biol.* **22:** R81-82

Du Q, Bert SA, Armstrong NJ, Caldon CE, Song JZ, Nair SS, Gould CM, Luu P-L, Peters T, Khoury A, Qu W, Zotenko E, Stirzaker C & Clark SJ (2019) Replication timing and epigenome remodelling are associated with the nature of chromosomal rearrangements in cancer. *Nat Commun* **10:** 1–15

Duriez B, Chilaka S, Bercher J-F, Hercul E & Prioleau M-N (2019) Replication dynamics of individual loci in single living cells reveal changes in the degree of replication stochasticity through S phase. *Nucleic Acids Res.* **47:** 5155–5169

Fang D, Lengronne A, Shi D, Forey R, Skrzypczak M, Ginalski K, Yan C, Wang X, Cao Q, Pasero P & Lou H (2017) Dbf4 recruitment by forkhead transcription factors defines an upstream rate-limiting step in determining origin firing timing. *Genes Dev.* **31:** 2405–2415

Foti R, Gnan S, Cornacchia D, Dileep V, Bulut-Karslioglu A, Diehl S, Buness A, Klein FA, Huber W, Johnstone E, Loos R, Bertone P, Gilbert DM, Manke T, Jenuwein T & Buonomo SCB (2016) Nuclear Architecture Organized by Rif1 Underpins the Replication-Timing Program. *Molecular Cell* **61:** 260–273

Hassan-Zadeh V, Chilaka S, Cadoret J-C, Ma MK-W, Boggetto N, West AG & Prioleau M-N (2012) USF binding sequences from the HS4 insulator element impose early replication timing on a vertebrate replicator. *PLoS Biol.* **10:** e1001277

Hildebrandt ER & Cozzarelli NR (1995) Comparison of recombination in vitro and in E. coli cells: measure of the effective concentration of DNA in vivo. *Cell* **81:** 331–340

Hiraga S-I, Alvino GM, Chang F, Lian H-Y, Sridhar A, Kubota T, Brewer BJ, Weinreich M, Raghuraman MK & Donaldson AD (2014) Rif1 controls DNA replication by directing Protein Phosphatase 1 to reverse Cdc7-mediated phosphorylation of the MCM complex. *Genes Dev.* **28:** 372–383

Imakaev M, Fudenberg G, McCord RP, Naumova N, Goloborodko A, Lajoie BR, Dekker J & Mirny LA (2012) Iterative correction of Hi-C data reveals hallmarks of chromosome organization. *Nat. Methods* **9:** 999–1003

Jodkowska K, Pancaldi V, Almeida R, Rigau M, Graña-Castro O, Fernández-Justel JM, Rodríguez-Acebes S, Rubio-Camarillo M, Pau ECS, Pisano D, Al-Shahrour F, Valencia A, Gómez M & Méndez J (2019) Three-dimensional connectivity and chromatin environment mediate the activation efficiency of mammalian DNA replication origins. *bioRxiv***:** 644971

Knott SRV, Peace JM, Ostrow AZ, Gan Y, Rex AE, Viggiani CJ, Tavaré S & Aparicio OM (2012) Forkhead transcription factors establish origin timing and long-range clustering in S. cerevisiae. *Cell* **148:** 99–111

Langmead B & Salzberg SL (2012) Fast gapped-read alignment with Bowtie 2. *Nat Methods* **9:** 357–359

Letessier A, Millot GA, Koundrioukoff S, Lachagès A-M, Vogt N, Hansen RS, Malfoy B, Brison O & Debatisse M (2011) Cell-type-specific replication initiation programs set fragility of the FRA3B fragile site. *Nature* **470:** 120–123

Li G, Ruan X, Auerbach RK, Sandhu KS, Zheng M, Wang P, Poh HM, Goh Y, Lim J, Zhang J, Sim HS, Peh SQ, Mulawadi FH, Ong CT, Orlov YL, Hong S, Zhang Z, Landt S, Raha D, Euskirchen G, et al (2012) Extensive promoter-centered chromatin interactions provide a topological basis for transcription regulation. *Cell* **148:** 84–98

Lieberman-Aiden E, van Berkum NL, Williams L, Imakaev M, Ragoczy T, Telling A, Amit I, Lajoie BR, Sabo PJ, Dorschner MO, Sandstrom R, Bernstein B, Bender MA, Groudine M, Gnirke A, Stamatoyannopoulos J, Mirny LA, Lander ES & Dekker J (2009) Comprehensive mapping of long-range interactions reveals folding principles of the human genome. *Science* **326:** 289–293

Litt MD, Simpson M, Recillas-Targa F, Prioleau MN & Felsenfeld G (2001) Transitions in histone acetylation reveal boundaries of three separately regulated neighboring loci. *EMBO J.* **20:** 2224–2235

Massip F, Laurent M, Brossas C, Fernández-Justel JM, Gómez M, Prioleau M-N, Duret L & Picard F (2019) Evolution of replication origins in vertebrate genomes: rapid turnover despite selective constraints. *Nucleic Acids Res.* **47:** 5114–5125

Maya-Mendoza A, Petermann E, Gillespie DAF, Caldecott KW & Jackson DA (2007) Chk1 regulates the density of active replication origins during the vertebrate S phase. *EMBO J.* **26:** 2719–2731

Picard F, Cadoret J-C, Audit B, Arneodo A, Alberti A, Battail C, Duret L & Prioleau M-N (2014) The Spatiotemporal Program of DNA Replication Is Associated with Specific Combinations of Chromatin Marks in Human Cells. *PLoS Genet* **10:** e1004282

Prioleau M-N & MacAlpine DM (2016) DNA replication origins-where do we begin? *Genes Dev.* **30:** 1683–1697

Prioleau MN, Nony P, Simpson M & Felsenfeld G (1999) An insulator element and condensed chromatin region separate the chicken beta-globin locus from an independently regulated erythroid-specific folate receptor gene. *EMBO J.* **18:** 4035–4048

Ryba T, Hiratani I, Lu J, Itoh M, Kulik M, Zhang J, Schulz TC, Robins AJ, Dalton S & Gilbert DM (2010a) Evolutionarily conserved replication timing profiles predict long-range chromatin interactions and distinguish closely related cell types. *Genome Res.* **20:** 761–770

Ryba T, Hiratani I, Lu J, Itoh M, Kulik M, Zhang J, Schulz TC, Robins AJ, Dalton S & Gilbert DM (2010b) Evolutionarily conserved replication timing profiles predict long-range chromatin interactions and distinguish closely related cell types. *Genome Res.* **20:** 761–770

Schwarzer W, Abdennur N, Goloborodko A, Pekowska A, Fudenberg G, Loe-Mie Y, Fonseca NA, Huber W, Haering CH, Mirny L & Spitz F (2017) Two independent modes of chromatin organization revealed by cohesin removal. *Nature* **551:** 51–56

Sima J, Chakraborty A, Dileep V, Michalski M, Klein KN, Holcomb NP, Turner JL, Paulsen MT, Rivera-Mulia JC, Trevilla-Garcia C, Bartlett DA, Zhao PA, Washburn BK, Nora EP, Kraft K, Mundlos S, Bruneau BG, Ljungman M, Fraser P, Ay F, et al (2019) Identifying cis Elements for Spatiotemporal Control of Mammalian DNA Replication. *Cell* **176:** 816-830.e18

Therizols P, Illingworth RS, Courilleau C, Boyle S, Wood AJ & Bickmore WA (2014) Chromatin decondensation is sufficient to alter nuclear organization in embryonic stem cells. *Science* **346:** 1238–1242

Valton A-L, Hassan-Zadeh V, Lema I, Boggetto N, Alberti P, Saintomé C, Riou J-F & Prioleau M-N (2014) G4 motifs affect origin positioning and efficiency in two vertebrate replicators. *EMBO J.*

West AG, Huang S, Gaszner M, Litt MD & Felsenfeld G (2004) Recruitment of histone modifications by USF proteins at a vertebrate barrier element. *Mol. Cell* **16:** 453–463

Yamazaki S, Ishii A, Kanoh Y, Oda M, Nishito Y & Masai H (2012) Rif1 regulates the replication timing domains on the human genome. *EMBO J.* **31:** 3667–3677

Figure Legends

Figure 1. Quantitative analysis of RT shifts reveals cooperation between two combinations of *cis*-regulatory elements.

Distribution of RT shifts calculated with the -ΔL+ΔE method described in Appendix Figure S1. Different transgenes in a mid-late-replicating region are compared: the *IL2R* reporter gene under the control of the β^A-*globin* promoter (β^Apro*)* containing an inactive (i, N=10) or an active origin (ii, N=8) flanked by two copies of FIV(2xFIV), the *blasticidin* resistance gene (*BsR*) under the control of the *β-actin* promoter (*β-act* pro) (iii, N=7) or a combination of these two transgenes (iv, N=8). Data information: Blue and black triangles represent reactive *loxP* sites and recombined inactive *loxP* sites respectively. Rectangle edges correspond

to the 0.25 and 0.75 quartiles, the thick black lines represent the median, the white triangles represent the mean and the whiskers extend to the smallest and largest -ΔL+ΔE values. Statistical analysis was performed with Wilcoxon nonparametric two-tailed tests (ns, not significant; $**p<0.01$; $***p<0.001$).

Figure 2. One autonomous replicon inserted in the mid-late region perturbs the RT over a 250 kb region through cooperation with an endogenous strong origin

A. UCSC genome browser visualization of the mid-late insertion site of chromosome 1 (genomic positions: chr1:71,000,000-74,100,000 bp, 3.1 Mb; galGal5). RT weighted average (WA) values for the wt and the *β^A-globin+β-actin* cell lines are shown. Early-replicated regions (E) are represented in orange and late replicating regions (L) in blue. Annotated genes (Ref Seq genes) are represented below. The mid-late insertion site is indicated with a red arrow and dotted line.

B. UCSC genome browser visualization of the mid-late insertion site of chromosome 1 (genomic positions: chr1:72,450,000-72,650,000 bp; 200 kb; galGal5). Tracks of nascent strands (NS) enrichments in the four S phase fractions were represented separately (S1 to S4) for the wt and the 2x(*β^A-globin+β-actin*) cell lines. NS enriched and depleted regions for each fraction are represented in purple and blue respectively. Single reads form SNS aligned and track of replication origins (Ori peaks) determined in (Massip *et al*, 2019) are reported in between. The three mid-late insertion sites 1, 2 and 3 are indicated with red arrows. Annotated genes and CpG Islands are shown below. Initiation zones (IZ) and termination zones (TZ) are reported.

Figure 3. Two advanced replicons separated by 30 kb cooperate to form a synthetic early-replicated region that is more associated with A compartments

A. Distribution of -ΔL+ΔE values for clonal cell lines containing one advanced replicon (*β^A-globin+β-actin*) inserted at site 1 (i, N=8) or 3 (iii, N=3) or at both sites on the same chromosome with one *GFP* reporter construct composed of the *GFP* reporter gene under the control of the *β^A-globin* promoter/origin linked to a 1.6 kb fragment of human chromosome 7 (h.K7) inserted at site 2, either on the same chromosome as 1 and 3 (1+2+3), or on the other chromosome (1+3) (ii, N=5). Data information: Blue and black triangles represent

reactive *loxP* sites and recombined inactive *loxP* sites respectively. Black vertical bars represent insertion sites. Rectangle edges correspond to the 0.25 and 0.75 quartiles, the thick black lines represent the median, the white triangles represent the mean and the whiskers extend to the smallest and largest -ΔL+ΔE values. Statistical analysis was performed with Wilcoxon nonparametric two-tailed tests (**p<0.01).

B. Schematic representation of alleles 1+3 and 2. Data information: Blue and black triangles represent reactive *loxP* sites and recombined inactive *loxP* sites respectively. Black vertical bars represent insertion sites.

C. Interaction profiles of allele 1+3/2 with chr1 for combined Hi-C libraries: distance-corrected interactions, *i.e.* observed/expected (OE), binned at 500 kb with corresponding compartment (EV1) tracks. Red arrows represent the loci that show preferred interactions with allele 1+3 and that coincide with A compartment.

D. OE interactions of allele 1+3 (orange rectangles) and allele 2 (blue rectangles) averaged over A and B compartments for p and q-arms at 100kb bin size. A random compartment status permutation test was made and then we calculated the one-sided p-value for the observed value of 'difference allele 1+3 / 2 A – B'. Values corresponding to OE interactions of allele 1+3 and allele 2 averaged over shuffled A (red circles, N=1000) and B compartments (blue circles, N=1000) for p and q-arms. ns, not significant; **p<0.01;***p<0.001.

E. Scatterplot of density of interactions between allele 1+3 and allele 2 with chromosomes larger than 5,000,000 bp.

Figure 4. The constitutive *β-actin* promoter/origin is necessary for the formation of the early-replicating domain

A. Distribution of -ΔL+ΔE values for clonal cell lines containing one *β-actin* construct at site 1 (i, N=7) or at site 1 and 3 (ii, N=5), on the same chromosome.

B. Distribution of -ΔL+ΔE values for clonal cell lines containing one β^A-*globin* construct at site 1 (i, N=8) or at site 1 and 3 (ii, N=6), on the same chromosome.

Data information: (A,B) Data information: Blue and black triangles represent reactive *loxP* sites and recombined inactive *loxP* sites respectively. Black vertical bars represent insertion sites.

Rectangle edges correspond to the 0.25 and 0.75 quartiles, the thick black lines represent the median, the white triangles represent the mean and the whiskers extend to the smallest and largest -ΔL+ΔE values. Statistical analysis was performed with Wilcoxon nonparametric two-tailed tests (**p<0.01).

Figure 5. The formation of the early-replicating domain is associated with the establishment of local interactions between the two advanced replicons separated by 30 kb

A. Clones 1+2+3, 1+3 and *β-actin* (1+3) described in Figure 3, together with control clones containing one β^A-*globin*+*β-actin* construct at site 3 and one *loxP_LE* sequence inserted at site 1 on the same chromosome with the *GFP* reporter construct inserted at site 2 on the other chromosome *loxP_LE* (1)+ β^A-*globin*+*β-actin* (3) were tested for their capacity to recombine after induction of the Cre recombinase. Yellow and green triangles represent reactive *loxP_RE* and *loxP_LE* sites, respectively, and black triangles represent recombined inactive *loxP* sites. Black vertical bars represent insertion sites.

B. Recombination between the upstream *loxP_RE* element (yellow triangle) inserted at site 3 and the downstream *loxP_LE* element (green triangle) inserted at site 1 leads to a large 1+3 and *loxP_LE* (1) + β^A-*globin*+*β-actin* (3) or *β-actin* (1+3) excision product.

C. After 1, 8, 24 and 48 h of 4-hydroxytamoxifen treatment, genomic DNA was extracted and quantified by semi-quantitative PCR (see Appendix Figure S6). Error bars correspond to the standard deviation for PCR duplicates. The percentages of cells with the large 1+3 and *loxP_LE* (1) + β^A-*globin*+*β-actin* (3) or *β-actin* (1+3) excision at each time point are shown for different cell lines.

Figure 6. The close proximity of the two advanced replicons is not associated with an increase in chromatin accessibility.

A, B. Clones 1+2+3, 1+3 (A) and *loxP_LE* (1) + *β^A-globin+β-actin* (3) (B) were used to assess chromatin accessibility within the transgenes. The positions of the amplicons used for quantification in each shifting construct individually (thick black lines; 5' 2xFIV-1 or -3, *β-actin* pro-1 or -3, *BsR* gene, *PuroR* gene, *LoxP* site), in both shifting constructs (*β^A* pro 1 and 2, *IL2R* gene, 3' 2xFIV1-3) or in the *GFP* reporter construct (*β^A-GFP*, *GFP* gene, h.K7) are shown. The insertion sites on the wt chromosome (insertion sites 1, 2 and 3) and a genomic region located 5 kb downstream from the insertion site (insertion site +5kb) were used as controls for the targeted genomic region. The endogenous active *MED14* promoter was analyzed as a control. Data information: (A, B) Blue and black triangles represent reactive *loxP* sites and recombined inactive *loxP* sites respectively. Black vertical bars represent insertion sites.

Quantifications by real-time qPCR of total chromatin (input) extracted from two 1+2+3, 1+3 and *loxP_LE* (1)+ *β^A-globin+β-actin* (3) clonal cell lines, after digestion with micrococcal nuclease (MNAse, 2.5 U, 10 U, 40 U, 160 U/mL) and size selection were shown. Error bars indicate the standard deviation for qPCR triplicates, for two independent clones. Data are presented as total chromatin input relative to the condensed genomic regions (cond1 and cond2) used for the normalization.

Figure 7. Genome wide overview of genomic features at the targeted insertion sites in DT40.

A, B. UCSC genome browser visualization of two parts of chromosome 1 containing the insertion sites (genomic positions: chr1:69,000,000-74,200,000; 5.2 Mb (A) and chr1: 175,300,000-180,500,000; 5.2 Mb (B); galGal5). RT weighted average (WA) values obtained after cells sorting into four S-phase fractions, BrdU pulse-labeled nascent strands (NS) immunoprecipitation and sequencing are shown. Early-replicated regions are represented in orange and late-replicating regions in blue. Below, track of eigenvector 1 values corresponding to A/B compartments at 100 kb resolution after Hi-C analysis in wt cells, track of replication origins determined in (Massip *et al*, 2019) (Ori peaks) and annotated genes are reported. The three sites chosen for insertion are indicated with red arrows and dotted lines (mid-late, late 1 (A) and late 2 (B) insertion).

At the bottom, an enlargement of late insertion sites (chr1: 69,500,000-71,500,000 (A), chr1: 177,000,000-179,000,000 (B); galGal5), displaying genes, mRNAs and ESTs for the chicken and all other species together with track of replication origins determined in (Massip *et al*, 2019) (Ori peaks) is shown. Tracks of RefSeq genes are represented in blue, tracks of Ensembl genes in red, tracks of AUGUSTUS ab initio gene predictions and TransMap alignements in green and tracks of mRNAs and ESTs in black. Insertion sites are indicated with red dotted lines and black dotted lines determine the borders of the enlarged regions.

Figure 8. Two late-replicating environments are permissive to a shift toward earlier replication after the site-specific insertion of a large autonomous replicon.

A, B. RT profiles of chromosomal alleles following the targeted integration of a β^A-*globin*+*β-actin* construct into two late-replicating loci, 1 (A) and 2 (B) in two or three clonal cell lines respectively. Nascent strands (NS) were quantified by real-time qPCR in four S phase fractions. Specific primer pairs determine the RT profile for the modified allele (With), the wt allele (Without) and both alleles (Both). The endogenous *β-globin* locus was analyzed as an early-replicated control. The modified (Mod) and wild-type (wt) alleles are shown. Difference -ΔL+ΔE values calculated at the target site following transgene integration are indicated (see Appendix Figure S1). Error bars correspond to the standard deviation for qPCR duplicates. The black vertical bars represent the precise insertion position.

Figure EV1. Additional RT assays for transgenes shifting the timing of replication.

A, B. RT profiles of each chromosomal allele are determined after targeted transgene integration using the allele-specific analysis of RT method by real-time PCR quantification described in Appendix Figure S1. Differences in -ΔL+ΔE values calculated at the target site following transgene integration are indicated. Data information: (A, B) Blue triangles represent reactive *loxP* sites. Error bars correspond to the standard deviation for qPCR duplicates. Analysis of six *β-actin* clonal cell lines (A) or two β^A-*globin*+*β-actin* clonal cell lines (B) described in Figure 1 is reported. Black vertical bars represent insertion sites.

Figure EV2. One advanced replicon inserted at site 1 or at site 3 directs a shift to earlier replication independently of the presence of a *GFP* reporter construct inserted at site 2.

RT profiles of each chromosomal allele are determined after targeted transgene integration using the allele-specific analysis of RT method by real-time PCR quantification described in Appendix Figure S1. Differences in -ΔL+ΔE values calculated at the target site following transgene integration are indicated.

A. Analysis of one clonal cell line containing one *GFP* reporter construct composed of the *GFP* reporter gene under the control of the *β^A-globin* promoter (*β^A* pro*)* and linked to a 1.6 kb fragment of human chromosome 7 (h.K7) inserted at site 2.

B, C. Analysis of clonal cell lines containing one *β^A-globin+β-actin* construct described in Figure 1 inserted at site 1 and one *GFP* reporter construct inserted at site 2 on the same chromosome (B) or on the other chromosome (C).

D, E. Analysis of clonal cell lines containing one *β^A-globin+β-actin* construct inserted at site 3 and one *GFP* reporter construct inserted at site 2 on the same chromosome (D) or on the other chromosome (E).

Data information: Blue and black triangles represent reactive *loxP* sites and recombined inactive *loxP* sites respectively. Black vertical bars represent insertion sites. Error bars correspond to the standard deviation for qPCR duplicates.

Figure EV3. Two *β^A-globin+β-actin* constructs as well as two *β-actin* constructs inserted at sites 1 and 3 form an early-replicated domain.

A-C. RT profiles of each chromosomal allele are determined after targeted transgene integration using the allele-specific analysis of RT method by real-time PCR quantification described in Appendix Figure S1. Differences in -ΔL+ΔE values calculated at the target site following transgene integration are indicated. Error bars correspond to the standard deviation for qPCR duplicates. (A, B) Analysis of two 1+2+3 (A) and three 1+3 (B) clonal cell lines described in Figure 3A. (C) Analysis of five clonal cell lines containing two *β-actin* constructs inserted at sites 1 and 3 on the same chromosome described in Figure 3B. Data information: Blue and black triangles represent reactive *loxP* sites and recombined inactive *loxP* sites

respectively. Black vertical bars represent insertion sites. Error bars correspond to the standard deviation for qPCR duplicates.

Figure EV4. The open chromatin structure of the whole advanced replicon is imposed by the active *β-actin* promoter.

A. Relative quantification, by real-time qPCR, of mRNA expression levels (RT-QPCR+) or background levels (RT-QPCR-), was performed in the *β^A-globin* and *β^A-globin+β-actin* clonal cell lines. For relative quantification, mRNA levels were normalized against *BU1A* mRNA levels arbitrarily set at 100 (first table). Crossing point (Cp) values for RT-QPCR+ and RT-QPCR- experiments are reported in the second table. NA corresponds to non-amplified samples, NS to non-specific signals and LD to the limit of detection.

B-D. The *β^A-globin* (B), *β-actin* (C) and *β^A-globin+β-actin* (D) transgenes are shown on the left, with the positions of the amplicons used for quantification (thick black lines with names indicated above). The endogenous active *MED14* promoter, two genomic regions located within the condensed region upstream from the *β-globin* locus (cond1 and cond2) were analyzed as controls. Quantification, by real-time qPCR, of total chromatin (input) extracted from the *β^A-globin* (B), *β-actin* (C) and *β^A-globin+β-actin* (D) clonal cell lines after digestion with increasing concentrations of micrococcal nuclease (MNAse, 2.5U, 10U, 40U, 160U/mL). Error bars indicate the standard deviation for qPCR triplicates made on two independent clones.

E. Immunoprecipitations of H3K9K27 acetylation (ac), H3K4 trimethylation (me3) or H3K4 dimethylation (me2) on formaldehyde-crosslinked chromatin extracted from the *β^A-globin* (green) and *β^A-globin+β-actin* (purple) clonal cell lines. The endogenous active *BU1A* promoter (*BU1A pro*) was analyzed as a control. Data are presented as enrichments of immunoprecipitated material relative to input DNA and normalized against *BU1A* enrichment. Error bars indicate the standard deviation for at least qPCR duplicates made on two independent clones.

Figure EV5: Two *β^A-globin* constructs inserted at sites 1 and 3 are not sufficient to form an early-replicated domain.

RT profiles of each chromosomal allele are determined after targeted transgene integration using the allele-specific analysis of RT method by real-time PCR quantification described in Appendix Figure S1. Differences in -ΔL+ΔE values calculated at the target site following transgene integration are indicated. Error bars correspond to the standard deviation for qPCR duplicates. Analysis of six *β^A-globin* (1+3) clonal cell lines described in Figure 4B.

Figure 1

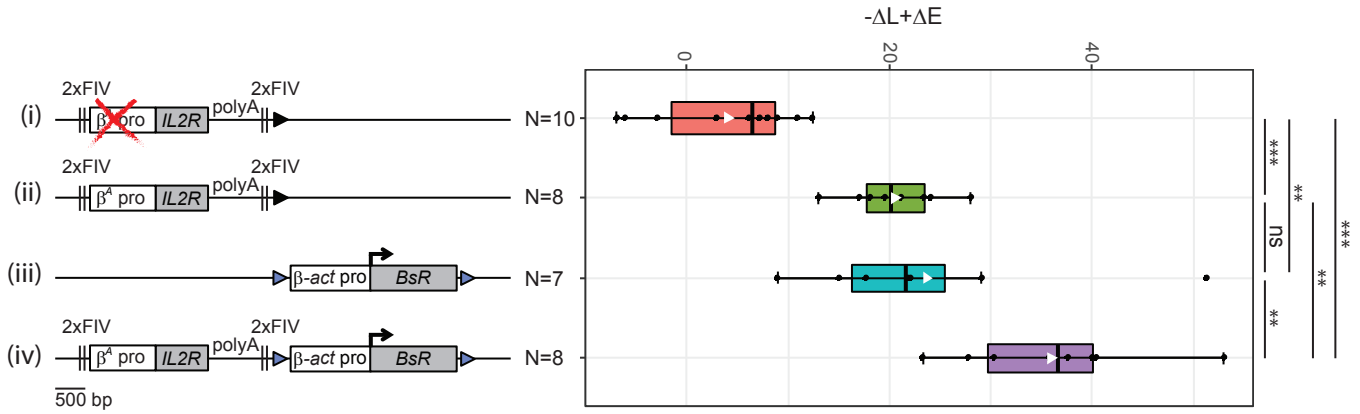
-ΔL+ΔE
0
20
40
(i)
(ii)
(iii)
(iv)
2xFIV
polyA
IL2R
BsR
β-act pro
N=10
N=8
N=7
N=8
***
**
ns
**
**
***
500 bp

Figure 2

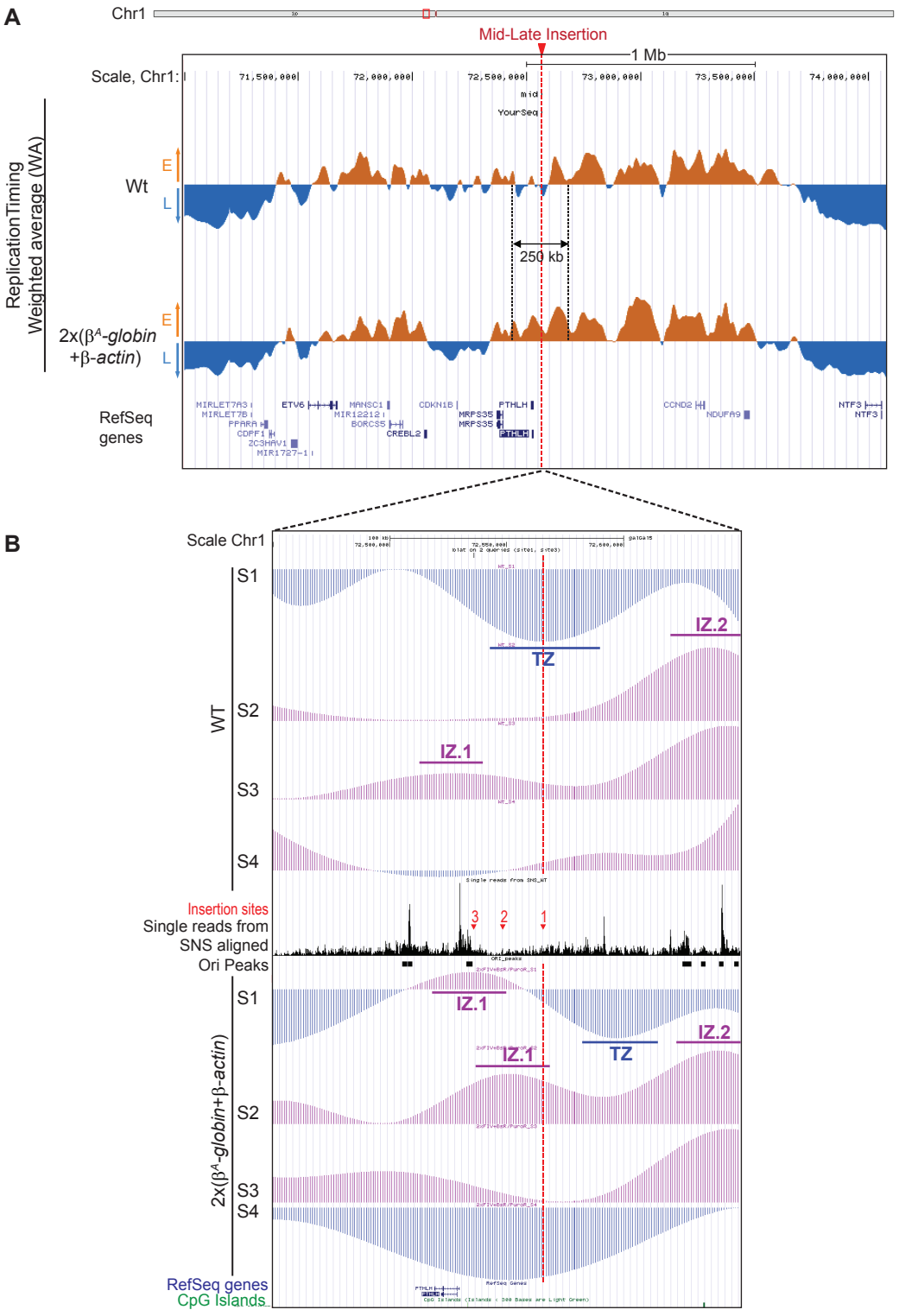
A
Chr1
Mid-Late Insertion
1 Mb
Scale, Chr1:
71,500,000
72,000,000
72,500,000
73,000,000
73,500,000
74,000,000
mid
YourSeq
ReplicationTiming
Weighted average (WA)
E
Wt
L
250 kb
E
2x(βA-globin
+β-actin)
L
RefSeq
genes
MIRLET7A3
MIRLET7B
PPARA
CDPF1
ZC3HAV1
MIR1727-1
ETV6
MANSC1
MIR12212
BORCS5
CREBL2
CDKN1B
PTHLH
MRPS35
MRPS35
PTHLH
CCND2
NDUFA9
NTF3
NTF3
B
Scale Chr1
WT
S1
S2
S3
S4
IZ.2
TZ
IZ.1
Insertion sites
Single reads from
SNS aligned
Ori Peaks
3
2
1
2x(βA-globin+β-actin)
S1
S2
S3
S4
IZ.1
IZ.2
TZ
IZ.1
RefSeq genes
CpG Islands

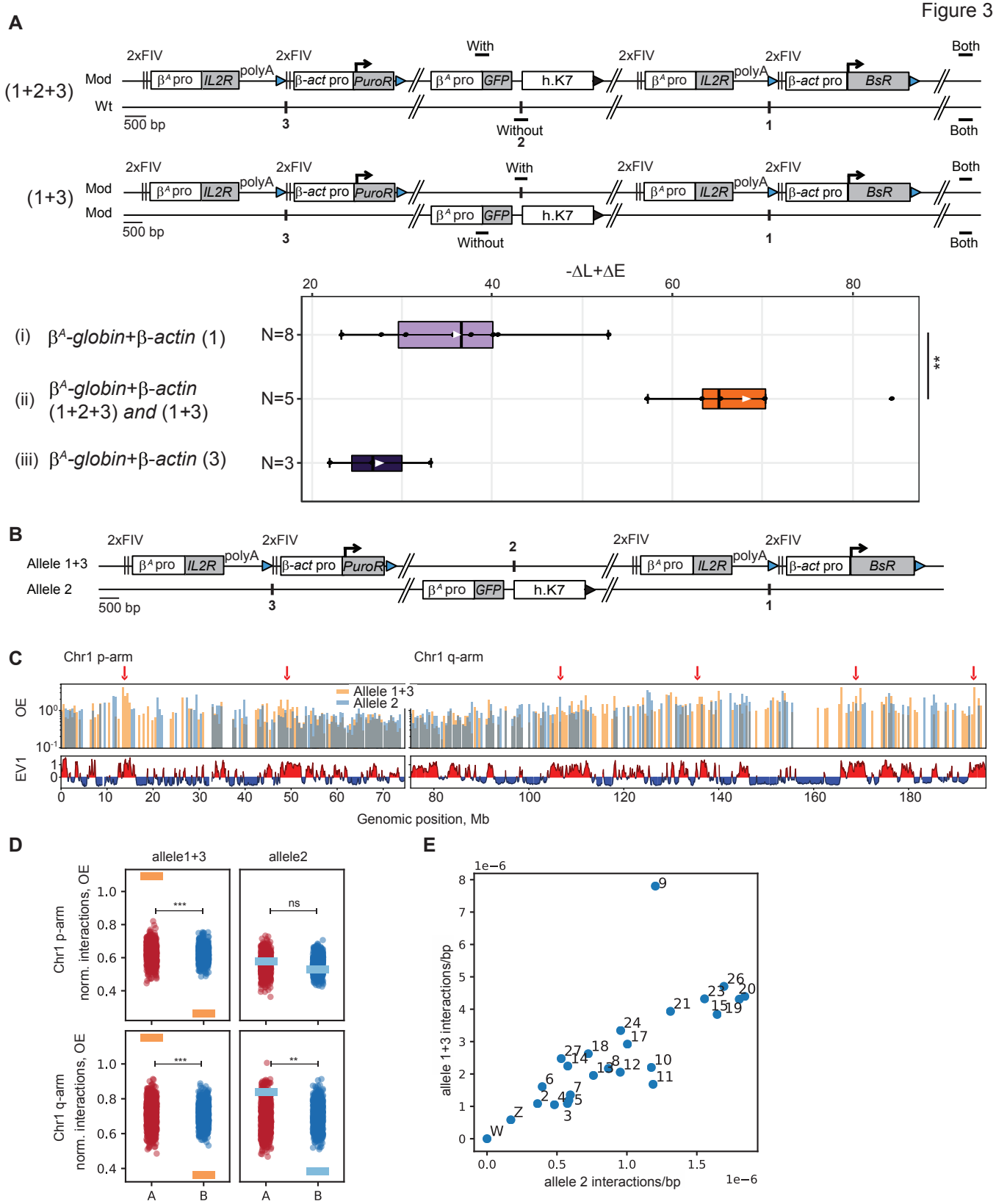
A
(1+2+3)
(1+3)
Mod
Wt
2xFIV
polyA
With
Without
Both
500 bp
(i) βA-globin+β-actin (1)
(ii) βA-globin+β-actin (1+2+3) and (1+3)
(iii) βA-globin+β-actin (3)
-ΔL+ΔE
N=8
N=5
N=3
**
B
Allele 1+3
Allele 2
C
Chr1 p-arm
Chr1 q-arm
OE
EV1
Genomic position, Mb
D
allele1+3
allele2
Chr1 p-arm
Chr1 q-arm
norm. interactions, OE
ns
E
allele 1+3 interactions/bp
allele 2 interactions/bp
1e−6

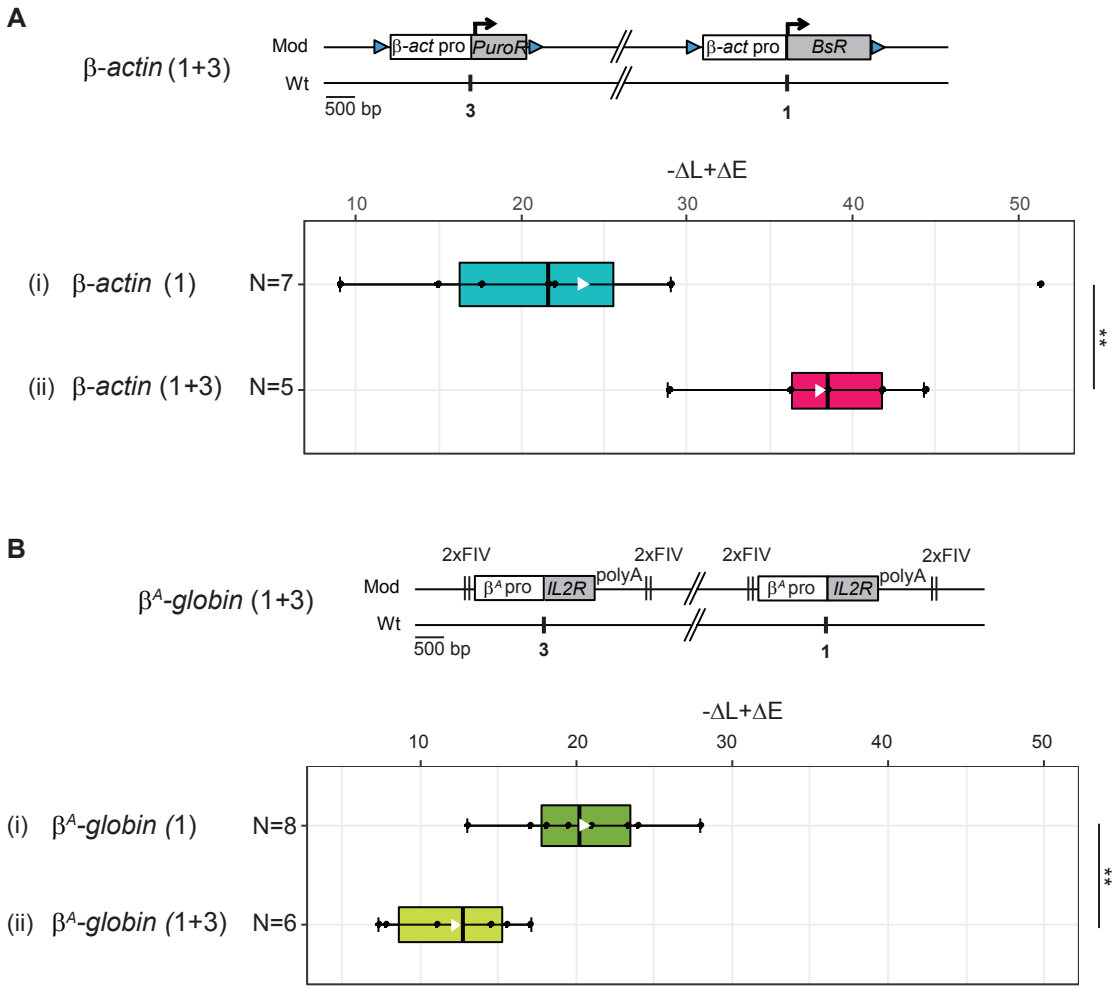
A
β-actin (1+3)
Mod
β-act pro
PuroR
β-act pro
BsR
Wt
500 bp
3
1
-ΔL+ΔE
10
20
30
40
50
(i) β-actin (1)
N=7
(ii) β-actin (1+3)
N=5
**
B
βA-globin (1+3)
2xFIV
2xFIV
2xFIV
2xFIV
Mod
βA pro
IL2R
polyA
βA pro
IL2R
polyA
Wt
500 bp
3
1
-ΔL+ΔE
10
20
30
40
50
(i) βA-globin (1)
N=8
(ii) βA-globin (1+3)
N=6
**

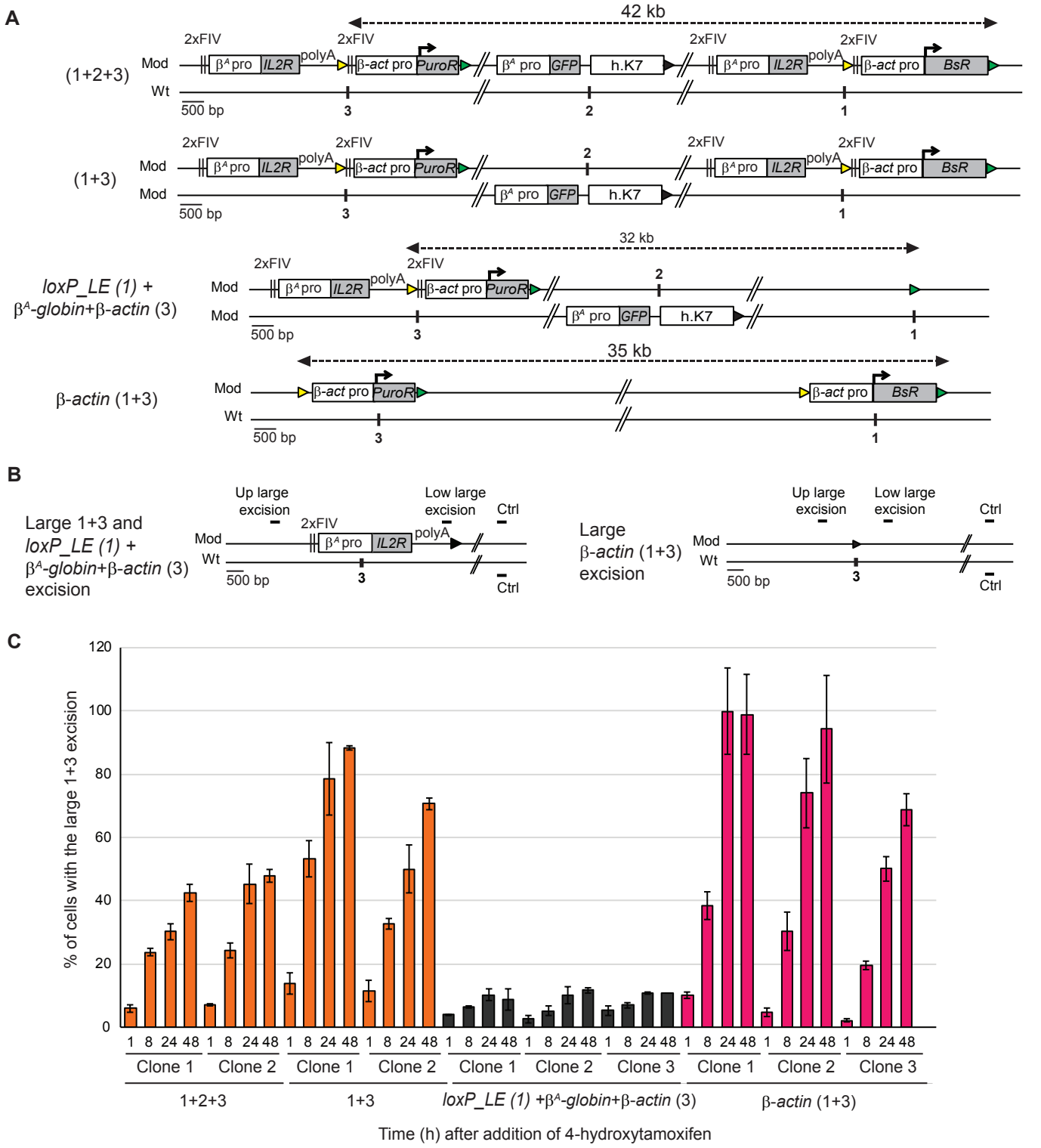
A
42 kb
(1+2+3)
Mod
Wt
2xFIV
βA pro
IL2R
polyA
β-act pro
PuroR
GFP
h.K7
BsR
500 bp
3
2
1
(1+3)
32 kb
loxP_LE (1) +
βA-globin+β-actin (3)
35 kb
β-actin (1+3)
B
Large 1+3 and
loxP_LE (1) +
βA-globin+β-actin (3)
excision
Up large
excision
Low large
excision
Ctrl
Large
β-actin (1+3)
excision
C
% of cells with the large 1+3 excision
0
20
40
60
80
100
120
1 8 24 48
Clone 1
Clone 2
Clone 3
1+2+3
1+3
loxP_LE (1) +βA-globin+β-actin (3)
β-actin (1+3)
Time (h) after addition of 4-hydroxytamoxifen

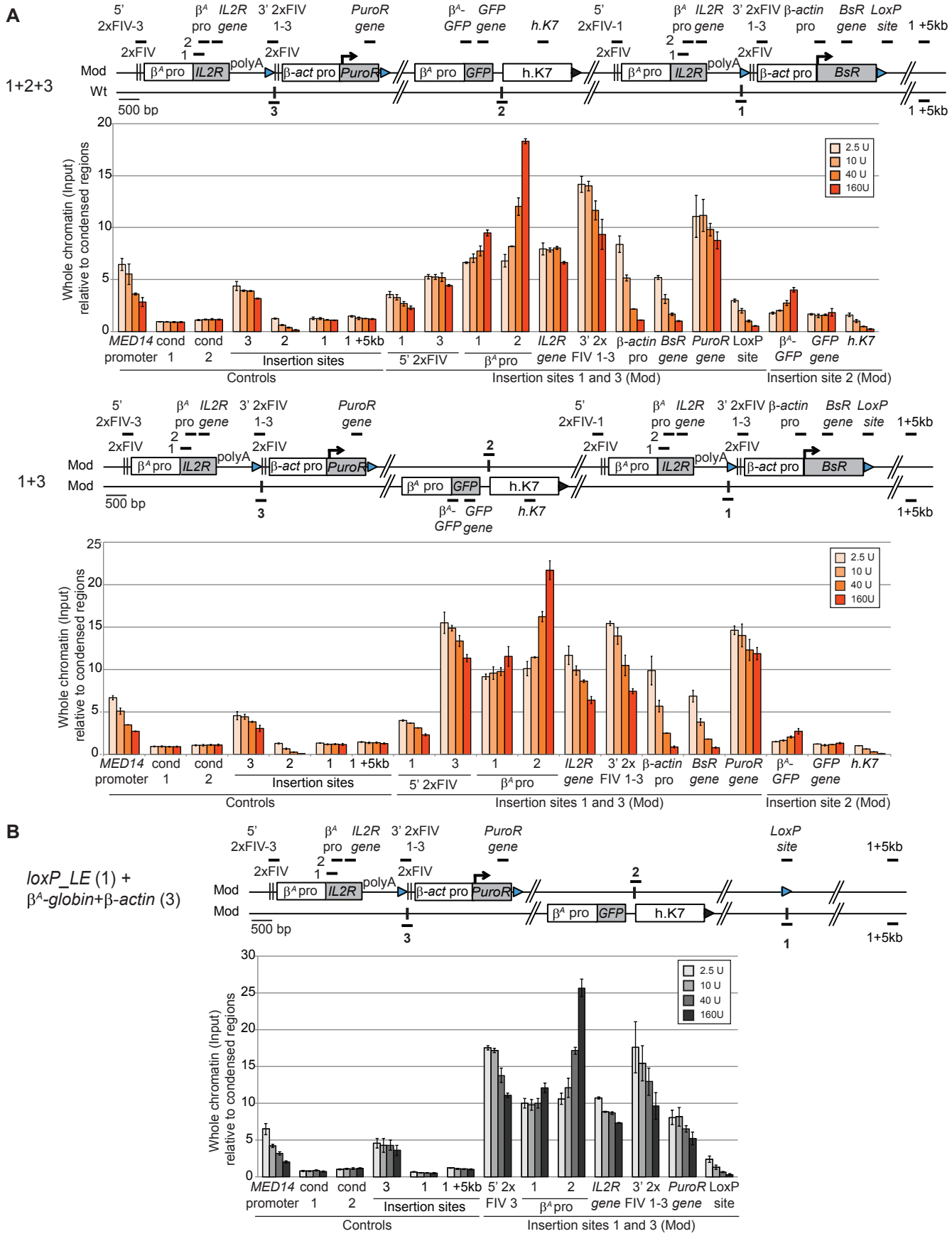
A
1+2+3
Mod
Wt
500 bp
polyA
Whole chromatin (Input) relative to condensed regions
2.5 U
10 U
40 U
160U
MED14 promoter
cond 1
cond 2
Insertion sites
Controls
5' 2xFIV
Insertion sites 1 and 3 (Mod)
Insertion site 2 (Mod)
1+3
B
loxP_LE (1) +
βA-globin+β-actin (3)

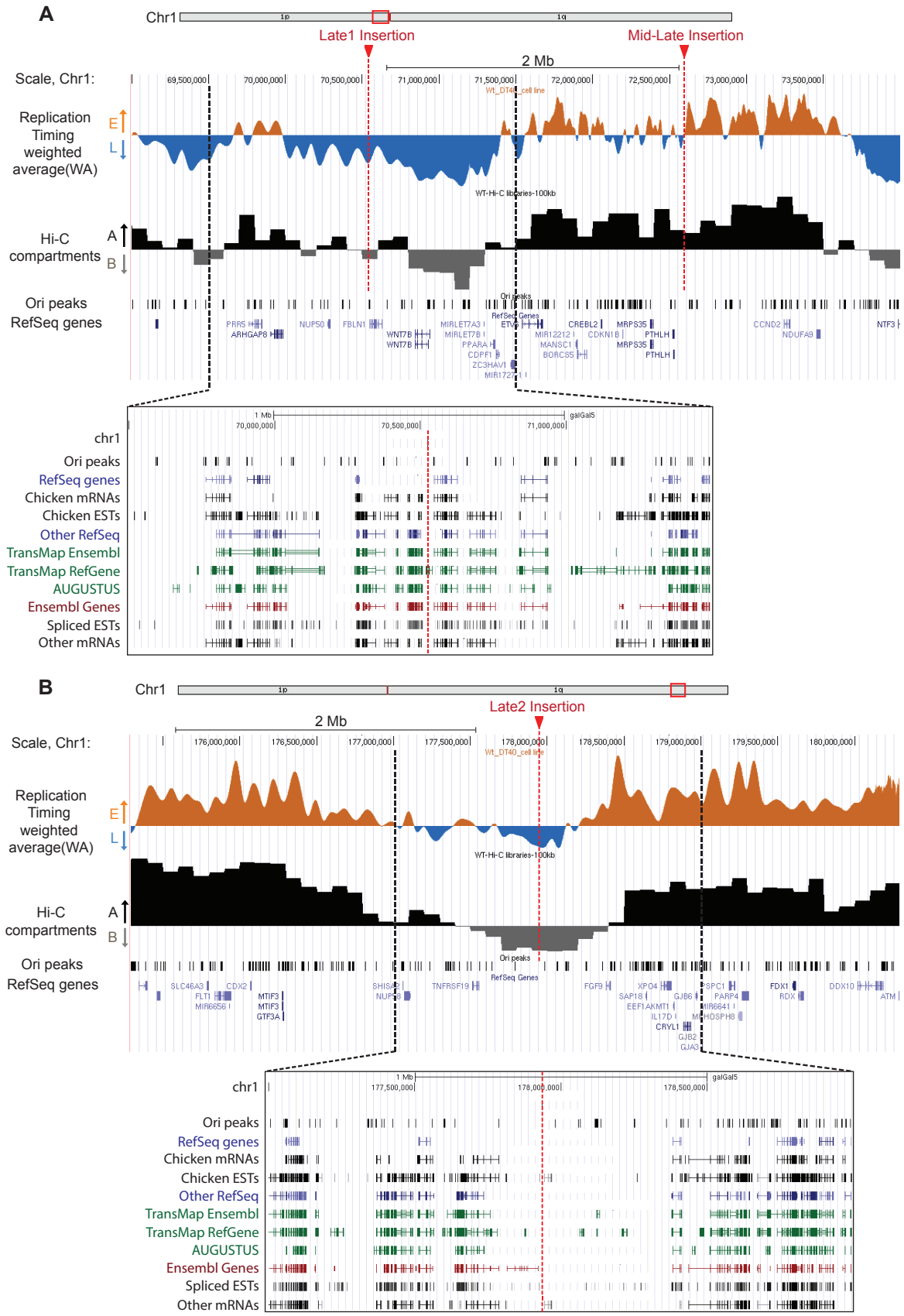
A
Chr1
Late1 Insertion
Mid-Late Insertion
2 Mb
Scale, Chr1:
Replication Timing weighted average(WA)
E
L
Hi-C compartments
A
B
Ori peaks
RefSeq genes
chr1
Ori peaks
RefSeq genes
Chicken mRNAs
Chicken ESTs
Other RefSeq
TransMap Ensembl
TransMap RefGene
AUGUSTUS
Ensembl Genes
Spliced ESTs
Other mRNAs
B
Chr1
Late2 Insertion
2 Mb
Scale, Chr1:
Replication Timing weighted average(WA)
Hi-C compartments
Ori peaks
RefSeq genes
chr1
Ori peaks
RefSeq genes
Chicken mRNAs
Chicken ESTs
Other RefSeq
TransMap Ensembl
TransMap RefGene
AUGUSTUS
Ensembl Genes
Spliced ESTs
Other mRNAs

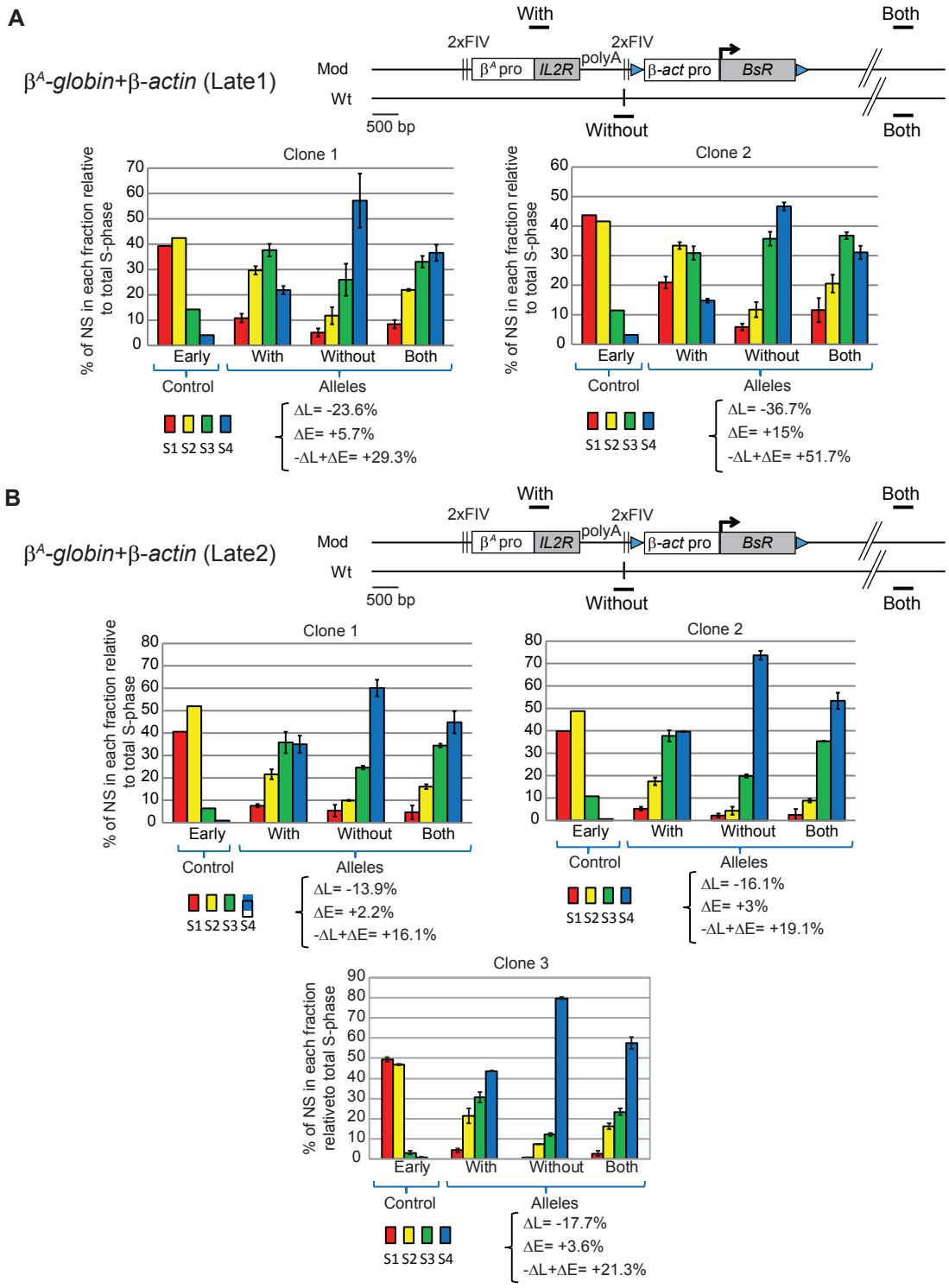
A
βA-globin+β-actin (Late1)
With
Both
2xFIV
2xFIV
Mod
βA pro
IL2R
polyA
β-act pro
BsR
Wt
500 bp
Without
Both
Clone 1
% of NS in each fraction relative to total S-phase
Early
With
Without
Both
Control
Alleles
S1 S2 S3 S4
ΔL= -23.6%
ΔE= +5.7%
-ΔL+ΔE= +29.3%
Clone 2
ΔL= -36.7%
ΔE= +15%
-ΔL+ΔE= +51.7%
B
βA-globin+β-actin (Late2)
ΔL= -13.9%
ΔE= +2.2%
-ΔL+ΔE= +16.1%
ΔL= -16.1%
ΔE= +3%
-ΔL+ΔE= +19.1%
Clone 3
% of NS in each fraction relativeto total S-phase
ΔL= -17.7%
ΔE= +3.6%
-ΔL+ΔE= +21.3%

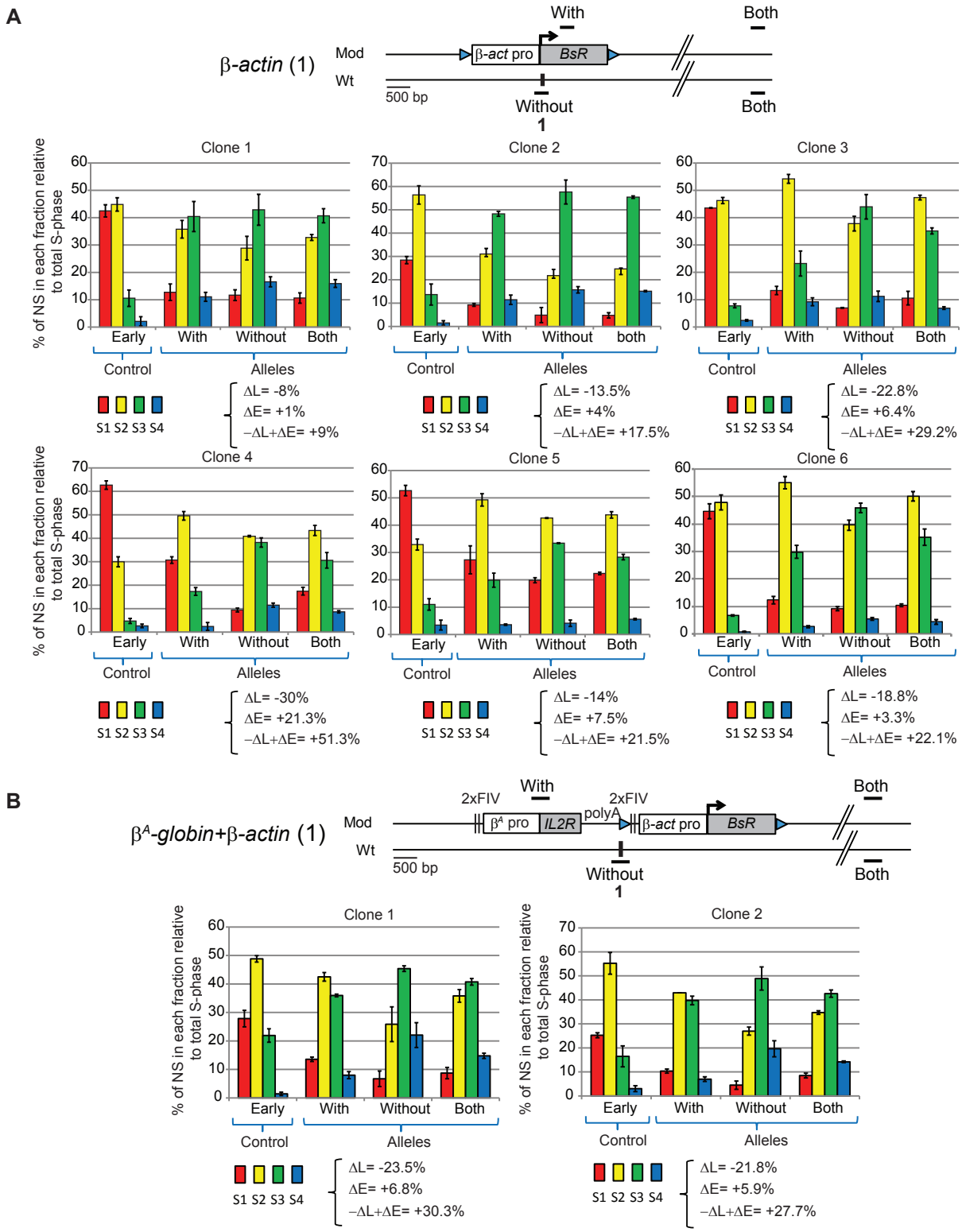
A
β-actin (1)
Mod
Wt
β-act pro
BsR
With
Both
500 bp
Without
1
Both
Clone 1
Clone 2
Clone 3
Clone 4
Clone 5
Clone 6
% of NS in each fraction relative to total S-phase
Early
With
Without
Both
both
Control
Alleles
S1 S2 S3 S4
ΔL= -8%
ΔE= +1%
−ΔL+ΔE= +9%
ΔL= -13.5%
ΔE= +4%
−ΔL+ΔE= +17.5%
ΔL= -22.8%
ΔE= +6.4%
−ΔL+ΔE= +29.2%
ΔL= -30%
ΔE= +21.3%
−ΔL+ΔE= +51.3%
ΔL= -14%
ΔE= +7.5%
−ΔL+ΔE= +21.5%
ΔL= -18.8%
ΔE= +3.3%
−ΔL+ΔE= +22.1%
B
βA-globin+β-actin (1)
2xFIV
βA pro
IL2R
polyA
β-act pro
BsR
ΔL= -23.5%
ΔE= +6.8%
−ΔL+ΔE= +30.3%
ΔL= -21.8%
ΔE= +5.9%
−ΔL+ΔE= +27.7%

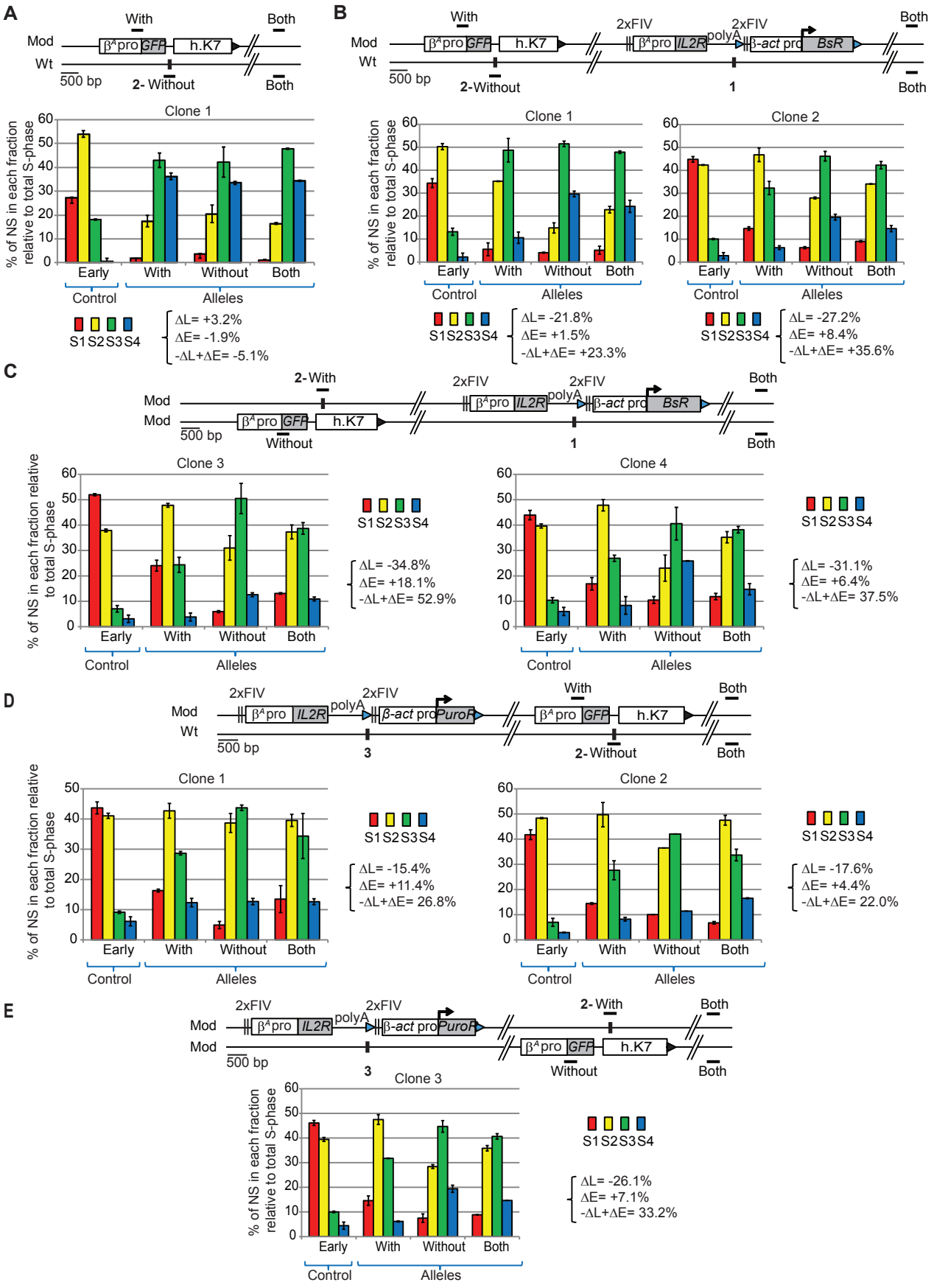
A
With
Both
Mod
Wt
βA pro GFP
h.K7
500 bp
2- Without
Both
Clone 1
% of NS in each fraction relative to total S-phase
Early
With
Without
Both
Control
Alleles
S1 S2 S3 S4
ΔL= +3.2%
ΔE= -1.9%
-ΔL+ΔE= -5.1%
B
With
2xFIV
2xFIV
Both
Mod
Wt
βA pro GFP
h.K7
βA pro IL2R
polyA
β-act pro BsR
500 bp
2-Without
1
Both
Clone 1
Clone 2
ΔL= -21.8%
ΔE= +1.5%
-ΔL+ΔE= +23.3%
ΔL= -27.2%
ΔE= +8.4%
-ΔL+ΔE= +35.6%
C
2- With
2xFIV
2xFIV
Both
Mod
Mod
βA pro GFP
h.K7
βA pro IL2R
polyA
β-act pro BsR
500 bp
Without
1
Both
Clone 3
Clone 4
ΔL= -34.8%
ΔE= +18.1%
-ΔL+ΔE= 52.9%
ΔL= -31.1%
ΔE= +6.4%
-ΔL+ΔE= 37.5%
D
2xFIV
2xFIV
With
Both
Mod
Wt
βA pro IL2R
polyA
β-act pro PuroR
βA pro GFP
h.K7
500 bp
3
2- Without
Both
Clone 1
Clone 2
ΔL= -15.4%
ΔE= +11.4%
-ΔL+ΔE= 26.8%
ΔL= -17.6%
ΔE= +4.4%
-ΔL+ΔE= 22.0%
E
2xFIV
2xFIV
2- With
Both
Mod
Mod
βA pro IL2R
polyA
β-act pro PuroR
βA pro GFP
h.K7
500 bp
3
Without
Both
Clone 3
ΔL= -26.1%
ΔE= +7.1%
-ΔL+ΔE= 33.2%

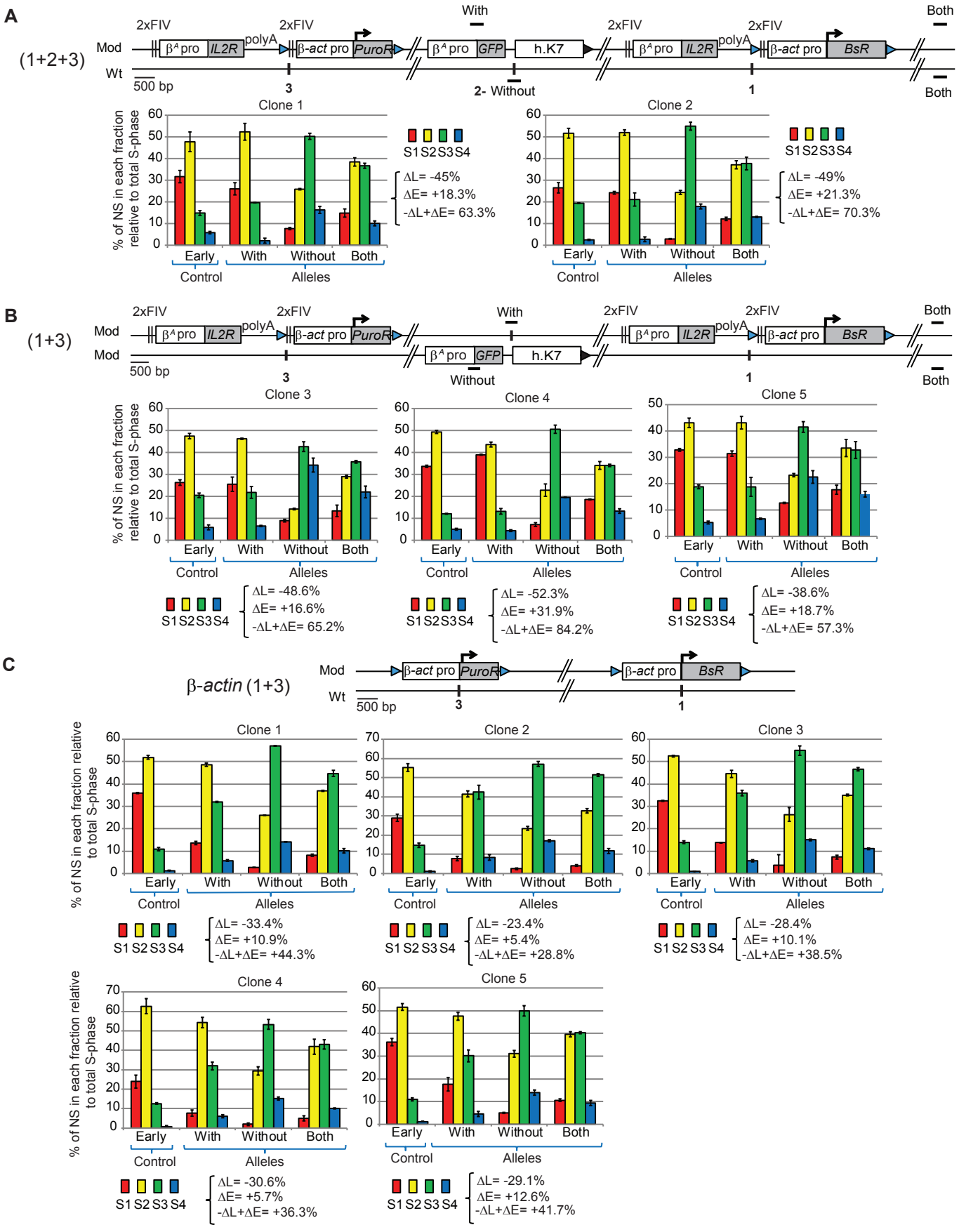
A
(1+2+3)
Mod
Wt
2xFIV
βA pro
IL2R
polyA
β-act pro
PuroR
With
GFP
h.K7
BsR
Both
500 bp
3
2- Without
1
Clone 1
Clone 2
% of NS in each fraction relative to total S-phase
S1 S2 S3 S4
ΔL= -45%
ΔE= +18.3%
-ΔL+ΔE= 63.3%
ΔL= -49%
ΔE= +21.3%
-ΔL+ΔE= 70.3%
Early
With
Without
Both
Control
Alleles
B
(1+3)
Clone 3
Clone 4
Clone 5
ΔL= -48.6%
ΔE= +16.6%
-ΔL+ΔE= 65.2%
ΔL= -52.3%
ΔE= +31.9%
-ΔL+ΔE= 84.2%
ΔL= -38.6%
ΔE= +18.7%
-ΔL+ΔE= 57.3%
C
β-actin (1+3)
ΔL= -33.4%
ΔE= +10.9%
-ΔL+ΔE= +44.3%
ΔL= -23.4%
ΔE= +5.4%
-ΔL+ΔE= +28.8%
ΔL= -28.4%
ΔE= +10.1%
-ΔL+ΔE= +38.5%
ΔL= -30.6%
ΔE= +5.7%
-ΔL+ΔE= +36.3%
ΔL= -29.1%
ΔE= +12.6%
-ΔL+ΔE= +41.7%

Figure EV4

A

Relative quantification values		*BU1A* gene	*MED14* gene	5' 2xFIV-1	β^A pro 2	*Il2R* gene	3' 2xFIV-1	*BsR* gene
RT-QPCR +	β^A-*globin* line (1)	100	2.51	NS	NS	NS	NS	
	β^A-*globin* line (2)	100	2.58	NS	NS	NS	NS	
RT-QPCR +	β^A-*globin* +β-*actin* line (1)	100	2.26	NS	0.097	0.091	LD	17
	β^A-*globin* +β-*actin* line (2)	100	3.06	NS	LD	LD	NS	6.6

Crossing point values		*BU1A* gene	*MED14* gene	5' 2xFIV-1	β^A pro 2	*Il2R* gene	3' 2xFIV-1	*BsR* gene
RT-QPCR +	β^A-*globin* line (1)	14.4	20	34.3	31.9	31.8	32.6	
	β^A-*globin* line (2)	14.1	19.7	33.7	32.1	31.9	33.9	
RT-QPCR -	β^A-*globin* line (1)	38.4	40.5	NA	33.1	33.4	32.9	
	β^A-*globin* line (2)	38.4	38.7	NA	NA	41.8	34.3	
RT-QPCR +	β^A-*globin* +β-*actin* line (1)	14	19.8	31	23.9	24.3	28.4	16.6
	β^A-*globin* +β-*actin* line (2)	14.4	19.7	33.9	29.1	29.3	31.2	18.4
RT-QPCR -	β^A-*globin* +β-*actin* line (1)	34.5	38.5	40.3	36.9	42.1	36.5	35.8
	β^A-*globin* +β-*actin* line (2)	32.2	37.3	44.4	36.8	43.6	33.8	34.4

B β^A-*globin* Line

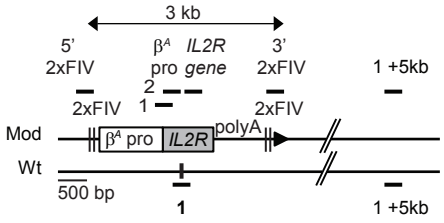

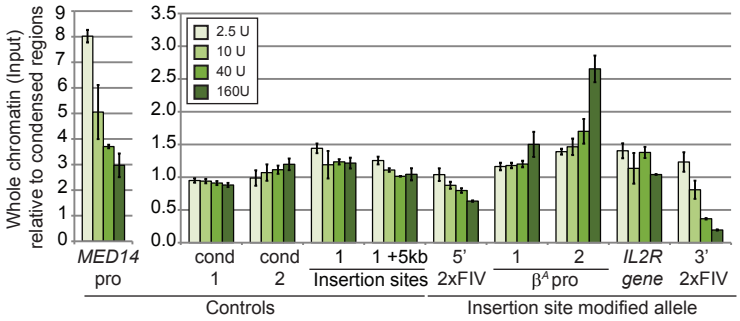

C β-*actin* Line

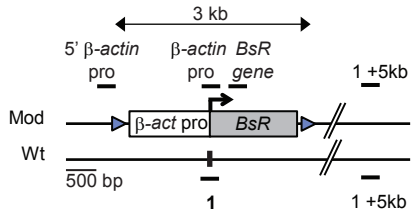

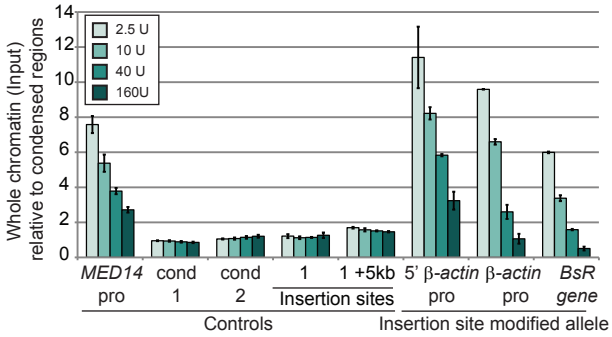

D β^A-*globin*+β-*actin* Line

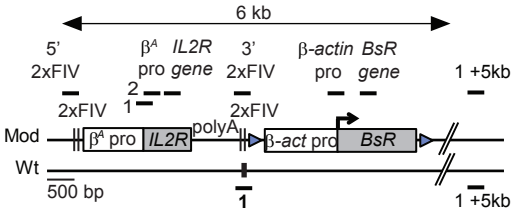

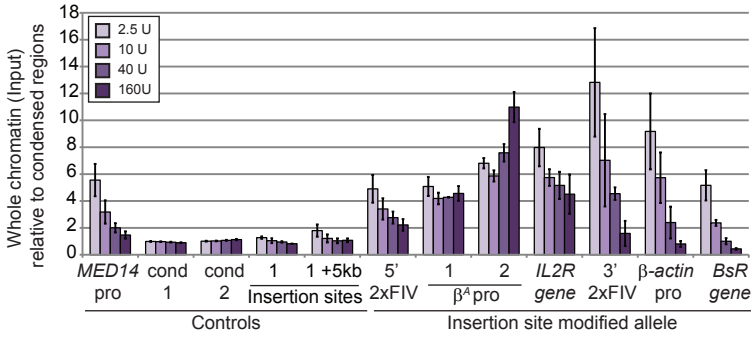

E

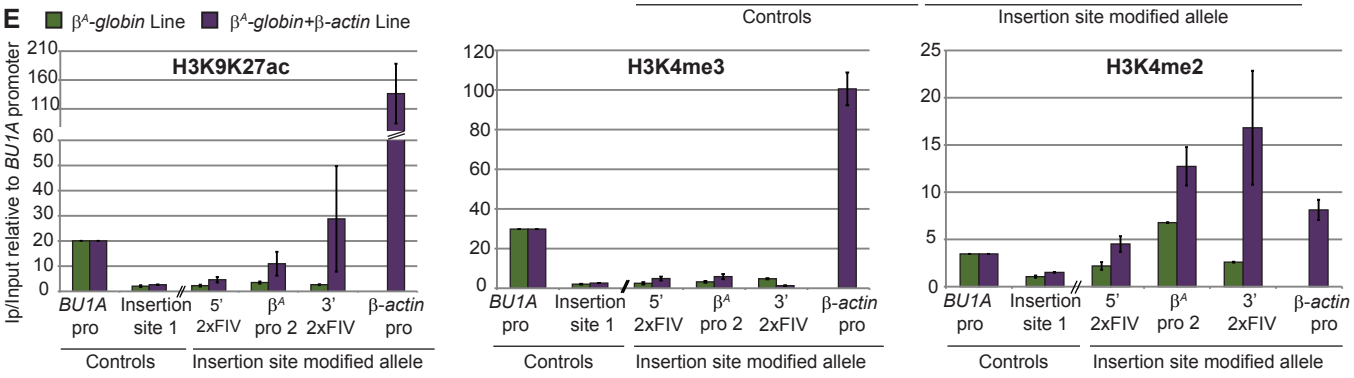

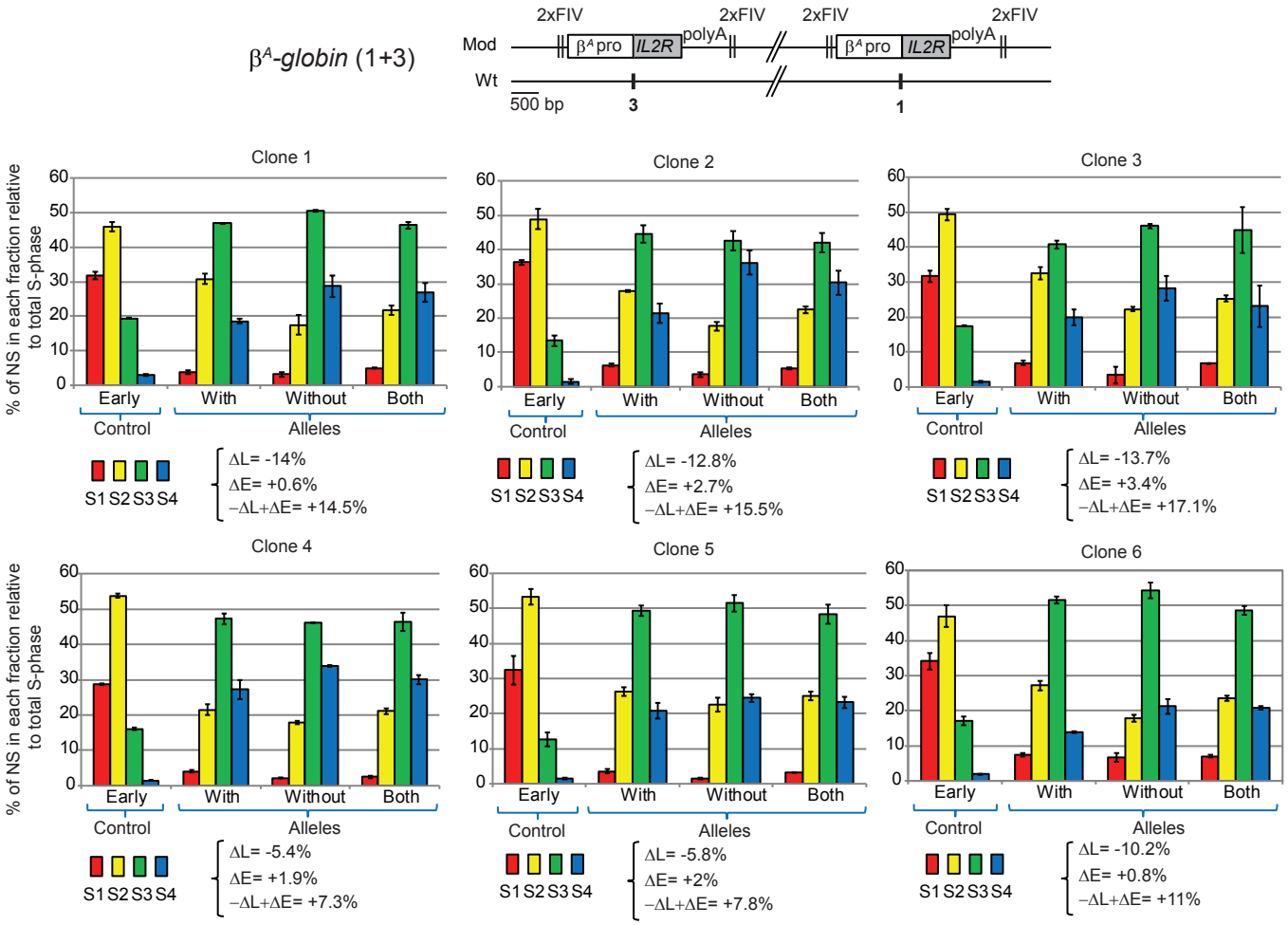
βA-globin (1+3)
2xFIV
2xFIV
2xFIV
2xFIV
Mod
βA pro
IL2R
polyA
βA pro
IL2R
polyA
Wt
500 bp
3
1
Clone 1
Clone 2
Clone 3
Clone 4
Clone 5
Clone 6
% of NS in each fraction relative to total S-phase
0
10
20
30
40
50
60
Early
With
Without
Both
Control
Alleles
S1 S2 S3 S4
ΔL= -14%
ΔE= +0.6%
−ΔL+ΔE= +14.5%
ΔL= -12.8%
ΔE= +2.7%
−ΔL+ΔE= +15.5%
ΔL= -13.7%
ΔE= +3.4%
−ΔL+ΔE= +17.1%
ΔL= -5.4%
ΔE= +1.9%
−ΔL+ΔE= +7.3%
ΔL= -5.8%
ΔE= +2%
−ΔL+ΔE= +7.8%
ΔL= -10.2%
ΔE= +0.8%
−ΔL+ΔE= +11%

Late replication
B Compartment

Late replication
B Compartment

Early replication
A Compartment

Schematic Figure

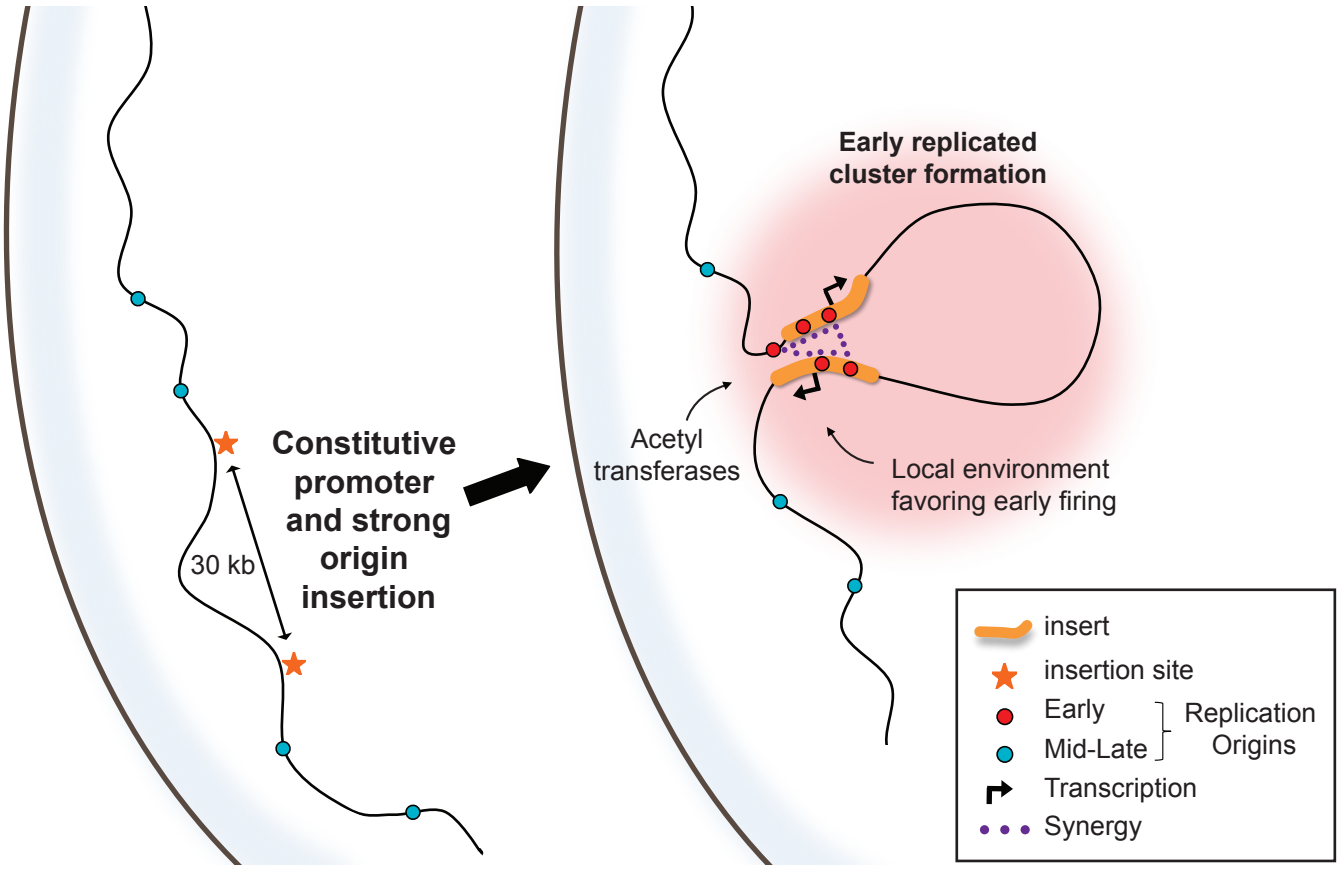

APPENDIX

Clustering of strong replicators associated with active promoters is sufficient to establish an early-replicating domain

Caroline Brossas[1], Anne-Laure Valton[2], Sergey V. Venev[2], Sabarinadh Chilaka[3], Antonin Counillon[1], Marc Laurent[1], Coralie Goncalves[1], Bénédicte Duriez[1], Franck Picard[4], Job Dekker[2,5] and Marie-Noëlle Prioleau[1]*

A

1) Asynchronous cells are BrdU pulse labelled for 1h

2) S-phase cells are sorted by flow cytometry into 4 fractions (S1 to S4)

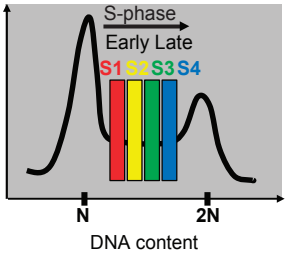

3) The nascent BrdU-labelled DNA is enriched by immunoprecipitation

4) and quantified with allele specific primer pairs by qPCR analysis

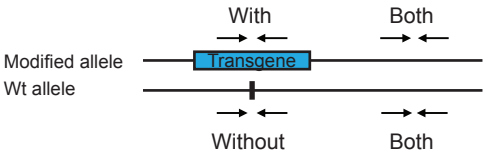

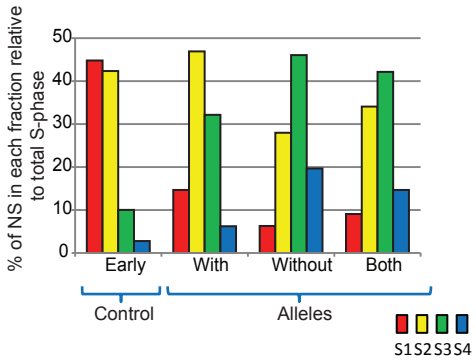

B

Method 1:

Proportion differences between early fractions and late fractions

- ΔL= -27.3%
- ΔE= +8.4%
- -ΔL+ΔE = 35.7%

$\Delta L = [(\%S3+\%S4)_{with}] - [(\%S3+\%S4)_{without}]$

$\Delta E = [(\%S1)_{with}] - [(\%S1)_{without}]$

Global timing shift value: $-\Delta L+\Delta E$

C

Method 2:

Slope differences (Δslope) on four fractions between the modified and the Wt allele

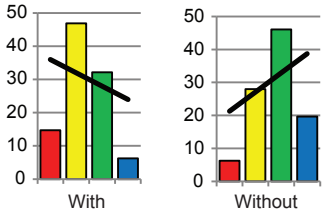

Linear regression equations:

y=-4.0066x+35.016 y=5.8147x+10.463

Δslope = -9.8

$\Delta slope = slope_{With} - slope_{Without}$

D

Correlation between the slope differences (Δslope) and the global timing shift value (-ΔL+ΔE)

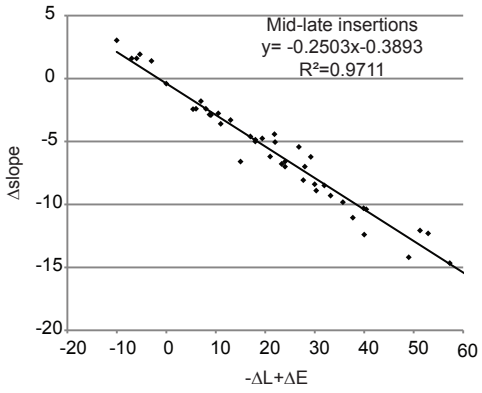

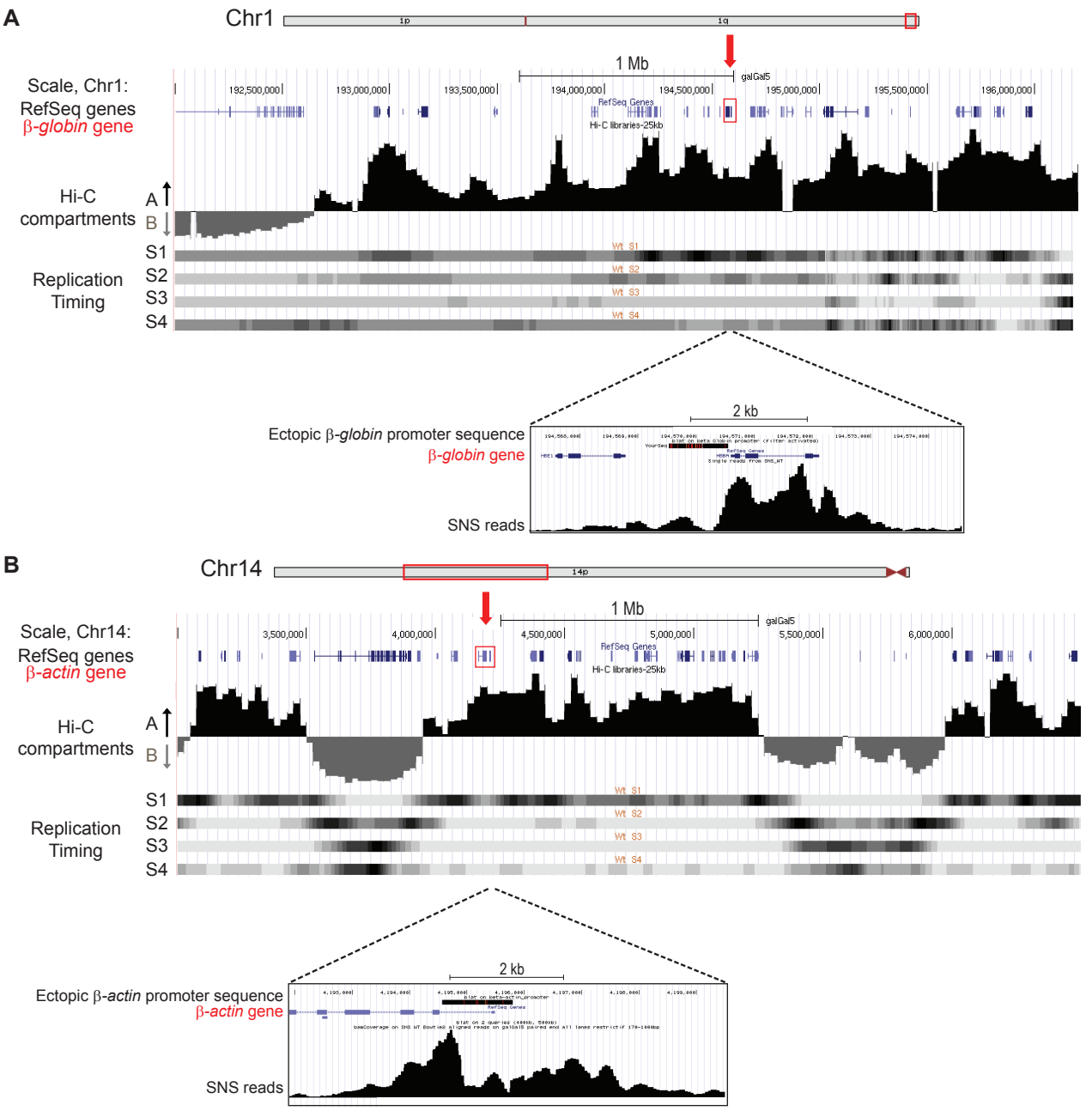
A
Chr1
1 Mb
galGal5
Scale, Chr1:
RefSeq genes
β-globin gene
Hi-C compartments
A
B
Replication Timing
S1
S2
S3
S4
Hi-C libraries-25kb
2 kb
Ectopic β-globin promoter sequence
β-globin gene
SNS reads
B
Chr14
Scale, Chr14:
RefSeq genes
β-actin gene
Ectopic β-actin promoter sequence
β-actin gene

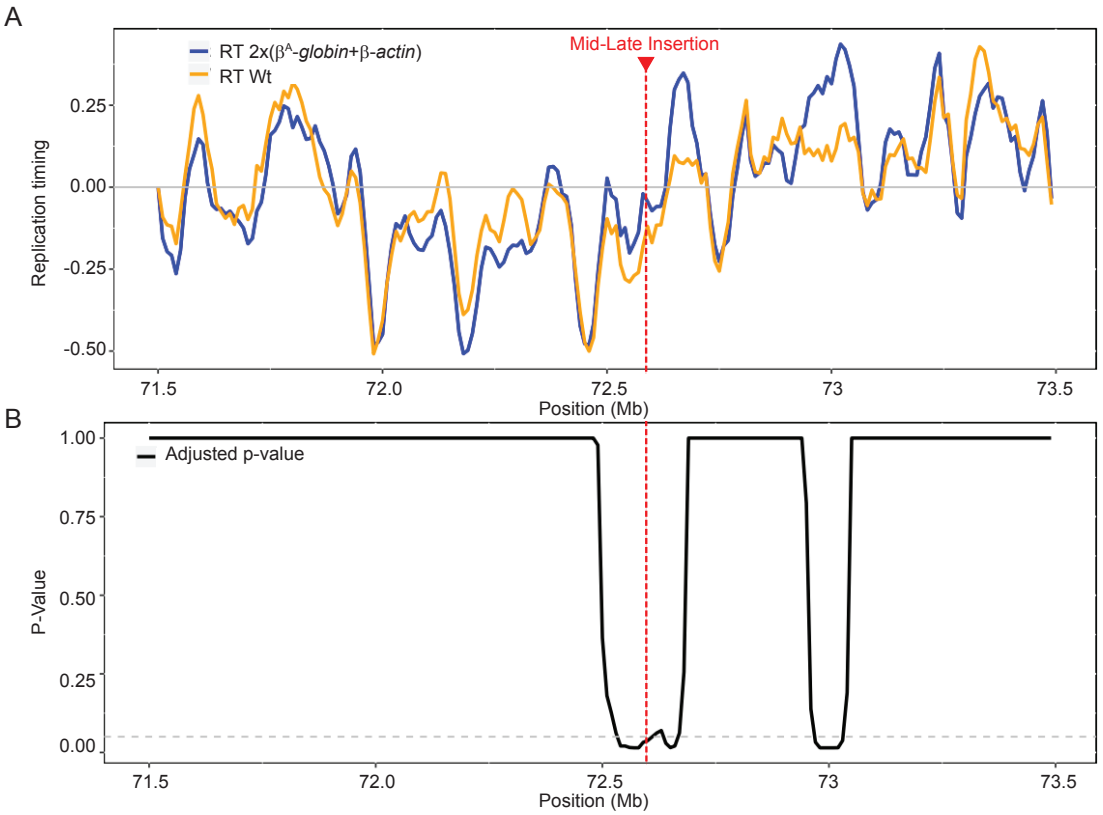
A
RT 2x(βA-globin+β-actin)
RT Wt
Mid-Late Insertion
Replication timing
0.25
0.00
-0.25
-0.50
71.5
72.0
72.5
73
73.5
Position (Mb)
B
Adjusted p-value
P-Value
1.00
0.75
0.50
0.25
0.00
71.5
72.0
72.5
73
73.5
Position (Mb)

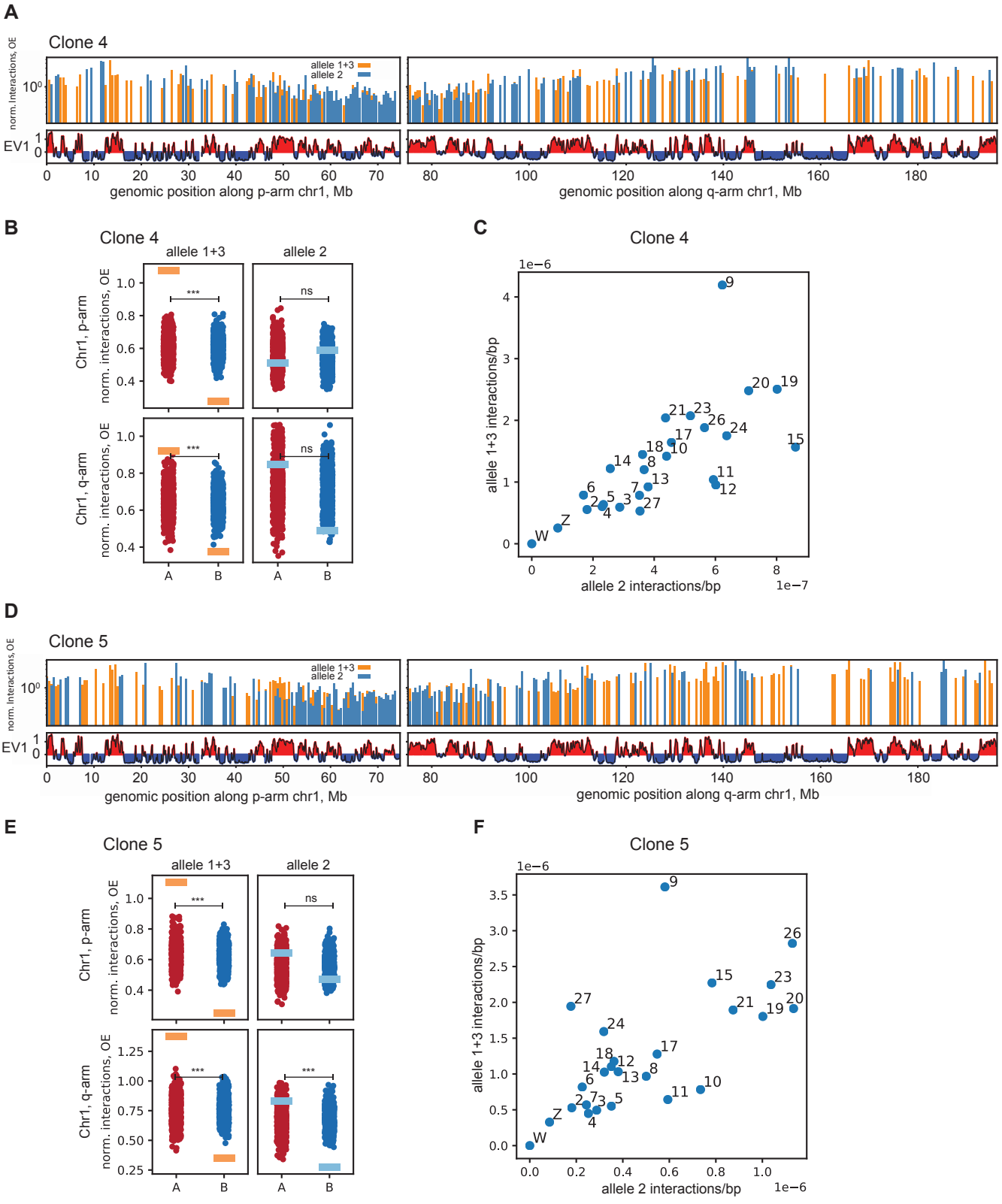
A
Clone 4
norm. interactions, OE
allele 1+3
allele 2
EV1
genomic position along p-arm chr1, Mb
genomic position along q-arm chr1, Mb
B
Clone 4
allele 1+3
allele 2
Chr1, p-arm
Chr1, q-arm
norm. interactions, OE
ns
C
Clone 4
allele 1+3 interactions/bp
allele 2 interactions/bp
D
Clone 5
E
Clone 5
F
Clone 5

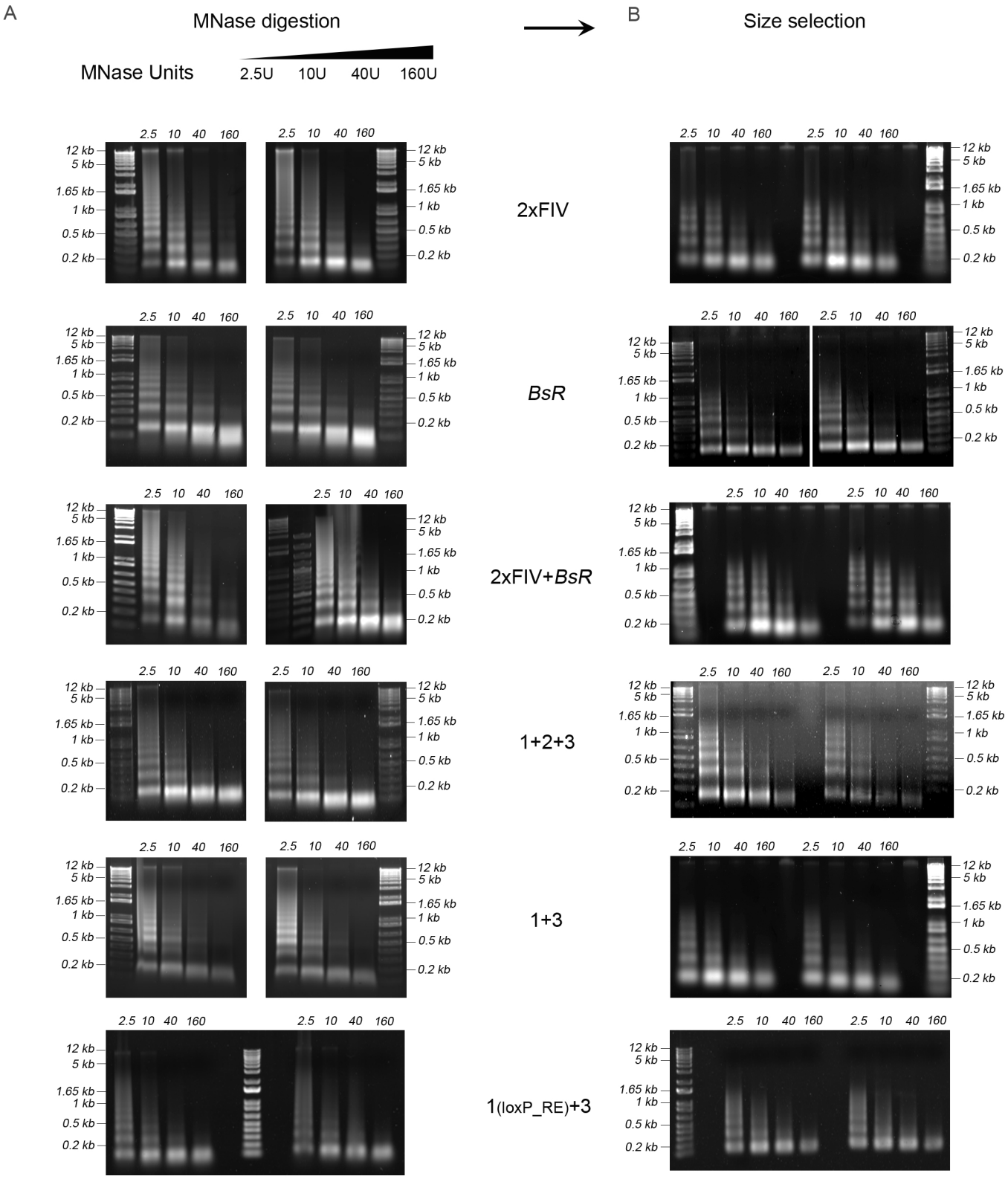
A
MNase digestion
MNase Units
2.5U
10U
40U
160U
B
Size selection
2.5 10 40 160
12 kb
5 kb
1.65 kb
1 kb
0.5 kb
0.2 kb
2xFIV
BsR
2xFIV+BsR
1+2+3
1+3
1(loxP_RE)+3

A

Large 1+3 and *loxP_LE* (1)+β^A-*globin*+β-*actin* (3) excision

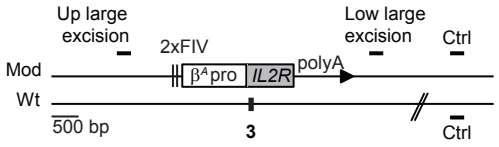

Large excision Up/Low

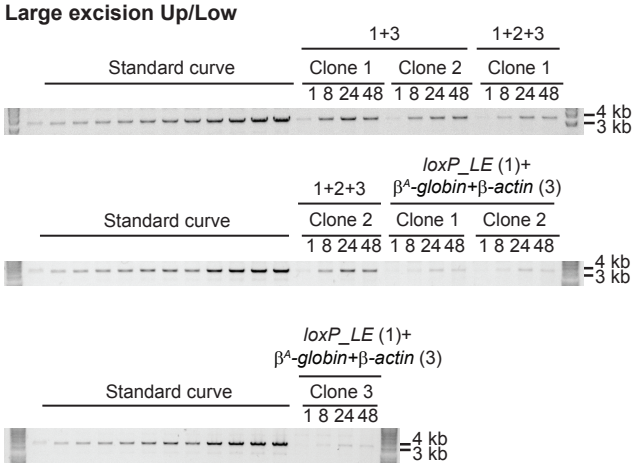

Ctrl

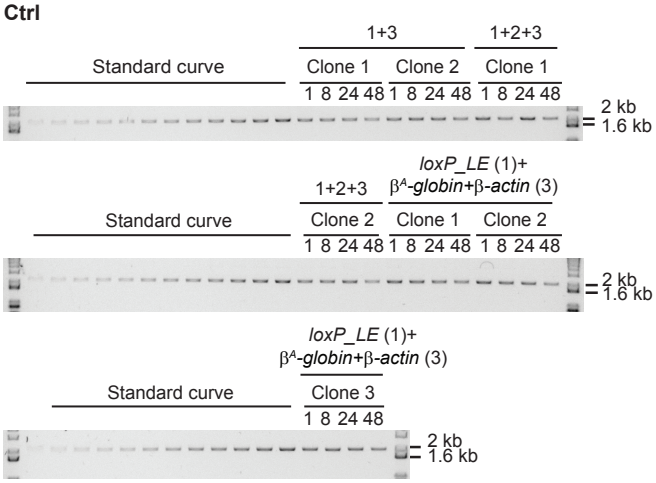

B

Large β-*actin* (1+3) excision

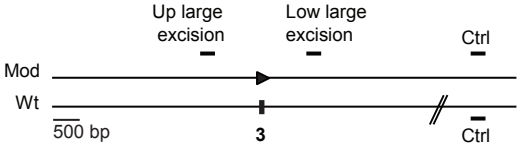

Large excision Up/Low

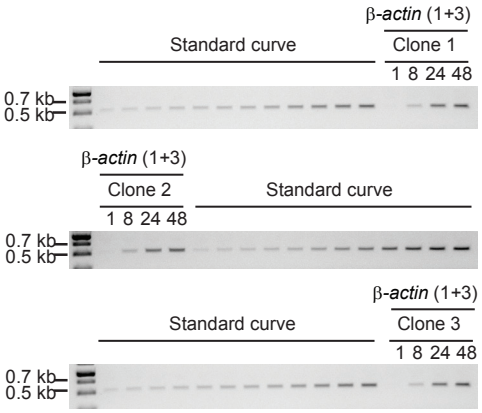

Ctrl

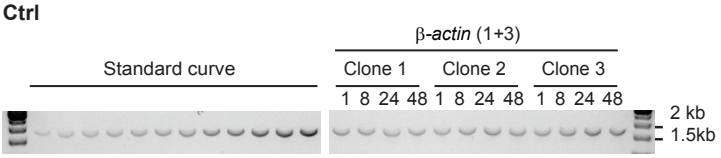

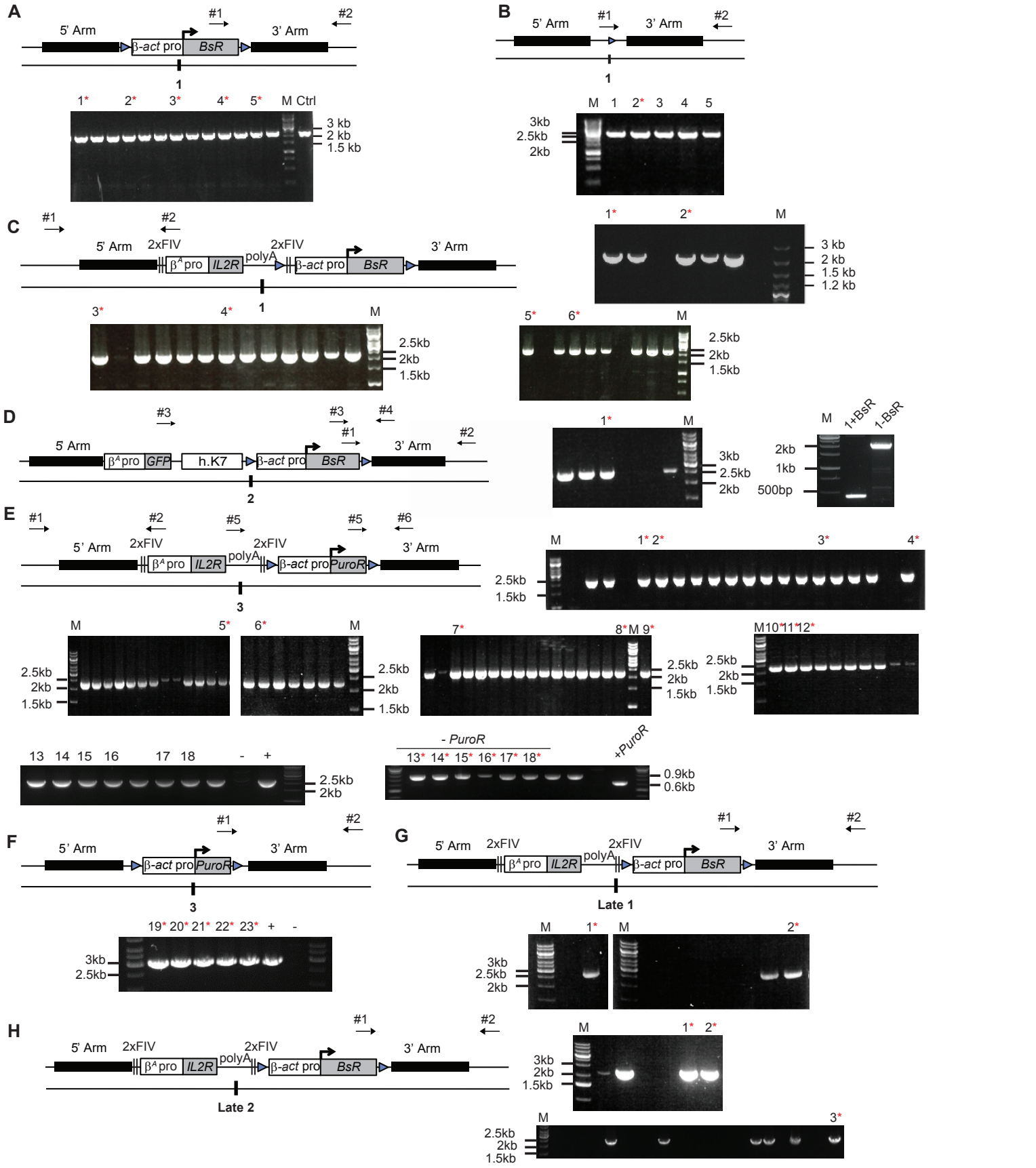
A
5' Arm
#1
#2
β-act pro
BsR
3' Arm
1
1* 2* 3* 4* 5* M Ctrl
3 kb
2 kb
1.5 kb
B
5' Arm
#1
3' Arm
#2
1
M 1 2* 3 4 5
3kb
2.5kb
2kb
C
#1
#2
5' Arm
2xFIV
β^A pro
IL2R
polyA
2xFIV
β-act pro
BsR
3' Arm
1
1* 2* M
3 kb
2 kb
1.5 kb
1.2 kb
3* 4* M
2.5kb
2kb
1.5kb
5* 6* M
2.5kb
2kb
1.5kb
D
#3
#3
#4
#1
#2
5 Arm
β^A pro
GFP
h.K7
β-act pro
BsR
3' Arm
2
1* M
3kb
2.5kb
2kb
M 1+BsR 1-BsR
2kb
1kb
500bp
E
#1
#2
#5
#5
#6
5' Arm
2xFIV
β^A pro
IL2R
polyA
2xFIV
β-act pro
PuroR
3' Arm
3
M 1* 2* 3* 4*
2.5kb
1.5kb
M 5* 6* M
2.5kb
2kb
1.5kb
7* 8* M 9*
2.5kb
2kb
1.5kb
M 10* 11* 12*
2.5kb
2kb
1.5kb
13 14 15 16 17 18 - +
2.5kb
2kb
- PuroR
13* 14* 15* 16* 17* 18*
+PuroR
0.9kb
0.6kb
F
#1
#2
5' Arm
β-act pro
PuroR
3' Arm
3
19* 20* 21* 22* 23* + -
3kb
2.5kb
G
#1
#2
5' Arm
2xFIV
β^A pro
IL2R
polyA
2xFIV
β-act pro
BsR
3' Arm
Late 1
M 1* M 2*
3kb
2.5kb
2kb
H
#1
#2
5' Arm
2xFIV
β^A pro
IL2R
polyA
2xFIV
β-act pro
BsR
3' Arm
Late 2
M 1* 2*
3kb
2kb
1.5kb
M 3*
2.5kb
2kb
1.5kb

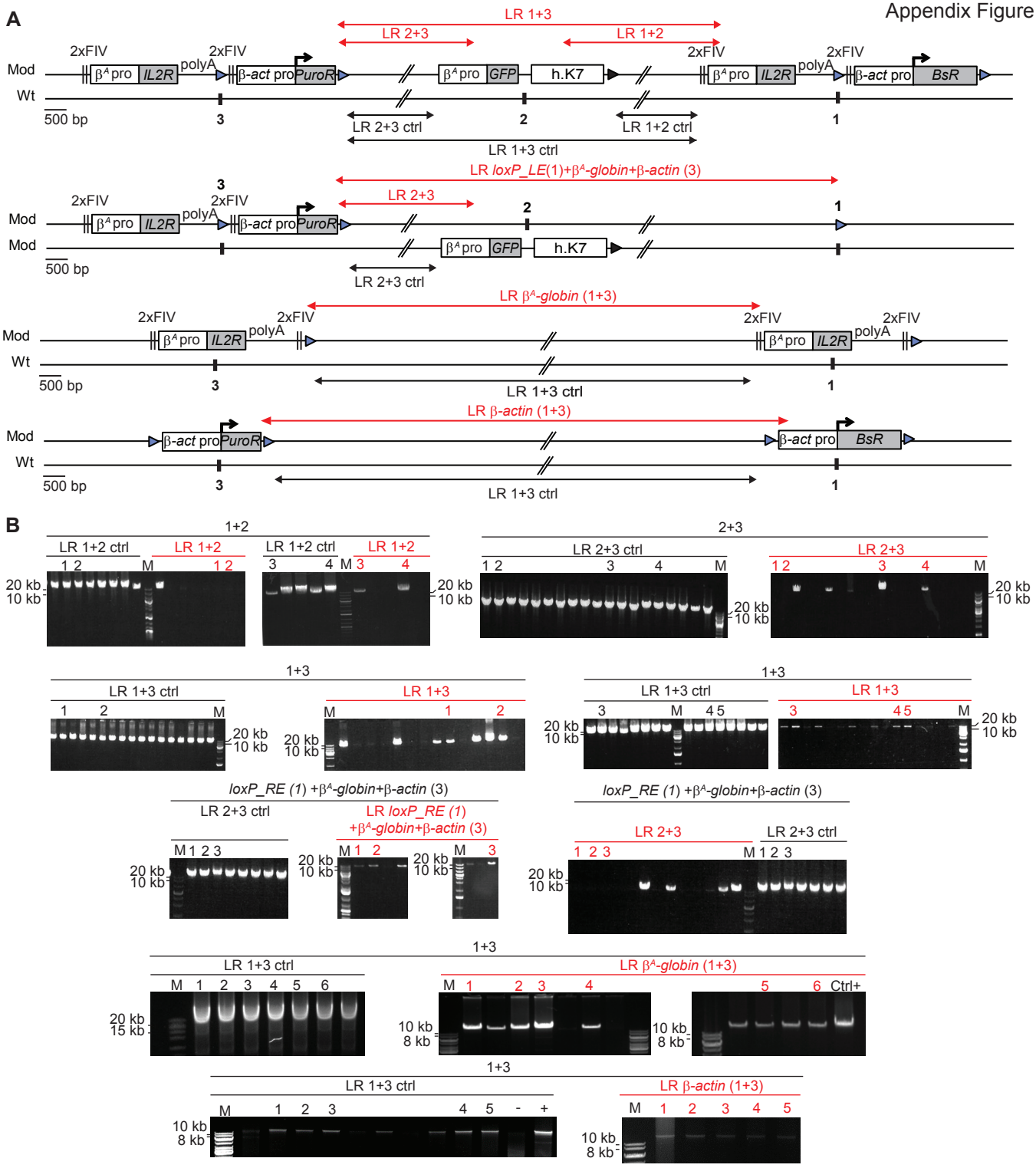
A
LR 1+3
LR 2+3
LR 1+2
2xFIV
polyA
Mod
Wt
βA pro
IL2R
β-act pro
PuroR
GFP
h.K7
BsR
500 bp
LR 2+3 ctrl
LR 1+2 ctrl
LR 1+3 ctrl
LR loxP_LE(1)+βA-globin+β-actin (3)
LR βA-globin (1+3)
LR β-actin (1+3)
B
1+2
2+3
1+3
LR 1+2 ctrl
LR 1+2
LR 2+3 ctrl
LR 2+3
LR 1+3 ctrl
LR 1+3
loxP_RE (1) +βA-globin+β-actin (3)
LR 2+3 ctrl
LR loxP_RE (1) +βA-globin+β-actin (3)
LR 2+3
LR 2+3 ctrl
LR 1+3 ctrl
LR βA-globin (1+3)
LR 1+3 ctrl
LR β-actin (1+3)
20 kb
10 kb
15 kb
8 kb
Ctrl+

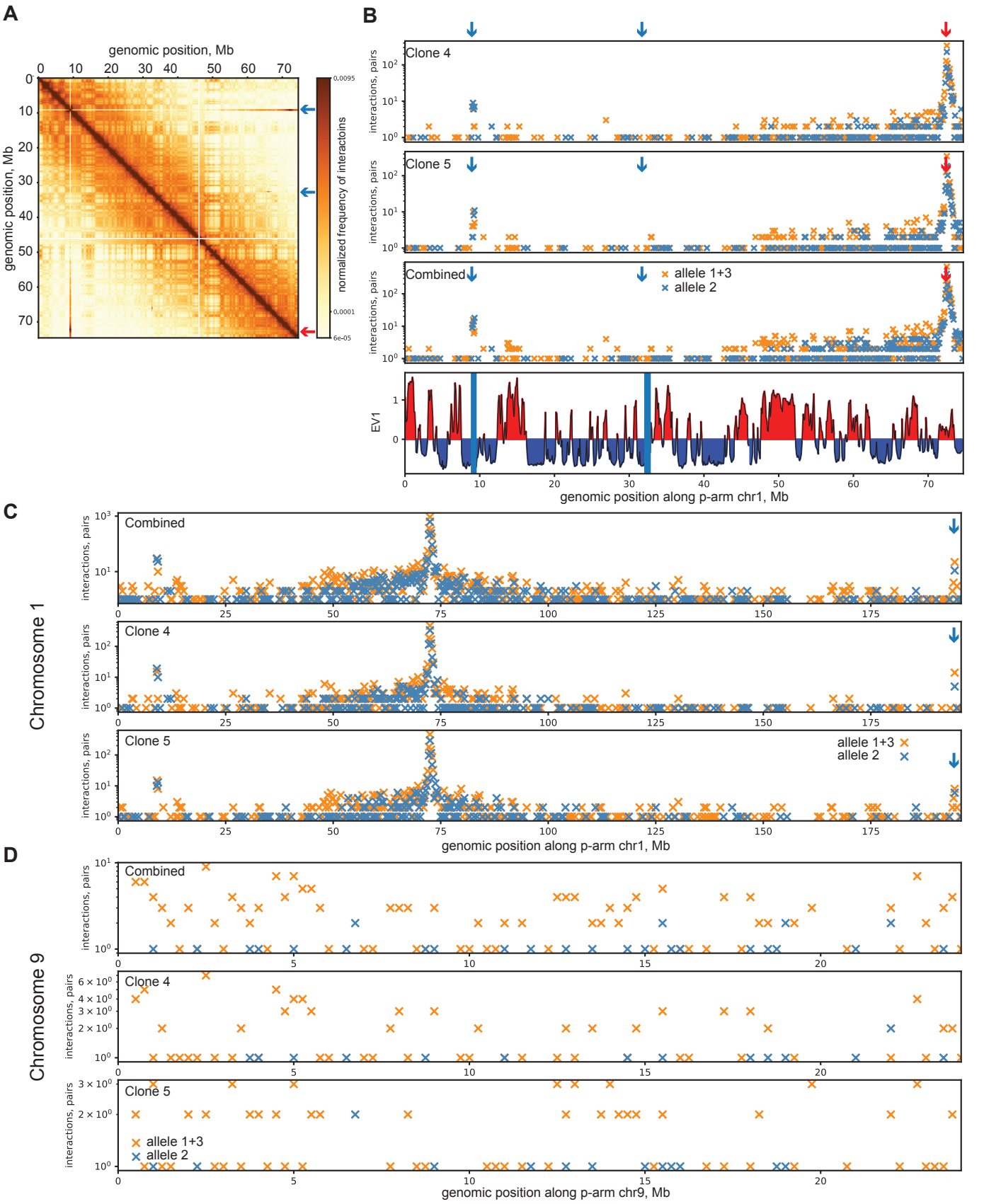
A
genomic position, Mb
genomic position, Mb
normalized frequency of interactoins
B
Clone 4
Clone 5
Combined
allele 1+3
allele 2
interactions, pairs
EV1
genomic position along p-arm chr1, Mb
C
Chromosome 1
Combined
Clone 4
Clone 5
allele 1+3
allele 2
interactions, pairs
genomic position along p-arm chr1, Mb
D
Chromosome 9
Combined
Clone 4
Clone 5
allele 1+3
allele 2
interactions, pairs
genomic position along p-arm chr9, Mb

Appendix Table S1

Site of insertion	Number of clones and source	RT shift Median values
Mid-Late (1)	Total= 44	
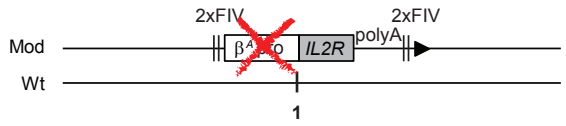	10 { 2 Hassan-Zadeh et al. 2012 (Figure 8); 8 Valton et al. 2014 (Figure 8C, S10) }	-ΔL+ΔE= +6.5%
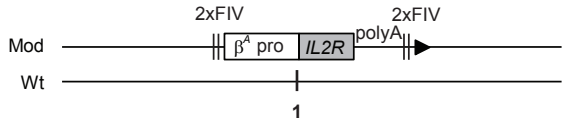	8 { 2 Hassan-Zadeh et al. 2012 (Figure 6B); 6 Valton et al. 2014 (Figure 8C, S9) }	-ΔL+ΔE= +20.2%
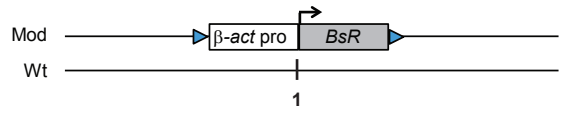	6 { 1 Hassan-Zadeh et al. 2012 (Figure 4A); 5 This study (Figure EV1A.) }	-ΔL+ΔE= +19.6%
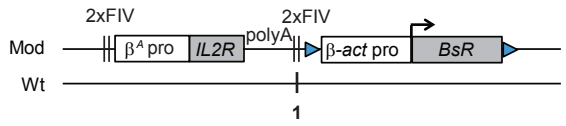	8 { 2 Hassan-Zadeh et al. 2012 (Figure 6A); 6 This study (Figure EV1B.,EV2B-C.) }	-ΔL+ΔE= +36.6%
Mid-Late (3)		
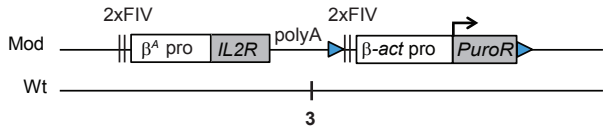	3 { This study (Figure EV2D-E.) }	-ΔL+ΔE= +26.8%
Mid-Late (1+3 and 1+2+3)		
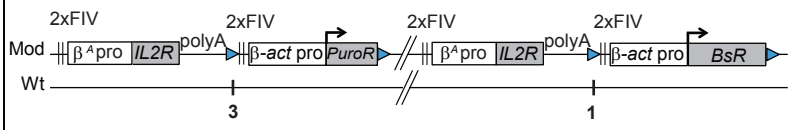	5 { This study (Figure EV3A-B.) }	-ΔL+ΔE= +65.2%
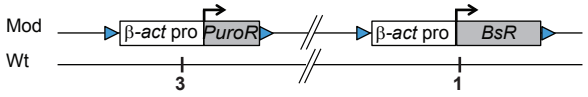	5 { This study (Figure EV3C.) }	-ΔL+ΔE= +38.5%
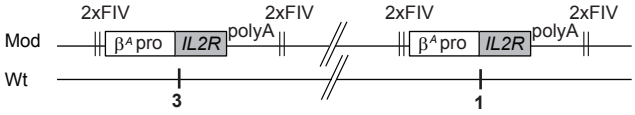	7 { This study (Figure EV5) }	-ΔL+ΔE= +11%
Late (1)		
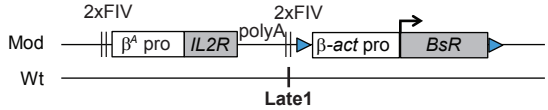	2 { This study (Figure 8A.) }	-ΔL+ΔE= +29.3% / +51.7%
Late (2)		
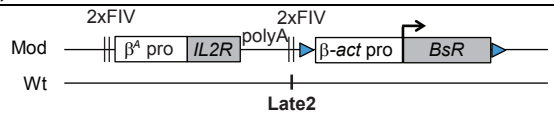	3 { This study (Figure 8B.) }	-ΔL+ΔE= +19.1%

	Construction tested / site	Both concentration	With concentration	Ratio With/Both
Insertions at site mid-1				
β-*actin* (1)	β-*actin* / 1	0.97	0.45	0.47
β-*actin* (2)		0.78	0.32	0.41
β-*actin* (3)		0.63	0.37	0.59
β-*actin* (4)		0.97	0.62	0.63
β-*actin* (5)		0.93	0.41	0.44
β^A-*globin*+β-*actin* (1)	β^A-*globin*+β-*actin* / 1	1.34	0.71	0.53
β^A-*globin*+β-*actin* (2)		1.29	0.65	0.5
β^A*GFP* h.K7+β^A-*globin*+β-*actin* (1)		0.81	0.45	0.55
β^A*GFP* h.K7+β^A-*globin*+β-*actin* (2)		0.84	0.43	0.51
β^A*GFP* h.K7+β^A-*globin*+β-*actin* (3)		0.74	0.4	0.54
β^A*GFP* h.K7+β^A-*globin*+β-*actin* (4)		0.91	0.45	0.49
LoxP_LE (1)	LoxP_LE / 1	0.58	0.28	0.48
Insertions at site mid-2				
β^A*GFP* h.K7 (1)	β^AGFP h.K7 / 2	1.12	0.54	0.49
Insertions at site mid-3				
β^A-*globin*+β-*actin* + β^A*GFP* h.K7 (1)	β^A-*globin*+β-*actin* / 3	1.04	0.57	0.55
β^A-*globin*+β-*actin* + β^A*GFP* h.K7 (2)		1.59	0.59	0.37
β^A-*globin*+β-*actin* + β^A*GFP* h.K7 (3)		1.08	0.43	0.4
Insertions at site mid-1 and mid-3				
β^A-*globin*+β-*actin* + β^A*GFP* h.K7+β^A-*globin*+β-*actin* (1)	β^A-*globin*+β-*actin* / 1 and 3	0.56	0.73	1.29
β^A-*globin*+β-*actin* + β^A*GFP* h.K7+β^A-*globin*+β-*actin* (2)		0.54	0.58	1.07
β^A-*globin*+β-*actin* + β^A*GFP* h.K7+β^A-*globin*+β-*actin* (3)		1.15	1.33	1.16
β^A-*globin*+β-*actin* + β^A*GFP* h.K7+β^A-*globin*+β-*actin* (4)		0.87	0.99	1.13
β^A-*globin*+β-*actin* + β^A*GFP* h.K7+β^A-*globin*+β-*actin* (5)		0.83	0.94	1.13
β^A-*globin*+β-*actin* +LoxP_LE (1)	LoxP_LE / 1	3.34	2.21	0.66
β^A-*globin*+β-*actin* +LoxP_LE (2)		2.19	1.39	0.63
β^A-*globin*+β-*actin* +LoxP_LE (3)		2.12	1.13	0.53
β-*actin* (1+3) (1)	β-*actin* / 3	1.17	0.71	0.61
β-*actin* (1+3) (2)		1.23	0.78	0.64
β-*actin* (1+3) (3)		1.22	0.7	0.57
β-*actin* (1+3) (4)		0.95	0.52	0.55
β-*actin* (1+3) (5)		1.04	0.57	0.54
β^A-*globin* (1+3) (1)	β^A-*globin* / 1 and 3	0.65	0.63	0.97
β^A-*globin* (1+3) (2)		0.74	0.62	0.83
β^A-*globin* (1+3) (3)		0.92	1.2	1.31
β^A-*globin* (1+3) (4)		0.77	1.0	1.30
β^A-*globin* (1+3) (5)		0.75	0.66	0.88
β^A-*globin* (1+3) (6)		0.2	0.22	1.1
Insertions at site late-1				
β^A-*globin*+β-*actin* (1)	β^A-*globin*+β-*actin* / late 1	2.15	0.96	0.45
β^A-*globin*+β-*actin* (2)		1.71	0.75	0.44
Insertions at site late-2				
β^A-*globin*+β-*actin* (1)	β^A-*globin*+β-*actin* / late 2	1.6	0.59	0.37
β^A-*globin*+β-*actin* (2)		1.37	0.5	0.36
β^A-*globin*+β-*actin* (3)		0.98	0.43	0.44

Appendix Table S3

Primer name	Primer sequence	Insertion site	galGal5 Assembly	Amplicon size
5'arm_ML1	(Hassan-Zadeh et al., 2012)	site mid-late 1	chr1:72,565,520	
3'arm_ML1				
5'arm_ML2_Up	CCAAACCAGGCCACTCTTAGT	site mid-late 2	chr1: 72,548,589	2,163 bp
5'arm_ML2_Low	AGTCACTTGGCATAAATAAGAAGCC			
3'arm_ML2_Up	CTGAGCAGGAAGGGAAACGA			2,068 bp
3'arm_ML2_Low	CCATAGTGCAGACCTGGCAT			
5'arm_ML3_Up	ACACACTCACCTCCTGCCTT	site mid-late 3	chr1: 72,536,060	2,054 bp
5'arm_ML3_Low	AGATCTCAGTCCTGCCAGCA			
3'arm_ML3_Up	AAGTTCGTAATACACAACCTTGAC			2,062 bp
3'arm_ML3_Low	GCTTCCCCGCTTCTTCCCTA			
5'arm_L1_Up	CAGTGAAACACAGGAGGAACA	site late 1	chr1:70,523,649	2,244 bp
5'arm_L1_Low	TAACTCCAAGAACGATCACTGC			
3'arm_L1_Up	GGAAATGTCTTGAATCTCACAAGG			2,137 bp
3'arm_L1_Low	ATGCCCACCAGTGTCCATAA			
5'arm_L2_Up	ACTTGTTGAGCCTTTATGGAGAAC	site late 2	chr1:177,936,192	1996 bp
5'arm_L2_Low	CGGTGTTACAGAGGAGTAAACTGA			
3'arm_L2_Up	ACCTTATGCATTTCGTTCCTATGT			2001 bp
3'arm_L2_Low	TAAGAAGAGAGATGGGGATCAAAC			
2XFIV_β^A*globin*-Up	GGGGACAACTTTGTATACAAAAGTTGAGGTGGCACGGGATCGCTTTCCTAGGTGGCACGGGATCGCTTTCCTCTGCCCACACCCTCCTG			
2XFIV_β^A*globin*-Low	GGGGACAACTTTGTATAGAAAAGTTGGGTGGGTACCACTAGTGATGATCCGTCATCCAGACATG			
2XFIV_β-*actin*-Up	GCTCGAGAGGTGGCACGGGATCGCTTTCCTAGGTGGCACGGGATCGCTTTCCTGTGAGC CCCACGTTCTGCTT			
2XFIV_β-*actin*-Low	CTTCTCTGTCGCTACTTCTAC			
XhoI+2xFIV-Up	GACTCTCGAGAGGAAAGCGATCCCGTGCCACCTAGGAAAGCGATCCCGTGCCACCTGCTAGCCCTGATCAATAACT			
XhoI+2xFIV-Low	AAGTCCTCGAGCGTATTACAATTCACTGGCCGT			
β^A-Up	CTGCCCACACCCTCCTG			
β^A-Low	TTCCTGACCCTTGGGACCA			
GFP-Up	GGGTCAGGAAATGGTGAGCAAGGGCGAGG			
GFP-Low	TGAAGCAGCATTTACGCCTTAAG			
h.K7-Up	TGCTGCTTCATTTCTGCTCTC			
h.K7-Low	GCAGAGCCAGAGTCCAAGAG			
loxP_RE-h.K7-Up	GGATCCATAACTTCGTATAGCATACATTATACGAACGGTAACTTGAGCCCAGGAGTTCGA			
loxP_RE-h.K7-rev	AGAGTTCCAACCCCAGCCTC			

Appendix Table S4

	Forward primer sequence	Reverse primer sequence	Genomic position (Build Dec 2015)
Replication timing analysis			
With on *GFP* reporter	GGAATTCGATAGCTTGGCGGC	GCTGAACTTGTGGCCGTTTAC	
With on insertion site 2	GTAATGAAATTCAGCAATGACAGGC	TCCTATCTGTTCAAATGTGCATCAG	chr1:72548543+72548676
With on β^A-*globin*+β-*actin*	GGGGACTGCTCACGTTCATCA	AATGTGGCGTGTGGGATCTC	
With on β-*actin*	TGCAGAAATCGGAGGAAGAAGA	GAATTGCCGCTCCCACATGA	
Without or Wt allele insertion site 1	CAGGACAGCAGGTATTCACA	GGCCTGAACACTGTGTCAAT	chr1:72565497+72565651
Without or Wt allele insertion site 2	GTAATGAAATTCAGCAATGACAGGC	TCCTATCTGTTCAAATGTGCATCAG	chr1:72548543+72548676
Without on *GFP* reporter site 2	GGAATTCGATAGCTTGGCGGC	GCTGAACTTGTGGCCGTTTAC	
Wt allele insertion site 3	TGGTACAGGCTGAGGACACC	TGATGACTGCAGCTTCCTTCT	chr1:72535996+72536105
Without or Wt allele insertion site late1	CCCTTGAATCAGACCCTTGA	CCCTCCTTTCTCCATAAAAACA	chr1:70523547+70523674
Without or Wt allele insertion site late 2	TTTACACTACTCCCACCCCTCG	TTGACCATATGCCACCAACACC	chr1:177936339+177936438
Controls			
Both or 1+ 5 kb	TCCATACAGCCACAACAGCA	TGTGGAAGAGTTTCAGTCCAGG	chr1:72570952+72571067
Both or late 1- 4.8 kb	TGTACTTCTCTGTGGACATGCA	TGGCACAGAGGACAGGTAAGA	chr1:70518727+70518810
Both or late 2 - 3.6kb	CAAGGTTTCCACCCCTAAAGA	TGATGGATGTGGGAAGAGAAA	chr1:177932452+ 177932533
Early timing control	GACGGTCAGGTTTGCCAAAG	TCCTGAGGATACGTTTTTCAG	chr1: 194563998+194564262
Mitochondrial DNA	CATCCCATGCATAACTCCTG	GTAGTCCAGGCTTCACTTGA	chrM :541+731
Chlps, Chromatin accessibility and RNA quantification			
5' 2xFIV-1	GGGCTATTCAGCTTGTCTAG	GCCACCTCAACTTTTGTATAC	
5' 2xFIV-3	TTATGCTGGCAGGACTGAGA	GTGGGCAGAGGAAAGCGAT	
β^A pro 1	GGGAGCAAGAGCCCAGAC	GTGAGCAGTCCCCACATCAG	
β^A pro 2	GGGACTGCTCACGTTCATCA	AATGTGGCGTGTGGGATCTC	
IL2R gene	CTACACAGAGGTCCTGCTG	GTGAAGAGAAGCCTCAGGCA	
3' 2xFIV-1	TGCATTCTAGTTGTGGTTTGTCC	ACCGTCGACCAACTTTGTATAGA	
3' 2xFIV 1-3	AAGCTTGGATCCCCTACCGT	GAGAGTGAAGCAGAACGTGGG	
5' β-*actin* pro	GTGGGACTTCTTCTAAAGGGCTA	TGATCAATAACTTCGTATAATGTATGCT	
β-*actin* pro	TGCAGAAATCGGAGGAAGAAGA	GAATTGCCGCTCCCACATGA	
BsR gene	CGGCAGTACATATTGAAGCGT	CCCTACACATACCACAAGGA	
PuroR gene	ACGACCTTCCATGACCGAGT	AGTTCTTGCAGCTCGGTGAC	
β^A-*GFP*	GGAATTCGATAGCTTGGCGGC	GCTGAACTTGTGGCCGTTTAC	
GFP gene	GCCCGACAACCACTACCTGAG	GCTTTACTTGTACAGCTCGTCCA	
h.K7	AAGTTTATCATTGTGTGGCAGTCA	GTTCTGGTTGGGTTGTATGTCAC	
LoxP site	CGCCCTATAGTGAGTCGTATTACA	TGTTTAAATGTTTGTAGCCTGCCT	
cond1	CATCTGTGCTCTGGGTCCA	AAGGAGTGGAAGGAACGCATC	chr1:194546368+194546497
cond 2	TTGGTGCAGTGCCTCAGATAG	ATGTCGCTTGTCACGATGGAT	chr1:194546457+194546563
MED 14 pro	GGATTCACACTGTTCCCCTCC	TGCATGTTTCTCTCATCCGAAGT	chr1:112227330+112227461
BU1A pro	CTCTGTAGCCAGATCGTCTTCTC	GTGTCAGCTCATCTAGGCAAATC	chr1:91922377+91922546
BU1A gene	AATGTCCCCAAAATGAGCTG	CCTCTTTTTCCACCCTCCTC	chr1:91923373+91923517
MED 14 gene	TGGGCTAATAATGCTGGAAAGGT	TAGAGAAGCCAGACGATCAGCA	chr1:112236082+112236823
Long-range amplifications			
LR 1+2	AAGGGTCAGCTTTCGTGATAATCTGG	ACCTCTCTTGCATTCACAGTTCAACA	
LR 1+2 ctrl	GCAAGATGGGCAGAGCTGAGTTAACAAT	TGTCCTGTAAGTCCTGGCAAAACAAAGA	chr1:72548824+72565503
LR 2+3	GAGCGTATTACAATTCACTGGCCGTC	CTTGCTCACCATTTCCTGACCCTTG	
LR 2+3 ctrl	GCAGTATAACAAGCACGCCTGAAGTAAA	CAGTCTTATCCCACCCCTTCCTGATAG	chr1:72536307+72548324
LR 1+3	GAGCGTATTACAATTCACTGGCCGTC	GATCCCGTGCCACCTCAACTTTTGTAT	
LR loxP LE(1)+ β^A-*globin*+β-*actin* (3)	GAGCGTATTACAATTCACTGGCCGTC	GACGTTGTGGCTGTTGTAGTTGTACTC	
LR β^A-*globin* (1+3)	TCCAATTCGCCCTATAGTGAGTCGTA	GATCCCGTGCCACCTCAACTTTTGTAT	
LR β-*actin* (1+3)	CTCCAATTCGCCCTATAGTGAGTCGTAT	GATACCGTCGACCAACTTTGTATAGAAAA	
LR 1+3 ctrl	GCAGTATAACAAGCACGCCTGAAGTAAA	TGTCCTGTAAGTCCTGGCAAAACAAAGA	chr1:72597486+72626682
Screening of targeted integration			
3'-screening-site 2 for *GFP* reporter	GCTCCAATTCGCCCTATAGTGA	GGCACTCCATTTCCATCTCCT	
5'-screening-site 3 for β^A-*globin*+β-*actin*	GGACTGGCTAGGGAACAAGAG	TCTGCCTTCTCCCTGATAACG	
5'-screening-site 1 for β^A-*globin*+β-*actin*	GTGCAGCATCAGTGGATAAAGT	TCTGCCTTCTCCCTGATAACG	
3'-screening-site 1 for β-*actin*	CCCCCTGAACCTGAAACATAA	CCACATGTTTATTGCATACGGC	
3'-screening site 1 for *loxP LE*	CCAATTCGCCCTATAGTGAGTCG	ACGTAACAAATCTACAGGTCTTCG	
3'-screening site 3 for *PuroR*	CCCCCTGAACCTGAAACATAA	CTTCCAACCCAGGCCACTATG	
3'-screening site late 1 for β^A-*globin*+β-*actin*	GAGCTCCAATTCGCCCTAT	ACTATTGTACCCCTCCCTGTTG	
3'-screening site late 2 for β^A-*globin*+β-*actin*	GAGCTCCAATTCGCCCTAT	GGTCTGATCCCTATCTCACTGG	
Screening of site specific excision			
BsR excision at site 2	CCCCCTGAACCTGAAACATAA	TATCCCACTGCCACTGGAGG	
PuroR excision at site 3	TGCATTCTAGTTGTGGTTTGTCC	GGTCTGAGAGGTCTTGCTGGA	
Large 1+3 excision Up/Low	GGTTCTGGTGCCCTCATTGAT	TGCTCTGCTAGAATTGCCTGT	chr1:72535815+72565623
Ctrl	ACCCAAGGCAGGCTACAAAC	TGAGTTACTTTGGCATTACTTTTCATC	chr1:72565577+72567483
No *PuroR* excision	CCCCCTGAACCTGAAACATAA	GCAGCCTTTTCCAGCAAGAC	
No *BsR* excision	ACGACCTTCCATGACCGAGT	AGTTCTTGCAGCTCGGTGAC	
PuroR excision	CACGCCACATTCAAAGCCATG	TCCAGCAAGACCTCTCAGACC	
BsR excision	CAGCGGAGACAGAGGAAGAGT	GGCATGGTTTTGATTTCTGGCC	
Copy number quantification			
loxP LE	CGCCCTATAGTGAGTCGTATTACA	TGTTTAAATGTTTGTAGCCTGCCT	
PuroR	ACGACCTTCCATGACCGAGT	AGTTCTTGCAGCTCGGTGAC	

name	length	GC	DpnII sites/bp	sample	total interactions	cis percent
allele1+3	2532	56.7	0.0043	clone 4	2433	67.41
allele1+3	2532	56.7	0.0043	clone 5	2369	69.78
allele2	2509	46.2	0.0032	clone 4	1318	80.2
allele2	2509	46.2	0.0032	clone 5	1290	78.53
chr1	196202544	40	0.0021	clone 4	121564119	81.08
chr1	196202544	40	0.0021	clone 5	116517761	80.63

Appendix Figure S1: Quantitative analysis of RT shifts by two distinct calculation methods reveals cooperation between two combinations of *cis*-regulatory elements

A. Method for allele-specific analysis of RT by real-time PCR quantification. BrdU pulse-labeled cells were sorted into four S-phase fractions (S1 to S4) and the immunoprecipitated newly synthesized strands (NS) were quantified by real-time qPCR in each fraction. Specific primer pairs determine the RT profile for the modified allele (With), the wt allele (Without) and both alleles (Both). The endogenous *β-globin* locus was analysed as an early-replicated control.

B-C. Two methods of calculation were used to determine the difference in RT between the wt and modified alleles: the -ΔL+ΔE method and the ΔSlope method.

D. The analysis of the correlation between the ΔSlope and the -ΔL+ΔE method for all clonal cell lines previously published (Hassan-Zadeh et al., 2012; Valton et al., 2014) or analysed for the first time here is shown. The linear regression curve is shown, with the corresponding equation and the coefficient of determination (R^2).

Appendix Figure S2: Endogenous genomic features of early-replicated domains containing the *β-globin* and *β-actin* loci

A-B. UCSC genome browser visualization (galGal5) of 4 Mb genomic windows inside either the *β-globin* locus of chromosome 1 or the *β-actin* locus of chromosome 14 are shown. Annotated genes are represented and the β^A*-globin* and the *β-actin* genes are indicated by a red arrow. Track of eigenvector 1 values corresponding to A/B compartments at 25 kb resolution after Hi-C analysis are represented. Tracks of nascent strands (NS) enrichments obtained after cells sorting into four S-phase fractions, BrdU pulse-labeled nascent strands (NS) immunoprecipitation, and sequencing were represented separately (S1 to S4) for the wt cell line in dense configuration. Below, an enlargement of either the β^A*-globin* or the *β-actin* promoter region with the ectopic sequence found in our constructs and the single reads from SNS aligned previously published (Massip et al., 2019) are reported.

Appendix Figure S3: P-value distribution for the effect of the *β^A-globin + β-actin* construct on RT in the mid-late locus

A. Replication timings of the WT and the 2x(*β^A-globin* + *β-actin*) insert were smoothed using 500kb sliding windows, then centered and normalized so that the variability of timings were comparable between the two conditions.

B. A t-test was performed for each window to assess the significance of the timing differences. Adjusted p-values were computed for each window and smoothed using the PLIS R-package (Wei et al., 2009) to account for their spatial genomic dependency. P-values were then adjusted by the Benjamini-Hochberg procedure to ensure the control of the False Discovery Rate. The dotted line corresponds to a FDR of 5%.

Appendix Figure S4: Interaction profiles of allele 1+3/2 with chromosome 1 for clones 4 and 5

A. Interaction profiles of allele 1+3/2 with chr1 for clone 4 Hi-C libraries: distance-corrected interactions, *i.e.* observed/expected (OE), binned at 500 kb with corresponding compartment (EV1) tracks.

B. OE interactions of allele 1+3 (orange rectangles) and allele 2 (blue rectangles) averaged over A and B compartments for p and q-arms at 100kb bin size for clone 4. Values corresponding to OE interactions of allele 1+3 and allele 2 averaged over shuffled A (red circles, N=1000) and B compartments (blue circles, N=1000) for p and q-arms. ns, not significant; *p<0.05; **p<0.01;***p<0.001.

C. Scatterplot of density of interactions between allele 1+3 and allele 2 with chromosomes larger than 5,000,000 bp for clone 4.

D. Interaction profiles of allele 1+3/2 with chr1 for clone 5 Hi-C libraries : distance-corrected interactions, *i.e.* observed/expected (OE), binned at 500 kb with corresponding compartment (EV1) tracks.

E. OE interactions of allele 1+3 (orange rectangles) and allele 2 (blue rectangles) averaged over A and B compartments for p and q-arms at 100kb bin size for clone 5. Values corresponding to OE interactions of allele 1+3 and allele 2 averaged over shuffled A (red circles, N=1000) and B compartments (blue circles, N=1000) for p and q-arms. ns, not significant; *p<0.05; **p<0.01;***p<0.001.

F. Scatterplot of density of interactions between allele 1+3 and allele 2 with chromosomes larger than 5,000,000 bp for clone 5.

Appendix Figure S5: Validation of MNase digestion patterns before and after size selection (Related to Figure 6 and EV4)

A-B. Chromatin was extracted from two clonal cell lines for each construct or combination (*β^A-globin*, *β-actin*, *β^A-globin*+*β-actin*, 1+2+3, 1+3 and *loxP_LE* (1)+ *β^A-globin*+*β-actin* (3) and partially digested with exponentially increasing concentrations of micrococcal nuclease (MNAse; 2.5, 10, 40 and 160 U/mL).

A. After purification, DNA molecules were subjected to a size selection process that removed most DNA molecules over 1000 bp.

B. The four digested DNA samples obtained for each clonal cell line were subjected to electrophoresis in a 1% w/v agarose gel before and after size selection and stained with SYBR safe. The DNA size marker was a commercial 1 kb plus ladder.

Appendix Figure S6: Validation of the semi-quantitative PCR approach used to determine the spatial proximity of different combination of *cis*-regulatory elements separated by 30 kb (Related to Figure 5)

A-B. Images of agarose gels used for the quantification of specific products obtainted after either the large 1+3 and *loxP_LE* (1)+ β^A*-globin*+*β-actin* (3) excision in 1+2+3, 1+3 and *loxP_LE* (1)+ β^A*-globin*+*β-actin* (3) clonal cell lines or the large *β-actin* (1+3) excision in *β-actin* (1+3) clonal cell line are shown. After 1, 8, 24 and 48 h of 4-hydroxytamoxifen treatment, genomic DNA was extracted and quantified by semi-quantitative PCR. PCR products specific for the large 1+3 or *loxP_LE* (1)+ β^A*-globin*+*β-actin* (3) excision (3.4 kb, in a thick black lines, Up and Low large excision, A left gels), and for the large *β-actin* (1+3) excision (542 bp, in a thick black lines, Up and Low large excision, B left gels) or used for normalization (1.9 kb, amplification from both chromosomes, in a thick black line, Ctrl, A and B right gels) were run on a 0.8% or 1% w/v agarose gel, respectively, and stained with SYBR safe. The DNA size marker was a commercial 1 kb plus ladder.

Appendix Figure S7: PCR validation of clones selected for homologous recombination

A-H. Schematic diagrams showing genomic region containing a site-specific integrated construct. The 5′ and 3′ arms of the targeted vector are shown as black boxes. Arrows #1 and #2 represent primer sets used for the analysis of correct integration of the constructs by homologous recombination. Other arrows represent primer sets used for the analysis of the correct excision of the *BsR* gene at site 2 (#3 and #4) or the correct excision of the *PuroR* gene at site 3 (#5 and #6). PCR products were subjected to electrophoresis in a 1-1.5% w/v agarose gel and stained with SYBR safe. The DNA size marker was a commercial 1 kb plus DNA ladder (M). Lanes marked with a red star correspond to clonal cell lines selected for further analysis.

A-C. Insertion site 1, containing the *β-actin* construct, one *loxP_LE* element or the β^A*-globin*+*β-actin* construct is shown.

D. Insertion site 2 containing the *GFP* reporter construct is shown.

E-F. Insertion site 3, containing the β^A*-globin*+*β-actin* or the *β-actin* construct construct is shown.

G-H. The two genomic regions containing the β^A*-globin*+*β-actin* construct inserted at the late 1 or late 2 site are shown.

A-H. The sizes of the different PCR products obtained after amplification with primers #1 and #2, to check for correct integration, are 2.4 kb (A), 2.6 kb (B), 2.3 kb (C), 2.6 kb (D, left gel), 2.3 kb (E except the last right gel), 2.9kb (F), 2.6 kb (G) and 2.2 kb (H). The sizes of the different PCR products for the screening of cell lines correctly recombined for the *BsR* gene cassette after amplification with primers #3 and #4 are 2.1 kb (D, insertion site 2, right gel) or 1.2 kb with the primers #5 and #6 (F, insertion site 3, last right gel). The clonal cell line containing the *GFP* reporter construct without the *BsR* cassette at site 2 (D, 1-*BsR*) was used for further insertions at site 1 (B, #2 and C, #3 to #6) or at site 3 (E, #1 to #4). The clonal cell lines containing the *GFP* reporter construct without the *BsR* cassette at site 2 and one autonomous replicon at site 1 (C, #3, #4, #5) were used for further insertions at site 3 (E #5 to #9). The clonal cell lines containing the *GFP* reporter construct without the *BsR* cassette at site 2 and one *loxP_LE* at site 1 (B, #2) were used for further insertions of an autonomous replicon at site 3 (E, #10 to #12). Clone 1 with the β^A-*globin* construct inserted at site 1, as previously obtained (Hassan-Zadeh 2012, Fig.6B), was used for the further insertion of a β^A-*globin*+*β-actin* construct at site 3 (E #13 to #18). Clonal cell lines containing two minimal β^A-*globin* modules at sites 1 and 3 were obtained after excision of the *PuroR* cassette at site 3 (E, -*PuroR*, #13 to 18). Clone 2 with the *β-actin* construct inserted at site 1 (B, #2) was used for further insertions of the *β-actin* construct at site 3 (F, #19 to #23).

Appendix Figure S8: Validation of transgene integration into the same chromosome

A. The insertion of transgenes into the same or a different chromosome was analyzed by long-range PCR, with a primer set composed of an upstream primer binding within one construct and a downstream primer binding to the other construct. The amplicons generated after PCR amplification to test for insertion into the same chromosome are represented by red arrows (LR1+2, LR2+3, LR1+3, LR loxP_LE (1)+ β^A-*globin*+*β-actin* (3), LR β^A-*globin* (1+3), LR *β-actin* (1+3)). The absence of an amplicon indicates that the two constructs were inserted into distinct chromosomes. The quality of the DNA was checked with primer sets amplifying, on the two chromosomes, a genomic region located between the two insertion sites (black arrows, LR 1+2 ctrl, LR 2+3 ctrl, LR 1+3 ctrl).

B. PCR products were subjected to electrophoresis in a 0.8% w/v agarose gel and stained with SYBR safe. The DNA size marker used was a commercial 20 kb plus ladder. 1+2 clonal lines #3 and #4 were used to generate 1+3 clonal lines #1 and #2 with the *GFP* reporter construct inserted at site 2 on the same chromosome and 1+2 clonal line #2 was used to generate 1+3 clonal lines #3 to #5 with the *GFP* reporter construct inserted at site 2 on the other chromosome. Clonal line with the *GFP* reporter construct inserted at site 2 was used to generate one clonal line with the *loxP_LE* element inserted at site 1, which itself generated *loxP_LE* (1)+ β^A*-globin*+*β-actin* (3) clonal lines #1, #2 and #3 with the *GFP* reporter construct inserted at site 2 on the other chromosome. Clonal line 1 with the β^A*-globin* construct inserted at site 1, as previously obtained (Hassan-Zadeh 2012, Fig.6B), was used to generate β^A*-globin* (1+3) clonal lines #1 to #6. Clonal line with the *β-actin* construct inserted at site 1 was used to generate *β-actin* (1+3) clonal lines #1 to #5.

Appendix Figure S9: Additional filtering of Hi-C interactions

A. Heatmap of interaction frequencies for p-arm of chr1, demonstrating the position of the insertion site (red arrow) relative to filtered translocations (blue arrows).

B. Raw and unfiltered interactions profiles for allele 1+3 and allele 2 with chr1 p-arm, observed in two clones and their combination, with the corresponding EV1 compartment track. Translocations are highlighted on the compartment track with light blue color and with blue arrows. The insertion site is highlighted with a red arrow.

C-D. Raw and unfiltered interactions profiles for allele 1+3 and allele 2 with chr1 and chr9, observed in two clones and their combination. Blue arrow indicates the location of the β^A*-globin* promoter.

Table 1: Summary of all clonal cell lines (previously published or new clonal lines) analysed in this study

Table 2: Transgene copy number determination in clonal cell lines

The table shows the qPCR results obtained with genomic DNA extracted from the clones selected for the experiments. For each clone, 2 ng of genomic DNA was amplified with a primer set amplifying a sequence within the construct (With) and another primer set amplifying a sequence 5 kb downstream from the insertion site for both alleles (Both). The ratio of the amounts of DNA obtained with the With and Both primer sets was used to determine transgene copy number in all clonal cell lines. For each line, the construct for which the copy number was tested is indicated with the corresponding insertion site.

Table 3: Primers sets used for plasmids constructions

Table 4: Primer sets used for quantitative PCR

Table 5: Characterization of the reference sequences of allele 1+3/2

Characterization of the sequences of allele 1+3 and allele 2 inserts and raw interactions involving the inserts obtained from Hi-C experiments for clones 4 and 5. Characterization of the entire chr1 is added as a reference.

References

Hassan-Zadeh, V., Chilaka, S., Cadoret, J.-C., Ma, M.K.-W., Boggetto, N., West, A.G., and Prioleau, M.-N. (2012). USF binding sequences from the HS4 insulator element impose early replication timing on a vertebrate replicator. PLoS Biol. *10*, e1001277.

Massip, F., Laurent, M., Brossas, C., Fernández-Justel, J.M., Gómez, M., Prioleau, M.-N., Duret, L., and Picard, F. (2019). Evolution of replication origins in vertebrate genomes: rapid turnover despite selective constraints. Nucleic Acids Res. *47*, 5114–5125.

Valton, A.-L., Hassan-Zadeh, V., Lema, I., Boggetto, N., Alberti, P., Saintomé, C., Riou, J.-F., and Prioleau, M.-N. (2014). G4 motifs affect origin positioning and efficiency in two vertebrate replicators. EMBO J. *33*, 732–746.

Wei, Z., Sun, W., Wang, K., and Hakonarson, H. (2009). Multiple testing in genome-wide association studies via hidden Markov models. Bioinformatics *25*, 2802–2808.